2-Methoxyestradiol and its derivatives decrease Ca^{2+} entry in human (*Homo sapiens*) and rat (*Rattus norvegicus*) T lymphocytes by inhibiting Ca^{2+} release-activated Ca^{2+} channels

Dissertation

zur Erlangung des Doktorgrades an der
Fakultät für Mathematik, Informatik und Naturwissenschaften
Fachbereich Biologie der Universität Hamburg

vorgelegt von

Anke Johnsen

aus Preetz

Hamburg, 2018

Vorsitzende der Prüfungskommission: Jun.-Prof. Dr. rer. med. Esther Diekhof

Erstgutachter: Prof. Dr. rer. nat. Dr. med. habil. Andreas H. Guse

Zweitgutachter: Prof. Dr. rer. nat. Christian Lohr

Datum der Disputation: 09.11.2018

Content

List of figures

List of tables

Abbreviations

2ME2: 2-Methoxyestradiol

ANOVA: analysis of variance

APC: antigen presenting cell

BAPTA: 1,2-bis(*o*-aminophenoxy)ethane-*N,N,N',N'*-tetraacetic acid

BSA: bovine serum albumin

$[Ca^{2+}]_i$: free cytosolic Ca^{2+} concentration

CaM: calmodulin

CD: cluster of differentiation

CFP: cyan fluorescent protein

CNS: central nervous system

ConA: concanavalin A

CRAC channels: Ca^{2+} release-activated Ca^{2+} channels

CRC: concentration-response curve

DAG: diacylglycerol

E1: estrone

E2: 17-β-estradiol

E3: estriol

EAE: experimental autoimmune encephalomyelitis

eGFP: enhanced green fluorescent protein

EGTA: ethylene glycol-bis(β-aminoethyl ether)-*N,N,N',N'*-tetraacetic acid

ER: endoplasmic reticulum

ERα: estrogen receptor α

ERβ: estrogen receptor β

EtOH: ethanol

FBS: fetal bovine serum

FoxP3: forkhead box P3 (FoxP3)

FRET: Förster resonance energy transfer

GPER: G protein-coupled estrogen receptor

HS: horse serum

I_{CRAC}: Ca^{2+} release-activated Ca^{2+} current

IFN-γ: interferon gamma

IL: interleukin

Iono: ionomycin

IP_3: D-*myo*-inositol 1,4,5-trisphosphate

IP_3R: IP_3 receptor

ITC: isothermal titration calorimetry

Kd: dissociation constant

LAT: linker for activated T cells

LCK: lymphocyte-specific protein tyrosine kinase

MBP: myelin basic protein

MCU: mitochondrial Ca^{2+} uniporter

MHC: major histocompatibility complex

MOG: myelin oligodendrocyte glycoprotein

MS: Multiple Sclerosis

NCS: newborn calf serum

NFAT: nuclear factor of activated T cells

NF-κB: nuclear factor 'kappa-light-chain-enhancer' of activated B cells

OKT3: an αCD3 antibody

PenStrep: penicillin-streptomycin

PIP_2: phosphatidyl inositol bisphosphate

PLL: poly-L-lysine

PLP: proteolipid protein

PMCA: plasma membrane Ca^{2+} ATPase

Prog: Progesterone

RM: restimulation medium

Rpip: resistance of the micropipette

RRMS: relapsing-remitting MS

Rseries: series resistance

RT: room temperature

RyR: ryanodine receptor

SD: standard deviation

SERCA: sarco-endoplasmic reticulum Ca^{2+} ATPase

SOCE: store-operated Ca^{2+} entry

STIM: stromal interaction molecule

Tes: testosterone

TCGF: T cell growth factor medium

TCM: T cell medium

TCR: T cell receptor

T_{eff} lymphocytes: effector T lymphocytes

TG: Thapsigargin

Th: T helper lymphocytes

T_{MBP} lymphocytes: restimulated, primary rat T lymphocytes specific for MBP

TNF-α: tumor necrosis factor α

T_{reg} lymphocytes: regulatory T lymphocytes

Tris: Tris(hydroxymethyl)aminomethane

YFP: yellow fluorescent protein

ZAP70: ζ-chain-associated protein kinase of 70 kDa

Abstract

2-Methoxyestradiol (2ME2) is an endogenous estradiol (E2) metabolite which is considered to be non-estrogenic as it binds to the estrogen receptors with an at least 500 fold lower affinity compared to E2 (LaVallee et al., 2002). 2ME2 is well known for inhibiting tumor growth by downregulating proliferation of tumor cells and angiogenesis (Fotsis et al., 1994). More recently, 2ME2 was shown to also ameliorate the symptoms in experimental autoimmune encephalomyelitis (EAE), an animal model of Multiple Sclerosis (MS; Duncan et al., 2012). In this model, 2ME2 downregulates the activation of T lymphocytes by inhibiting the translocation of NFAT (nuclear factor of activated T cells), a mechanism which requires increased Ca^{2+} entry resulting in elevation of the free cytosolic Ca^{2+} concentration ($[Ca^{2+}]_i$; Duncan et al., 2012; Kar et al., 2016). However, it still remains unresolved if 2ME2 inhibits NFAT translocation by interfering with Ca^{2+} signalling pathways or with any other mechanism like directly inhibiting the dephosphorylation of NFAT. Thus, the central aim of the current study was to investigate the impact of 2ME2 on Ca^{2+} signalling pathways in T lymphocytes and if other endogenous steroid hormones possess similar effects. The analysis of Fura2 loaded Jurkat T lymphocytes stimulated with thapsigargin in a nominal Ca^{2+} free buffer revealed that increasing 2ME2 concentrations decrease Ca^{2+} entry after Ca^{2+} re-addition with an IC_{50} of 20 µM. In contrast to this, E2 also inhibited Ca^{2+} entry but not as potently as 2ME2, suggesting that the 2-methoxy group is crucial for inhibiting Ca^{2+} entry in T lymphocytes. On the basis of these results, 25 derivatives of 2ME2 with different side chains were analysed. This analysis revealed that the most potent 2ME2 derivatives possess 2-ethyl, a 3-hydroxy or 3-sulfamoyloxy and a hydrogen bond acceptor group at C17 which was different from a sulfamoyloxy group. The most potent compounds decreased Ca^{2+} entry with an IC_{50} of about 1 µM.

To analyse the mechanism of Ca^{2+} entry inhibition, I investigated K^+ channels via whole cell patch clamp recordings, Ca^{2+} independent mechanisms by Mn^{2+} quenching and Ca^{2+} entry through CRAC/Orai channels covalently bound to a genetically encoded Ca^{2+} indicator (GECO). This study revealed that K^+ channels and Ca^{2+} dependent mechanisms are not influenced but the fluorescence of GECO bound to Orai channels was decreased by 2ME2 and its derivatives. These data indicate inhibition of the STIM/Orai mediated Ca^{2+} entry as the target of the endogenous E2 metabolite 2ME2

in T lymphocytes. The potency of 2ME2 was increased by derivatisation, leading to a new series of potent STIM/Orai inhibitors in T lymphocytes.

Zusammenfassung

2-Methoxyestradiol (2ME2) ist ein endogener Östradiol (E2)-Metabolit, der als nicht-östrogen angesehen wird, da er im Vergleich zu E2 mit einer mindestens 500-fach geringeren Affinität an die Östrogenrezeptoren bindet (LaVallee et al., 2002). 2ME2 ist bekannt für seine Inhibition des Wachstums von Tumoren durch die Reduktion der Proliferation der Tumorzellen sowie der Angiogenese (Fotsis et al., 1994). Außerdem wurde gezeigt, dass 2ME2 die Symptome in der experimentellen autoimmunen Enzephalomyelitis (EAE), einem Tiermodell der Multiplen Sklerose, abmildert (Duncan et al., 2012). In diesem Model bewirkt 2ME2 eine verminderte Proliferation und Aktivierung der T-Lymphozyten durch die Inhibition der Translokation von NFAT (nukleärer Faktor aktivierter T-Zellen), eines Mechanismus‘, der einen verstärkten Ca^{2+}-Einstrom und eine daraus resultierende höhere freie zytosolische Ca^{2+}-Konzentration ($[Ca^{2+}]_i$) benötigt (Duncan et al., 2012; Kar et al., 2016). Bisher ist immer noch ungeklärt, ob 2ME2 die Translokation von NFAT durch die Ca^{2+}-Signalwege oder durch andere Mechanismen, wie die direkte Hemmung der Dephosphorylierung von NFAT, inhibiert. Daher ist das zentrale Ziel dieser Studie die Untersuchung des Einflusses von 2ME2 auf die Ca^{2+}-Signalwege in T-Lymphozyten und die Analyse, ob andere endogene Steroidhormone ähnliche Effekte aufweisen. Die Untersuchung von Fura2-beladenen Jurkat T-Lymphozyten, die mit Thapsigargin in einem nominal Ca^{2+}-freien Puffer stimuliert wurden, zeigte, dass 2ME2 den Ca^{2+}-Einstrom nach Ca^{2+}-Zugabe bei einer Konzentration von 20 µM halbmaximal inhibiert. Im Gegensatz hierzu zeigte E2 eine schwächere Inhibition des Ca^{2+}-Einstroms, was darauf hindeutet, dass die Methoxylgruppe an C2 entscheidend für die Inhibition des Ca^{2+}-Einstroms der T-Lymphozyten ist. Auf Grundlage dieser Ergebnisse wurden 25 Derivate von 2ME2 mit unterschiedlichen Seitengruppen auf ihre Wirksamkeit hin untersucht. Diese Analyse zeigte, dass die potentesten Derivate eine 2-Ethyl-, eine 3-Hydroxyl- oder 3-Sulphamoyloxyl-Gruppe sowie einen Akzeptor für Wasserstoffbindungen an C17 beinhielten, wobei eine Sulfamoyloxyl-Gruppe als Akzeptor für Wasserstoffbindungen keinen positiven Effekt zeigte. Diese potentesten Substanzen inhibierten den Ca^{2+}-Einstrom mit einer IC_{50} von etwa 1 µM.

Um den Mechanismus für die Inhibierung des Ca^{2+}-Einstroms aufzuklären, habe ich K^+-Kanäle per Spannungsklemmen-Ableitungen im Ganzzell-Modus, Ca^{2+}-unabhängige Mechanismen mittels Mn^{2+}-Quenching und den Ca^{2+}-Einstrom durch CRAC/Orai-Kanäle durch genetisch kodierte Ca^{2+}-Indikatoren (GECO), die kovalent an die Orai-Kanäle gebunden wurden, untersucht. Die Ergebnisse zeigen, dass weder K^+-Kanäle noch Ca^{2+}-abhängige Mechanismen, sondern die Fluoreszenz der an Orai-Kanäle gebundenen GECO-Fluorophore durch 2ME2 und seine Derivate inhibiert werden. Diese Ergebnisse deuten darauf hin, dass 2ME2 auf den STIM/Orai-vermittelten Ca^{2+}-Einstrom in T-Lymphozyten wirkt. Durch Derivatisierung wurde die Wirksamkeit von 2ME2 um das 20-fache erhöht. Somit stellen diese Substanzen eine neue Klasse von STIM/Orai-Inhibitoren in T-Lymphozyten dar.

1. Introduction

Usually the immune system protects the body from numerous threats like bacteria, viruses, fungi, parasites and further “foreign and dangerous” substances as well as tumor cells. But if the immune system is directed against body cells, autoimmune diseases can arise. One such autoimmune disease is Multiple Sclerosis (MS) which is characterized by inflammation of the CNS. Interestingly, symptoms of MS are ameliorated during pregnancy, especially in the last trimester (Confavreux et al., 1998).

1.1 Multiple Sclerosis – an autoimmune disease

Multiple Sclerosis is an autoimmune disease which is characterized by inflammation and neurodegeneration of the CNS. This disease often occurs as a relapsing-remitting disease marked by time periods with a high degree of disability which are intermitted by time periods with a decreased degree of disability (reviewed in Stys et al., 2012). MS at this state is called relapsing-remitting MS (RRMS). After several years of RRMS, MS often develops into a progressive form which is characterized by neurodegeneration whereas the central feature of the relapsing-remitting disease is inflammation (Frischer et al., 2009). The immune response as well as the neurodegeneration cause an impaired propagation of neuronal signals resulting in a slower or abolished signal transduction by neurons. Depending on which neurons are affected, different symptoms can occur of which impaired sensation and impaired control of body functions occur most frequently (Stuke et al., 2009).

The proper and fast signal transduction in the CNS is usually mediated by the myelin sheath built up by oligodendrocytes (reviewed in Bunge, 1968). It surrounds and insulates neurons and provides fast signal transduction. There is good evidence that the myelin sheath, particularly certain proteins within the myelin sheath, play a central role in causing disability in MS. These proteins encompass myelin oligodendrocyte glycoprotein (MOG) and myelin basic protein (MBP) as antibodies against them are associated with an increased relapse rate (Berger et al., 2003). One further protein is proteolipid protein (PLP) which, like MOG and MBP, is able to induce MS like symptoms in the experimental autoimmune encephalomyelitis (EAE), an animal model

of MS (reviewed in Martin et al., 1995; Robinson et al., 2014). Furthermore, a transfer of T lymphocytes reactive against any of these proteins from affected animals can induce inflammation in otherwise healthy animals (Ben-Nun et al., 1981). This observation suggests that T lymphocytes are the main mediators for MS although a contribution of other immune cells, like macrophages or microglia, are also discussed (Chiang et al., 1996). Furthermore, autoantibodies produced by B lymphocytes were found in the CNS of MS patients (Linington et al., 1988). However, it is not known until now if T lymphocytes cause inflammation which results in cytodegeneration (outside-in model) or if a T lymphocytes mediated inflammation arises in response to cytodegeneration (inside-out model; Stys et al., 2012). Furthermore, it has not been revealed yet whether T lymphocytes become activated in the periphery and cross the blood brain barrier as lymphoblasts or if the blood brain barrier is leaky before, facilitating the crossing of immune cells (reviewed in Pinheiro et al., 2016).

Nonetheless, the inflammation can be dampened by regulatory T lymphocytes (T_{reg} lymphocytes) which downregulate effector T lymphocytes (T_{eff} lymphocytes) mediating inflammation. Increased numbers of T_{reg} lymphocytes are found during remission compared to relapses (Frisullo et al., 2009). However, T_{reg} lymphocytes from MS patients are either less effective in downregulating T_{eff} lymphocytes or T_{eff} lymphocytes are resistant to downregulation by T_{reg} lymphocytes (Viglietta et al., 2004). Symptoms can further be ameliorated by rebuilding the myelin sheath, a process which is called remyelination (reviewed in Chari, 2007).

As this section shows, T lymphocytes play a central role in mediating MS. How T lymphocytes become activated and cause an inflammation is described in the next section.

1.2 Immune response mediated by T lymphocytes

It is a striking feature of immune cells that they identify dangerous foreign or abnormal cells and structures. This identification can be either mediated by unique features of foreign cells, like lipopeptides or lipopolysaccharides on the cell membrane of e.g. bacteria, or by recognition of specific antigens (reviewed in Bittar & Bittar, 1996, p. 53). The first characteristic is used by cells of the unspecific immune system which is made up by natural killer cells, macrophages and dendritic cells among others (reviewed in

Hato & Dagher, 2015). In contrast to cells of the unspecific immune system, T and B lymphocytes recognize specific peptides, a feature which makes T lymphocytes together with B lymphocytes belong to the specific immune system (reviewed in Hohlfeld, 1997). While B lymphocytes are able to take up antigens on their own, T lymphocytes require peptides bound to polypeptide chains. These polypeptide chains are called major histocompatibility complex (MHC; reviewed in Bittar & Bittar, 1996, p. 7 ff.). MHCs can bind peptides which derive from protein digestion. Digested peptides are bound to the MHC and presented on the cell surface where T lymphocytes can detect them. MHCs can be differentiated into MHC I and MHC II. MHC I and II differ concerning the origin of bound peptides and cells identifying them. In case of MHC I, proteins originating from the same cell are digested and bound to the complex (reviewed in Bittar & Bittar, 1996, p. 54). After presentation on the cells' surface, these peptides can be identified by $CD8^+$ cytotoxic T lymphocytes (CTLs). If peptides presented on MHC I do not belong to the peptides which are usually expressed by the cell, e.g. in case of a tumor or a virus infected cell, CTLs can cause the death of the cell by inducing apoptosis (reviewed in Bittar & Bittar, 1996, p. 276). Some viruses supress MHC I expression I on the cell surface resulting in non-identification by CTLs. These cells are eliminated by NK cells (Kärre et al., 1986).

While MHC I is expressed on almost every cell, MHC II is only expressed on very few cell types which are called antigen presenting cells (APCs; reviewed in Lin & Loré, 2017). APCs are made up by monocytes, macrophages, dendritic cells, B lymphocytes and are discussed to also include granulocytes which express low amounts of MHC II (Vono et al., 2017). Peptides presented on MHC II do not derive from endogenous proteins but originate from dead cells or proteins which entered the body. These proteins have to be taken up by APCs via phagocytosis. Subsequently, proteins are cleaved into peptides and bound to MHC II where peptides can be detected by $CD4^+$ T lymphocytes, so called T helper (Th) cells (reviewed in Bittar & Bittar, 1996, p. 53). CD4 is made up by polypeptide chains which are accompanied by T cell receptors (TCR). Upon antigen recognition, $CD4^+$ cells become activated and in turn activate specific B lymphocytes by cytokine secretion and by binding of CD40 on the B lymphocyte to its ligand on T lymphocytes (reviewed in Clark & Ledbetter, 1994; Zhu & Paul, 2008). Upon activation, B lymphocytes proliferate and differentiate into plasma cells secreting

antibodies (reviewed in Yang & Reth, 2015). Besides B lymphocyte activation, T lymphocytes mediate macrophage activation by IFN-γ as well as macrophage deactivation by secretion of IL-4, IL-10 and IL-13 (reviewed in Hohlfeld, 1997).

To identify many different antigens, individual T lymphocytes express different TCRs each of which only binds to a specific peptide presented on MHC (reviewed in Merwe and Dushek, 2011). This specificity requires a high variability and selectivity of TCR which derives from its structure. It is composed of two segments which are either an α and a β chain ($\alpha\beta^+$ T cells) or a γ and a δ chain ($\gamma\delta^+$ T cells) among which the first are present in the majority of T lymphocytes (reviewed in Hohlfeld, 1997). These chains stabilize the binding of TCR to MHC. Each of these chains is built up by freely combinable and independently expressed gene segments (reviewed in Attaf et al., 2015). The random combination of different gene segments is responsible for the high variability which is necessary to react to a large number of antigens. By chance, TCRs can be generated which identify endogenous peptides resulting in so-called self-reactive T lymphocytes. To ensure that self-reactive T lymphocytes do not harm the body, T lymphocytes are negatively selected in the thymus as many of the proteins present in the periphery are also present in the thymus (reviewed in Goodnow et al., 2005; Hohlfeld, 1997). Usually, self-reactive T lymphocytes undergo apoptosis in the thymus. But if this mechanism fails, self-reactive T lymphocytes can enter the periphery and can cause inflammations resulting in autoimmune diseases like MS (Laufer et al., 1996). Self-reactive T lymphocytes are thought to identify peptide sequences which occur in many proteins from different sources (Birnbaum et al., 2014; Wucherpfennig & Strominger, 1995; reviewed in Sewell, 2012). This mechanism is called molecular mimicry (Wucherpfennig & Strominger, 1995) or cross-reactivity (Birnbaum et al., 2014). Self-reactive T lymphocytes can pass negative selection in the thymus by reacting only very weak to self-peptides. If these cells become activated in the periphery by foreign peptides, they can develop into memory T lymphocytes which can be activated by lower peptide concentrations (Sewell, 2012).

In dependence of the cytokine pattern released by $CD4^+$ T lymphocytes, these cells can further be subdivided into Th1, Th2 and Th17 lymphocytes and less often into Th3 and Th0 lymphocytes (reviewed in Hohlfeld, 1997). The most important subclasses among these are Th1 and Th2 lymphocytes. They can also be discriminated by the expression of CD30

which is only expressed by Th2 lymphocytes (Del Prete et al., 1995). Th1 lymphocytes typically express IFN-γ and IL-2 and mediate cellular immunity caused by the natural killer cells (reviewed in Hohlfeld, 1997). This immune response is predominantly present in MS patients during the active disease (Correale et al., 1995; Voskuhl et al., 1993). In contrast to Th1 cells, Th2 lymphocytes mainly release IL-4, IL-5, IL-6, IL-9, IL-10, and IL-13 and support humoral immunity mediated by antibody secreting B lymphocytes (reviewed in Hohlfeld, 1997). T lymphocytes from MS patients express Th1 lymphocytes cytokines during the active phase whereas the proportion of Th2 lymphocytes increases during the remission phase (Correale et al., 1995; Voskuhl et al., 1993). Furthermore, an induced Th2 immune response can prevent the symptoms in EAE (Falcone & Bloom, 1997).

Among $CD4^+$ T lymphocytes, there are not only T_{eff} lymphocytes which secrete pro-inflammatory cytokines but also T_{reg} lymphocytes which are able to suppress the inflammation by secreting anti-inflammatory cytokines. T_{reg} lymphocytes can be separated from other $CD4^+$ cells by the expression of different proteins of which the forkhead box P3 (FoxP3) is the best known (Fontenot et al., 2017; Hori et al., 2003; reviewed in Piccioni et al., 2014). T_{reg} lymphocytes are thought to suppress the immune response to avoid an overshoot and thereby avoid an uncontrolled or systemic inflammation.

Besides association of CD4 or CD8 with TCR, the latter is further accompanied by CD3 which is responsible for signal transduction (reviewed in Bittar & Bittar, 1996, p. 54). This mechanism and the central role of Ca^{2+} is described in the next section.

1.2.1 Activation of T lymphocytes

Second messenger formation

If TCRs bind to a peptide, a signalling cascade is initiated at the associated CD3 which is composed of γ, δ, ε and ζ chains (reviewed in Brownlie & Zamoyska, 2013). First of all LCK (lymphocyte-specific protein tyrosine kinase) is phosphorylated (Lovatt et al., 2006). In turn, LCK binds to CD4 or CD8 which moves LCK to immunoreceptor tyrosine-based activation motifs (ITAMs; Artyomov et al., 2010; Veillette et al., 1988). There, LCK phosphorylates ITAMs of ε and ζ chains as well as ζ-chain associated protein kinase of 70 kDa (ZAP70; Acuto et al., 2008). The latter phosphorylation results in a conformational change of ZAP70 which mediates, among others, the phosphorylation of linker for activated T lymphocytes

(LAT; Deindl et al., 2007). This phosphorylation activates many other downstream molecules, one of which is PLCγ. PLCγ cleaves phosphatidylinositol 4,5-bisphosphate (PIP_2) into diacylglycerol (DAG) and D-*myo*-inositol 1,4,5-trisphosphate (IP_3; reviewed in Feske, 2007). Furthermore, upon TCR engagement, nicotinic acid adenine dinucleotide phosphate (NAADP) and cyclic adenosine diphosphate ribose (cADPR) are formed (Gasser et al., 2006; Guse et al., 1999). NAADP is formed and degraded within the first 20 s after TCR engagement in Jurkat T lymphocytes, indicating that this is the first second messenger relevant for Ca^{2+} signalling (Gasser et al., 2006). About 3 min after stimulation via TCR, IP_3 concentration reaches its maximum while cADPR concentration reaches a long lasting plateau after 10 min, indicating that these second messenger evoke Ca^{2+} signals in a temporally coordinated way (Guse et al., 1993, 1999). All of these second messengers bind to receptors in the membrane of the endoplasmic reticulum (ER). While IP_3 binds to its specific IP_3 receptor (IP_3R), NAADP and cADPR bind to ryanodine receptors (RyR) all of which are ligand-gated Ca^{2+} ion channels (Kunerth et al., 2004; Langhorst et al., 2004; reviewed in Feske, 2007). As the free Ca^{2+} concentration is much higher in the ER (100 – 800 µM) than in the cytosol (100 nM), a large chemical gradient results in Ca^{2+} ions moving through these ion channels along this chemical gradient from the ER into the cytosol (reviewed in Feske, 2007). This Ca^{2+} release is the starting point for Ca^{2+} signalling.

Ca^{2+} signalling pathways

Ca^{2+} signalling is initiated by Ca^{2+} release from the ER and involves many ion channels and pumps. Ca^{2+} signalling pathways and its consequences for T lymphocyte activation are depicted in Figure 1. Ca^{2+} release from the ER by IP_3R and RyR on the one hand increases the free cytosolic Ca^{2+} concentration ($[Ca^{2+}]_i$) and on the other hand decreases the luminal Ca^{2+} concentration within the ER. The latter mechanism favours the dissociation of Ca^{2+} from the EF-hand of the stromal interaction molecule (STIM). STIM is a Ca^{2+} sensing molecule spanning the ER membrane (Liou et al., 2005). Dissociation of Ca^{2+} from STIM causes STIM phosphorylation resulting in cluster formation and oligomerization (Luik et al., 2008). Subsequently, STIM binds to Orai channels located in the plasma membrane. Orai channels form hetero-hexamers and open upon STIM binding (Hou et al., 2012; Kawasaki et al., 2009). Activation of Orai channels leads to Ca^{2+} entry due to the chemical gradient as extracellular Ca^{2+}

concentrations (about 1 mM) are much higher at physiological conditions than $[Ca^{2+}]_i$ (approx.. 100 nM in resting cells, 1 µM in activated cells; reviewed in Feske, 2007). This particular Ca^{2+} entry is also called store operated Ca^{2+} entry (SOCE) or Ca^{2+} release-activated Ca^{2+} entry (CRAC; reviewed in Feske, 2007).

$[Ca^{2+}]_i$ is regulated not solely by Ca^{2+} release and Ca^{2+} entry but also by pathways decreasing $[Ca^{2+}]_i$. The latter are important to refill Ca^{2+} stores, decrease $[Ca^{2+}]_i$ after stimulation, and buffer local Ca^{2+} in close proximity to Orai channels. These so-called Ca^{2+} clearance mechanisms are crucial for Ca^{2+} signalling and include Ca^{2+} reuptake into the ER by serco/endoplasmic reticulum Ca^{2+}-ATPases (SERCAs), Ca^{2+} extrusion to the extracellular space by plasma membrane Ca^{2+}-ATPases (PMCAs) and Ca^{2+} uptake into mitochondria by mitochondrial Ca^{2+} uniporter (MCUs: Samanta et al., 2014; Tang et al., 2015; SERCA: Redondo et al., 2008; PMCA: Domi et al., 2007). Buffering local Ca^{2+} is particularly important for mediating sustained Ca^{2+} entry as Orai channels are inhibited by local Ca^{2+} (Hoth et al., 2000).

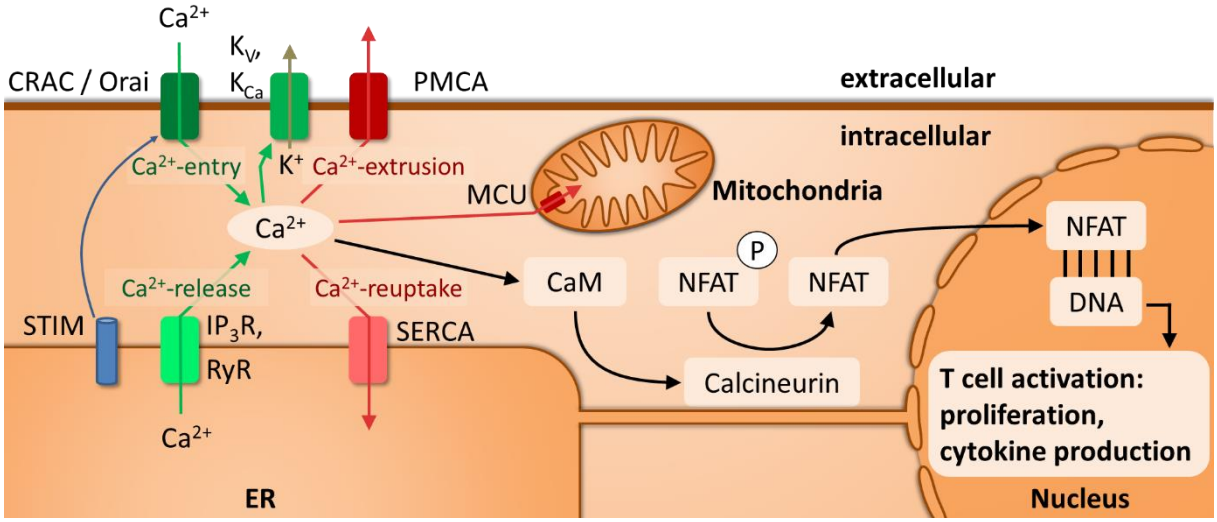

Figure 1: Ca^{2+}-signalling pathways in T lymphocytes.

Upon second messenger formation, Ca^{2+} is released from the ER into the cytosol is mediated resulting in a transient increase in $[Ca^{2+}]_i$. Ca^{2+} release decreases luminal Ca^{2+} concentration in the ER causing Ca^{2+} dissociating the EF-hand of STIM. Thereby, STIM is activated by phosphorylation resulting in oligomerisation and cluster formation. Upon oligomerization, STIM can bind to and activate Orai channels in the plasma membrane mediating Ca^{2+} entry. Upon Ca^{2+} entry, the cytosol depolarizes and activate K^+ channels which counteract the depolarisation and maintain Ca^{2+} entry. These three mechanisms are referred to as Ca^{2+} increasing mechanisms. Increased $[Ca^{2+}]_i$ facilitates binding of Ca^{2+} to CaM which in turn activates the phosphatase calcineurin. Calcineurin dephosphorylates NFAT which can then translocate to the nucleus and activate production of proteins required for T lymphocytes activation. Increased $[Ca^{2+}]_i$ can be decreased by Ca^{2+} clearance mechanisms which consist of Ca^{2+}-reuptake into the ER by SERCAs, Ca^{2+}-extrusion to the extracellular space by PMCAs and Ca^{2+} uptake into mitochondria by MCUs. (modified from Feske, 2007).

T cell activation is further regulated by K^+ channels which mediate a K^+ efflux. This monovalent cation efflux counteracts the divalent cation influx provided by Ca^{2+} entry and thereby maintains the electrical gradient for Ca^{2+} which is required for sustained Ca^{2+} entry and T lymphocyte activation (Beeton et al., 2001a; Fanger et al., 2001; Ghanshani et al., 2000). In T lymphocytes, two different kinds of K^+ channels are activated, namely voltage-dependent K_V channels and Ca^{2+}-activated K_{Ca} channels. K_V channels activate upon depolarization (Cahalan et al., 2001). These channels are particularly important in resting T lymphocytes but also in mediating inflammation (Beeton et al., 2001a, 2001b). K_{Ca} channels open upon increased $[Ca^{2+}]_i$ which is of special importance in activated T lymphocytes as these channels become highly upregulated during T lymphocyte activation and inhibition of K_{Ca} channels inhibit Ca^{2+} entry (Fanger et al., 2001; Ghanshani et al., 2000; Grissmer et al., 1993).

All of these mechanisms help to regulate $[Ca^{2+}]_i$ after TCR engagement. Increased $[Ca^{2+}]_i$ mediates many downstream events, one of which is the modulation of gene expression. One important transcription factor activated upon increased $[Ca^{2+}]_i$ is the nuclear factor of activated T cells (NFAT).

NFAT translocation and regulation of cytokine production

One important consequence of an increased $[Ca^{2+}]_i$ is the translocation of transcription factors into the nucleus. The most important one in T lymphocytes is the nuclear factor of activated T cells (NFAT). NFAT regulates the expression of IL-2 as well as IFN-γ (Negulescu et al., 1994; Sica et al., 1997).

The impact of Ca^{2+} on gene regulation was first described by (Negulescu et al., 1994). Elevated $[Ca^{2+}]_i$ facilitates binding of Ca^{2+} ions to the Ca^{2+} binding protein calmodulin (CaM) which in turn activates the phosphatase calcineurin (reviewed in Cahalan et al., 2001; Feske, 2007). Calcineurin dephosphorylates NFAT which subsequently can translocate to the nucleus regulating expression of several genes (reviewed in Feske, 2007). NFAT has different isoforms. Interestingly, translocation of these isoforms require Ca^{2+} signals in different compartments and different amplitudes (Kar et al., 2016; reviewed in Liu et al., 2016). NFAT1 translocates to the nucleus upon local Ca^{2+} entry and an elevated $[Ca^{2+}]_i$ whereas NFAT4 requires Ca^{2+} in the nucleus which is mediated by IP_3R located in the ER membrane facing to the nucleus (Kar et al., 2016).

Interestingly, NFAT translocation is inhibited by 2-methoxyestradiol (2ME2), an endogenous estradiol (E2) metabolite, resulting in downregulation of T lymphocytes and amelioration of EAE (Duncan et al., 2012). Furthermore, several endogenous hormones interfere with T lymphocytes which are described in the next section.

1.3 Immunomodulation by steroid hormones

Ca^{2+} signals and subsequent NFAT translocation are directly connected to cytokine production by T lymphocytes. They play central roles in T lymphocyte activation and inflammation, independently of whether T lymphocytes recognize foreign or endogenous antigens. Downregulation of T lymphocytes is one treatment for autoimmune diseases like MS.

Interestingly, about 20 years ago, Confavreux et al. showed that symptoms as well as frequency of relapses in patients with MS are decreased during pregnancy, esp. in the last trimester (Confavreux et al., 1998; confirmed by a meta-data analysis: Finkelsztejn et al., 2011). This time period correlates with an increased amount of steroid hormones like E2 and progesterone (Prog; Doria et al., 2002). E2 and Prog but also other steroid hormones were described to directly influence cytokine production of immune cells. The effect of estrogens and androgens are controversially described in the literature as some groups showed a suppression of the immune system while others showed an activation (e.g. Ackerman, 2006; Correale et al., 1998; Engler et al., 2017; Hoffman et al., 2001; Marzi et al., 1996; McMurray et al., 2001; Paavonen et al., 1981; Polanczyk et al., 2004; Stefano et al., 2000; Stubelius et al., 2014; Voskuhl & Palaszynski, 2001; Wegmann et al., 1993). E2 as well as Prog shift composition of T lymphocytes by inhibiting T_{eff} lymphocytes resulting in an increased proportion of T_{reg} lymphocytes (Engler et al., 2017; Polanczyk et al., 2004). Furthermore, it is well established that pregnancy, most probably the particular high concentration of E2 and Prog, induces a shift from a Th1- to a Th2-immune response (Ackerman, 2006; Marzi et al., 1996; Wegmann et al., 1993; reviewed in Khan & Ahmed, 2016; Whitacre, 1999).

The change of the immune system response during pregnancy is thought to facilitate the foeto-maternal immune tolerance so that the maternal immune system does not reject the foetus which contains foreign proteins originating from the paternal genes

(reviewed in Arck & Hecher, 2013; Pankratz et al., 2016). The foetus and the placenta secretes cytokines like IL-10 which dampens the cellular immunity by the mother (Confavreux et al., 1998). This shift is thought to be induced by an increase in concentrations of steroid hormones, like E2 and Prog (Ito et al., 2001; Piccinni et al., 1995). The action of androgens is thought to be largely mediated also by estrogens as the androgens are converted to estrogens by aromatase (Grossman, 1985). A shift towards Th2 is thought to ameliorate T lymphocyte mediated autoimmune diseases like MS and rheumatoid arthritis while B lymphocyte mediated autoimmune diseases like systemic lupus erythematosus are worsened (Chen et al., 2015; Confavreux et al., 1998; de Man et al., 2008).

High levels of estrogens, Prog and testosterone (Tes) mediate differentiation of Th lymphocytes into Th2 lymphocytes (Ackerman, 2006; reviewed in Whitacre, 1999). Besides E2, Prog, estrone (E1) and estriol (E3) also influence cytokine production by T lymphocytes. E2, E1 and E3 were shown to stimulate IL-10 and IFN-γ production in a concentration dependent manner whereas these steroid hormones do not influence IL-4 or TGF-β secretion (Correale et al., 1998). Inhibition of IL-10 and IFN-γ production at high estrogen concentrations resembles a Th2 like, anti-inflammatory immune response at concentrations typical for pregnancy (Gilmore et al., 1997). Shifting immune responses towards Th2 not only affects T lymphocytes but also production of inflammatory mediators secreted by astrocytes, microglia and macrophages (reviewed in Melcangi et al., 2016). However, Ito and colleagues argue that the effect of E2 on EAE is not mediated by a shift from Th1 to Th2 because EAE symptoms are ameliorated in mice deficient of important cytokines expressed by Th2 lymphocytes like IL-3, IL-10 and IFN-γ (Ito et al., 2001). Additionally, Elenkov and colleagues claim that changes in cytokine production are due to increased concentrations of cortisol, norepinephrine and dihydroxyvitamin D3 as 10 pM to 10 µM E2 or Prog does neither affect IL-12, TNF-α nor IL-10 production (Elenkov et al., 2001). Thus, although it is well established that pregnancy induces the shift from a Th1 to a Th2 immune response, the underlying mechanism is also not unravelled in detail by now.

Furthermore, women are about 2 to 3 times more often affected by MS than men (reviewed in Whitacre, 1999). This so-called sex bias also occurs in other autoimmune diseases, like rheumatoid arthritis or systemic lupus erythematosus (reviewed in

Rubtsova et al., 2015). In MS, the disease also develops differently in men and women. The first symptoms in women usually occur in early adulthood whereas the first symptoms in men occur when they are around 40 years old who additionally show a faster disease progression (reviewed in Confavreux & Vukusic, 2002). This suggests that the disease and thereby the immune system are directly affected by the steroid hormones or by the sex chromosomes (reviewed in Pennell et al., 2012). The current study investigated the impact of steroidal hormones as well as their metabolites and derivatives on T lymphocytes by interfering Ca^{2+} signalling pathways.

There are a lot of papers showing immunomodulation by different steroid hormones as described earlier. Not only the steroid hormones themselves supress immune reactions but also their metabolites. One such interesting metabolite is 2-methoxyestradiol (2ME2).

1.3.1 2-Methoxyestradiol (2ME2)

2ME2 is an endogenous E2 metabolite which is formed by conversion of E2 to 2-hydroxyestradiol by Cytochrome P450, isoform CYP1B1 (reviewed in Dubey, 2017). 2-Hydroxyestradiol is further metabolized to 2ME2 by catechol-*O*-methyltransferase (COMT) in granulosa cells (reviewed in Zhu & Conney, 1998). All steroid hormones originate from cholesterol (Chol).

Physiological 2ME2 concentrations vary largely. Typical values are about 30 pM in adult male and 150 pg/ml (500 pM) in non-pregnant females, reaching concentrations up to 280 pg/ml (1 nM) in the last trimester of pregnancy (Shen et al., 2014; reviewed in D'Amato et al., 1994).

2ME2 is considered to be a non-estrogenic metabolite as it binds to estrogen receptors α and β with affinities about 500 fold and 3200 fold lower compared to E2, respectively (LaVallee et al., 2002). Furthermore, 2ME2 does not induce uterine growth in rodents (Martucci & Fishman, 1979).

2ME2 has been described to inhibit proliferation, angiogenesis, as well as the growth of different tumors (Ireson et al., 2004). Further, 2ME2 is more potent than E2 in inhibiting tumor cell proliferation (Seegers et al., 1989). This observation makes 2ME2 more

suitable as a potential drug for treating cancer. It was already tested in phase I and II clinical trials as an anti-cancer treatment (Bruce et al., 2012; Tevaarwerk et al., 2009).

More recently, 2ME2 was found to inhibit proliferation of many other cell types like lymphocytes, endothelial cells and microglia (Duncan et al., 2012; Fotsis et al., 1994; Lippert et al., 2000; Schaufelberger et al., 2016). Furthermore, 2ME2 suppresses autoimmune diseases, which was shown in EAE as well as in animal models of rheumatoid arthritis and uveitis, by downregulating activation and proliferation of T lymphocytes as well as causing an arrest in the G2/M phase of the cell cycle (Attalla et al., 1996; Duncan et al., 2012; Josefsson & Tarkowski, 1997; Stubelius et al., 2011, 2014; Xu et al., 2016). The latter effect was also evoked by 100 µg/ml E2 (370 µM) or Prog (320 µM; Jenkins et al., 2001). However, the underlying mechanism is still unresolved. One controversial hypothesis discussed claims that 30 µM 2ME2 causes cell cycle arrest by interfering with tubulin by binding to the colchicine binding site (D'Amato et al., 1994). In contrast to this, Attalla and colleagues showed that even 1 µM 2ME2 arrests cells in G2/M phase of cell cycle without disruption of tubulin (Attalla et al., 1996).

Duncan and colleagues have shown that NFAT translocation is largely decreased by 50 µM 2ME2 in T lymphocytes *in vitro* while the translocation of nuclear factor 'kappa-light-chain-enhancer' of activated B cells (NF-κB) was unaffected (Duncan et al., 2012). As NFAT, in contrast to NF-κB translocation, strongly depends on an increased $[Ca^{2+}]_i$ (see section 1.2.1 "Activation of T lymphocytes"), it is conceivable that 2ME2 may also interfere with Ca^{2+} signalling. Although STIM and Orai are quite abundantly expressed in the human body, patients with impaired Ca^{2+} currents mediated by these two proteins mainly show deficits in T lymphocyte activation as well as symptoms of myopathy, deficits in muscles and ectodermally derived tissues (reviewed in Hogan et al., 2010). As mainly the T lymphocytes are affected, compounds targeting the STIM / Orai mediated Ca^{2+} entry are especially attractive for treating autoimmune diseases.

Furthermore, 2ME2 is in principle suitable as a drug for treating autoimmune diseases like MS as it is non-estrogenic. Unfortunately, 2ME2 possesses only a very low oral bioavailability of about 1 % (Ireson et al., 2004). As a potential drug in cancer treatment, an improved 2ME2 derivative was synthesized which showed a bioavailability of about 85 % (Ireson et al., 2004). This compound is called 3,17-bis-sulfamoyloxy-2-methoxyestradiol (STX140).

2. Study aims

2ME2 is an endogenous E2 metabolite which diminishes the proliferation of T lymphocytes most likely by decreasing the nuclear translocation of NFAT but not NF-κB. Translocation of NFAT is in contrast to translocation of NF-κB highly dependent in an increase in cytosolic Ca^{2+} concentration. Therefore, the first central aim of this study is to investigate 2ME2's impact on Ca^{2+} signalling in T lymphocytes. In addition it will be checked whether interference with Ca^{2+} signalling is unique to 2ME2 or whether endogenous steroid hormones are also able to inhibit Ca^{2+} signalling in T lymphocytes.

2ME2 interferes not only with T lymphocyte activation and proliferation but also inhibits tumor growth. Therefore, numerous derivatives, some of them with largely improved potency in downregulating tumor cells, were developed during the last years. Although different targets might be affected, some of these derivatives might also show improved potency in T lymphocytes. This can reveal information about the importance of functional groups. In addition, the higher potency of these compounds would decrease the amount required compared to 2ME2 to exhibit the same action and might putatively diminish off-target effects.

After investigating the impact of 2ME2 and its derivatives on Ca^{2+} signalling pathways, the specific target will be identified. Regulation of $[Ca^{2+}]_i$ involves many different ion channels and pumps which might be affected by 2ME2 and its derivatives. These targets include Ca^{2+} release mediated by IP_3R and RyR, Ca^{2+} entry mediated by STIM and Orai channels, Ca^{2+} clearance mediated by PMCAs, MCUs and SERCAs as well as Ca^{2+} entry maintenance by K^+ channels.

3. Materials and methods

3.1 Materials

Aspartic acid, **$CaCl_2$** (* 2 H_2O), **(D)-glucose** (* H_2O), **KCl**, **$MgCl_2$** (* 6 H_2O), **$MgSO_4$** (* 7 H_2O), **NaH_2PO_4** (* H_2O) and **nitric acid** were purchased from Merck (Darmstadt, D).

Fura2-AM and **TG** were purchased from Calbiochem (Merck, EMD Millipore Corp., Billerica, MA USA).

AgCl, **(L)-Asparagine**, **BAPTA**, **BSA**, **CH_3SO_3Na**, **DMSO**, **E2**, **E3**, **EGTA**, **NaCl**, **NCS**, high-molecular **poly-L-lysine (PLL)** solution (100 µg/ml, 150 000 – 300 000 g/mol), **PLL hydrobromide** (70 000 – 150 000 g/mol), **Prog**, **Tes**, **Triton X-100** and **Tris** were purchased from Sigma-Aldrich Co. (St. Louis, MO USA) or Sigma-Aldrich Chemie GmbH (Steinheim, D).

Ethanol was purchased from Th. Geyer GmbH & Co. KG (Renningen, D).

HEPES was purchased from Carl Roth (Karlsruhe, D).

DMEM, **MEM non-essential amino acids**, **2-mercaptoethanol** (50 mM), **PenStrep**, **RPMI 1640 + GlutaMAX™-I + 25 mM HEPES + phenol red**, **RPMI 1640 + GlutaMAX™-I + 25 mM HEPES** and **sodium pyruvate** (100 mM) were purchased from Gibco (Life Technologies Corporation, Grand Island, NY USA).

FBS was purchased from Biochrom (Berlin, D).

NaOH was purchased from J.T. Baker (Deventer, NL).

ShK-Dap22 and **UCL1684** were purchased from Tocris Bioscience (Bristol, UK).

Synta66 was purchased from aobious Inc. (Gloucester, MA USA).

3.2 Solutions

Unless noted otherwise, all buffers were sterile filtered with a 0.2 µm filter (volumina ≥ 250 ml: Express PLUS, GP Millipore, Darmstadt, D. or Filtropur V50, Sarstedt Inc., Newton, NC USA; volumina ≤ 50 ml: Puradisc 25 AS, Whatman, GE Healthcare, Little

Chalfont, UK). Prepared buffers and stock solutions were stored at +4 °C up to several months. Unless otherwise noted, all experiments were performed at RT.

3.2.1 Cell culture Jurkat JMP T lymphocytes

JMP Medium: RPMI medium 1640 + GlutaMAX^{TM}-I supplemented with 25 mM HEPES and phenol red, additionally supplemented with 1 % (v/v) PenStrep (final concentration: 100 U/ml) and 7.5 % (v/v) NCS.

Transfection medium: RPMI medium 1640 + GlutaMAX™-I + 25 mM HEPES, supplemented with 7.5 % (v/v) NCS.

3.2.2 Cell culture T_{MBP} lymphocytes

T cell medium (TCM): 96 % (v/v) DMEM + GutaMAX^{TM}-I supplemented with 4.5 g/l D-glucose, without pyruvate, 1 % (v/v) MEM non-essential amino acids, 1 % (v/v) sodium pyruvate (final concentration: 1 mM), 1 % (v/v) PenStrep (final concentration: 100 U/ml), 1 % (v/v) L-asparagine (final concentration: 1 mM), 0.1 % (v/v) 2-mercaptoethanol (final concentration: 50 µM)

Restimulation medium (RM): 99 % (v/v) TCM, 1 % (v/v) rat (*Rattus norvegicus*) serum (kindly provided by Prof. Alexander Flügel, Department of neuroimmunology, University medical center, Göttingen, D)

T cell growth medium (TCGF): 85 % (v/v) TCM, 5 % (v/v) ConA supernatant (kindly provided by Prof. Alexander Flügel, Department of Neuroimmunology, University Medical Center, Göttingen, D.), 10 % (v/v) HS

Freezing medium: 40 % (v/v) TCM, 50 % (v/v) HS, 10 % (v/v) DMSO

3.2.3 Stock solutions

$CaCl_2$: 0.5 M in high-purity water; 1 ml aliquots for Ca^{2+} measurements were stored at -20 °C for several months; up to 15 ml aliquots for preparing electrophysiological buffers were sterile filtered and stored at +4 °C.

Fura2-AM: 1 mM in DMSO; 4.3 µl aliquots were stored at -20 °C for several months

Fluo4-AM: 1 mM in DMSO; 5.2 µl aliquots were stored at -20 °C for several months

ShK-Dap22: 1 mg/ml = 249 µM in high-purity water (MW: 4012.7 g/mol); 1 µl = 249 pmol aliquots were lyophilized for 15 min and stored at -20 °C for several months

Steroidal compounds and derivatives: 50 mM in DMSO; 20 µl aliquots stored at -20 °C for up to six months

Synta66: 10 mM in DMSO; 1 µl aliquots stored at -20 °C for several months

Thapsigargin: 1.67 mM in DMSO; 20 µl aliquots stored at -20 °C for several months

Tris-EGTA: 4 M Tris and 300 mM EGTA in high-purity water; 1 ml aliquots were stored at -20 °C for several months

Triton X-100: 10 % (w/v) in high-purity water; 1 ml aliquots were stored at -20 °C for several months

UCL1684: 2.5 mM in 50 % (v/v) DMSO and 50 % (v/v) high-purity water; 100 µl = 250 nmol aliquots were lyophilized for 45 min and stored at -20 °C for several months

3.2.4 2ME2 and its derivatives

Table 1: Paper describing compound synthesis.

Numbers in brackets indicate compounds' names in corresponding papers.

2ME2	Leese et al., 2005 (2)	STX1177	Jourdan et al., 2010 (47)
STX49	Leese et al., 2006 (20)	STX1306	Jourdan et al., 2011 (60)
STX68	Leese et al., 2005 (4)	STX1307	Jourdan et al., 2011 (61)
STX139	Bubert et al., 2007 (2)	STX2009	Bubert et al., 2007 (8)
STX140	Leese et al., 2006 (21)	STX2015	Bubert et al., 2007 (27)
STX243	Leese et al., 2006 (23)	STX2484	Leese et al., 2010 (6b)
STX505	Leese et al., 2008 (7)	STX2557	Dohle et al., 2014b (6b)
STX564	Leese et al., 2008 (8)	STX3119	Dohle et al., 2014b (6q)
STX640	Leese et al., 2008 (14)	STX3209	Dohle et al., 2014b (6r)
STX641	Leese et al., 2008 (15)	STX3327	Dohle et al., 2014b (6k)
STX738	Leese et al., 2006 (32)	STX3407	Dohle et al., 2014b (6f)
STX1175	Jourdan et al., 2010 (46)	STX3451	Dohle et al., 2014a (12f)

2ME2 as well as its derivatives were synthesized and kindly provided by Prof. Barry V. L. Potter and his colleague Dr. Wolfgang Dohle from the Department of Pharmacology at University of Oxford, GB. The synthesis of these compounds is described in detail in the papers named in Table 1. One paper describing the synthesis of STX3967, STX3969 and STX3971 is in preparation. The synthesis of STX2917 was not published (C Bubert & BVL Potter, unpublished data). The compounds' structure is shown in Table 2 as well as in Figure 4C, Figure 5D, Figure 6C, Figure 8A, Figure 9C, Figure 10C, Figure 11C, Figure 12C, and Figure 13C.

3.2.5 Ca^{2+} measurements

Ca^{2+} measurement buffer: 140 mM NaCl, 5 mM KCl, 1 mM $CaCl_2$, 1 mM $MgSO_4$, 1 mM NaH_2PO_4, 20 mM HEPES, 5.5 mM glucose; pH 7.4 adjusted with 7 M / 1 M NaOH

Nominal Ca^{2+} free measurement buffer: 140 mM NaCl, 5 mM KCl, 1 mM $MgSO_4$, 1 mM NaH_2PO_4, 20 mM HEPES, 5.5 mM glucose; pH 7.4 adjusted with 7 M / 1 M NaOH

3.2.6 Electrophysiology

Buffers used in electrophysiological experiments were prepared from the following stock solutions: 1 M NaCl, 1 M HEPES, 0.5 M glucose, 0.5 M $MgCl_2$, 0.5 M $CaCl_2$ and 0.5 M $MgSO_4$. Other compounds were added salts and freshly dissolved.

Extracellular buffer for measuring K_V channels (ECB K_V): 128 mM CH_3SO_3Na, 4 mM NaCl, 2 mM $CaCl_2$, 1 mM $MgCl_2$, 10 mM HEPES, 10 mM glucose; pH 7.4 adjusted with 7 M / 1 M NaOH (modified from Thakur & Fomina, 2010)

Intracellular buffer for measuring K_V channels (ICB K_V): 125 mM aspartic acid, 5 mM $MgCl_2$, 2 mM $MgSO_4$, 15 mM HEPES, 12 mM BAPTA; pH 7.2 adjusted with 7 M KOH (modified from Thakur & Fomina, 2010)

Extracellular buffer for measuring K_{Ca} channels (ECB K_{Ca}): 119.5 mM NaCl, 40 mM KCl, 2 mM $CaCl_2$, 1 mM $MgCl_2$, 5 mM HEPES, 10 mM glucose; pH 7.4 adjusted with 7 M / 1 M NaOH (Fanger et al., 2001)

Intracellular buffer for measuring K_{Ca} channels (ICB K_{Ca}): 130 mM aspartic acid, 8.55 mM $CaCl_2$, 2.08 mM $MgCl_2$, 10 mM HEPES, 10 mM EGTA; pH 7.2 adjusted with 7 M KOH; $[Ca^{2+}]_i$ = 1 µM, $[Mg^{2+}]_i$ = 2 mM (calculated with MaxChelator, http://maxchelator.stanford.edu/; Fanger et al., 2001)

3.3 Cell culture

3.3.1 Jurkat JMP T lymphocytes

Jurkat JMP T lymphocytes were cultured in JMP medium in T25 (10 ml) or T75 (30 ml) cell culture flasks (Sarstedt, Nümbrecht, D) and were kept in an incubator at 37 °C and 5 % CO_2 (Heraeus Instruments, Heraeus Holding GmbH, Hanau, D; Thermo Fisher Scientific Inc., Waltham, MA USA). Usually, cells were diluted every Monday, Wednesday and Friday by a factor of three. Cell densities were kept between 0.3 and 1.2 * 10^6 cells per ml. If a high cell density was required on Tuesday or Thursday, the cells were diluted 1.5 fold on the previous day.

3.3.2 T_{MBP} lymphocytes

Restimulated primary T lymphocytes specific for MBP (T_{MBP} lymphocytes) were kindly provided by the group of Prof. Alexander Flügel (Department of Neuroimmunology, University Medical Center, Göttingen, D). 10 days before cell isolation, Lewis rats (*Rattus norvegicus*) were immunized with 100 µg MBP in 200 µl complete Freud's adjuvant by injection into the tail base and flanks. After incubation time, popliteal, inguinal and paraaortal lymph nodes were isolated and placed into cold HEPES buffer. Cells were isolated by mincing the lymph nodes through a metal mesh, taken up at a cell density of 4 * 10^6 cells per ml in restimulation medium (RM) supplemented with 20 µg/ml MBP. Subsequently, 2 * 10^5 cells were placed into one well of a 96 well plate. After 2 days, 50 µl TCGF were added and one or two days thereafter, 50 µl of the

supernatant was removed and 100 µl TCGF supplemented with 0.4 mg/ml were added. On day 7, T lymphocytes are restimulated with irradiated thymocytes, including APCs. Therefore, the thymus of a Lewis rat (*Rattus norvegicus*) was removed and was irradiated with 3000 Rad. $1.4 * 10^6$ irradiated thymocytes were added to one well with lymphocytes and 10 µg/ml MBP as well as 0.4 mg/ml G418 were added. On the next day, 50 µl TCGF supplemented with 0.4 mg/ml G418 were added. On the following day, cells were pooled and transferred to 60 mm cell culture dishes. Cells were split on subsequent days if required. Every 7 days after first restimulation, T_{MBP} lymphocytes can be restimulated again. Therefore, $3.5 * 10^6$ lymphocytes and $7 * 10^7$ irradiated thymocytes were placed into a 60 mm cell culture dish supplemented with 10 µg/ml MBP and 0.4 mg/ml G418. On the second day after every restimulation, cells can be splitted by adding TCGF and 0.4 mg/ml G418.

4 to 6 days after the last restimulation, cells can be frozen in liquid nitrogen using freezing medium. 10^7 cells were pelleted at 300 xg for 5 min at RT, resuspended in 1 ml freezing medium. Cells were frozen in a polystyrene box at -80 °C for one night and afterwards transferred to liquid nitrogen.

Only cells at day 5 to 7 after the 2^{nd} to 4^{th} restimulation were used for Ca^{2+} measurements. Therefore, cells were thawed from liquid nitrogen, transferred to 10 ml JMP medium, pelleted at 300 xg for 5 min at RT, resuspended into 10 ml TCM supplemented with 10 % (v/v) HS and kept in a 10 cm cell culture dish in the incubator at 37 °C and 5 % CO_2 overnight.

3.4 Transfection

$12.5 * 10^6$ Jurkat T lymphocytes were pelleted and resuspended in 1 ml transfection medium. 30 µg plasmid DNA and Jurkat T lymphocytes were mixed in an electroporation cuvette (Biozym Scientific GmbH, Hessisch Oldendorf, D) and preincubated at 37 °C for 5 min. Afterwards, the cuvette was placed into an electroporation device and cells were treated with 960 µF and 240 V with a time constant τ of 14.7 s to 16 s (mean: 15.3 s). Subsequently, cells were allowed to chill at 37 °C for 10 min. Afterwards, they were transferred into a T-25 cell culture flask (Sarstedt, Nümbrecht, D) containing 10 ml JMP medium. The electroporation was

always performed in the afternoon. Transfected cells were used the next morning to early afternoon for live cell imaging experiments.

The vector for transfecting G-GECO1.2-Orai1 into Jurkat T lymphocytes (Figure 2) was purchased from Addgene (Cambridge, MA USA) and was first described by (Dynes et al., 2016). Cells transfected with this vector expressed Orai1 channels covalently bound to G-GECO on the intracellular site. GECO is a genetically encoded Ca^{2+} sensor for optical measurements. Ca^{2+} selectivity is performed by a CaM binding site and the protein is fluorescent by an eGFP. In general, GECO is designed to increase in fluorescence upon Ca^{2+} binding.

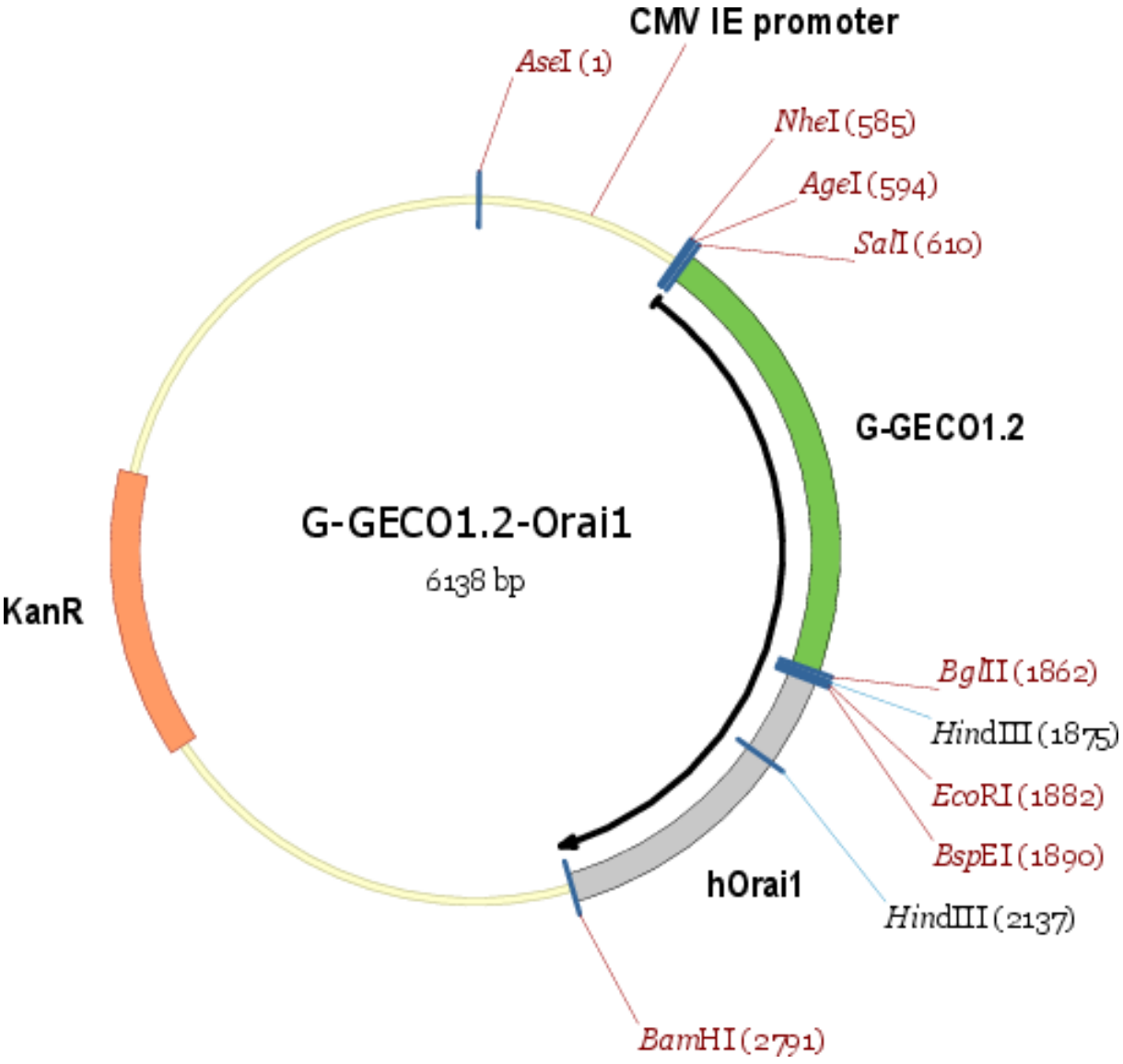

Figure 2: Vector map of G-GECO1.2-Orai1.

3.5 Ca^{2+} measurements using spectrofluorometry

For measuring $[Ca^{2+}]_i$, 2 * 10^7 Jurkat T lymphocytes or 5 to 10 * 10^6 T_{MBP} lymphocytes (mean: 7.7 * 10^6 T_{MBP} lymphocytes) were collected and pelleted at 450 xg for 5 min (JMP) or 300 xg for 8 min (T_{MBP}), respectively. Cells were taken up in 1 ml fresh medium and preincubated at 37 °C for 5 min. Then, 4 µl (4 µM) Fura2-AM was added and cells were incubated at 37 °C for 30 min. After addition of Fura2-AM, cells were kept in the dark. 15 min after initial addition of Fura2-AM, cells were diluted with 4 ml medium. After Fura2-AM incubation, cells were washed with 5 ml Ca^{2+} measurement buffer and finally taken up to a density of 2 * 10^6 cells per ml. Cells were allowed to chill for 20 min at RT prior to the first measurement to ensure complete hydrolysis of Fura2-AM esters.

In experiments using hydrophilic compounds STX2484, STX2557, STX3119, STX3209, STX3327, STX3407, STX3451, STX3967, STX3969 and STX3971, Jurkat T lymphocytes were loaded with Fluo4-AM instead of Fura2-AM. This method was similar to that described before, but the cells were incubated for 50 min at RT with 10 µl (10 µM) Fluo4-AM. 20 min after initial addition of Fluo4-AM, 4 ml medium were added.

In experiments using Ca^{2+} measurement buffer, 10^6 cells were mixed with fresh Ca^{2+} measurement buffer to a final volume of 1 ml. Cells and Ca^{2+} measurement buffer were placed in a quartz glass cuvette (Hellma analytics, Müllheim, D) providing a thickness of 10 mm and a maximal volume of 3.5 ml. In experiments using nominal Ca^{2+} free measurement buffer, 10^6 cells were pelleted, Ca^{2+} measurement buffer was carefully removed and replaced by 1 ml nominal Ca^{2+} free measurement buffer. Thus, at both conditions 10^6 cells were measured in 1 ml buffer.

The quartz glass cuvette was placed into a fluorescence spectrophotometer (model F-2710, Hitachi High-Technologies Corporation, Tokyo, Japan). The measurement was started and measurement conditions were controlled by using FLSolutions for F-2700 (Version 4.1, Hitachi High-Technologies Corporation, Tokyo, Japan). Fura2 was alternatively excited at 340 ± 10 nm and 380 ± 10 nm every 2 s and emission was measured at 495 ± 10 nm. In Mn^{2+} quenching experiments, cells were excited at Fura2's isosbestic point which was experimentally determined to be 357 nm. Upon T lymphocyte stimulation with TG, fluorescence at 357 nm did not change in contrast to

fluorescence at 340 as well as at 380 nm. For measuring cells loaded with Fluo4-AM, the dye was excited at 488 ± 10 nm and emission was measured at 520 ± 10 nm. Before the first addition, cells were kept in the fluorescence spectrophotometer for 3 min to measure basal $[Ca^{2+}]_i$. At the end of each measurement, the fluorescence was calibrated using 0.1 % (w/v) Triton X-100 for cell lysis and obtaining Rmax as cytosolic Fura2 binds to extracellular Ca^{2+} which is efficient for saturating Fura2. After 140 s, 3 mM EGTA and 40 mM Tris were added to chelate extracellular Ca^{2+} and to obtain Rmin as EGTA binds Ca^{2+} with higher affinity than Fura2. Tris is added for pH buffering. Rmin and Rmax and the corresponding highest and lowest light intensities were calculated and determined using the actual ratio values and light intensities in Excel. For calculation of the $[Ca^{2+}]_i$, the following equation described by (Grynkiewicz et al., 1985) was used:

$$[\mathrm{Ca}^{2+}]_\mathrm{i} = \mathrm{Kd} * \frac{\mathrm{R}-\mathrm{Rmin}}{\mathrm{Rmax}-\mathrm{R}} * \frac{\mathrm{F(380)max}}{\mathrm{F(380)min}} \quad (1)$$

$[Ca^{2+}]_i$ is the free cytosolic Ca^{2+} concentration. Kd refers to the dissociation constant which is 224 nM. R is the ratio of fluorescence at an excitation of 340 nm (F340) divided by fluorescence at an excitation of 380 nm (F380). Rmin and Rmax are the minimal and maximal ratio, respectively, which were obtained during calibration. F(380)max and F(380)min are maximal and minimal intensities measured at an excitation of 380 nm, respectively, which were measured during calibration. Measurements using Fluo4 were normalized to fluorescence intensity measured at the first time point (F/F0).

After measurements finished, artefacts due to compound addition were deleted from the tracings. Artefacts lasted about 8 s and were easily identified by an increased light intensity. Fluorescence intensities of deleted data points was interpolated from the fluorescence intensities just before and after the deleted intensities by using FLSolutions.

The excitation wavelength is generated by a Xenon short-arc lamp (Ushio Inc., Tokyo, Japan) and is set to a certain wavelength by a monochromator. The sample's fluorescence is detected in an angle of 90° compared to the excitation path to exclude interference with excitation light.

In these experiments, good care was taken to ensure that the time points of compound addition did not differ more than 2 s between individual experiments. Furthermore,

different compound concentrations were measured by dilution of stock solutions with DMSO. Thus, the same volume and DMSO concentration was added in every measurement. This was done to exclude off-target effects which might arise from different DMSO concentrations. Furthermore, only one DMSO control is efficient for all compound concentrations.

Data analysis was performed with Microsoft Excel 2013 (Microsoft Corporation, Redmond, WA USA) and Prism (Version 6.07, GraphPad Prism Software Inc, San Diego, CA USA). Unless noted otherwise, mean values ± SD are depicted in the graphs.

For concentration response curves (CRC), compound concentrations were log transformed and normalized by using GraphPad Prism. For log transformation, DMSO's compound concentration was set to be 100 times smaller than the smallest compound concentration measured. For normalization of dPlateau values, daily DMSO controls were set to 100 %. As it turned out, the smallest dPlateau values were measured by treating cells with 50 µM STX49. Thus, the mean dPlateau values of this condition was set to 0 % for all conditions.

Log transformed and normalized data were fitted by a nonlinear curve which resembles the inhibition of a dose-response curve in which the inhibitor's concentration is log transformed and the response is normalized ranging from 0 to 100. Furthermore, curves were fitted with variable slopes. For STX139 and STX243 only concentrations up to 50 and 20 µM were fitted to the nonlinear curve as the plateau values increased upon higher concentrations, respectively.

3.5.1 Data analysis: Kinetics of inhibition

In experiments in which cells were stimulated by thapsigargin in Ca^{2+} measurement buffer (see Figure 15), mean basal $[Ca^{2+}]_i$ concentrations were calculated between 75 s and 25 s before thapsigargin addition. It turned out that peak $[Ca^{2+}]_i$ after thapsigargin addition differed in every measurement. To circumvent this variety, the ratio between dPlateau values of stimulation (mean value between 75 s and 25 s before compound addition = mean value between 755 s and 805 s after stimulation)

and the minimal value after compound addition was calculated. This ratio provides a quantitative readout for $[Ca^{2+}]_i$ reduction after compound addition.

Compound concentrations were log transformed and ratios were normalized. For log transformation of compound concentration, DMSO concentration was set to be 100 times smaller than the smallest compound concentration measured. In these experiments, the smallest ratios were measured at 25 µM STX640, so these values were set to 0 % for all measurements. Daily DMSO controls of every condition was set to 100 %. These data were fitted to a nonlinear curve which resembles the inhibition of a dose-response curve in which the inhibitor's concentration is log transformed and the response is normalized ranging from 0 to 100. Furthermore, curves were fitted with variable slopes.

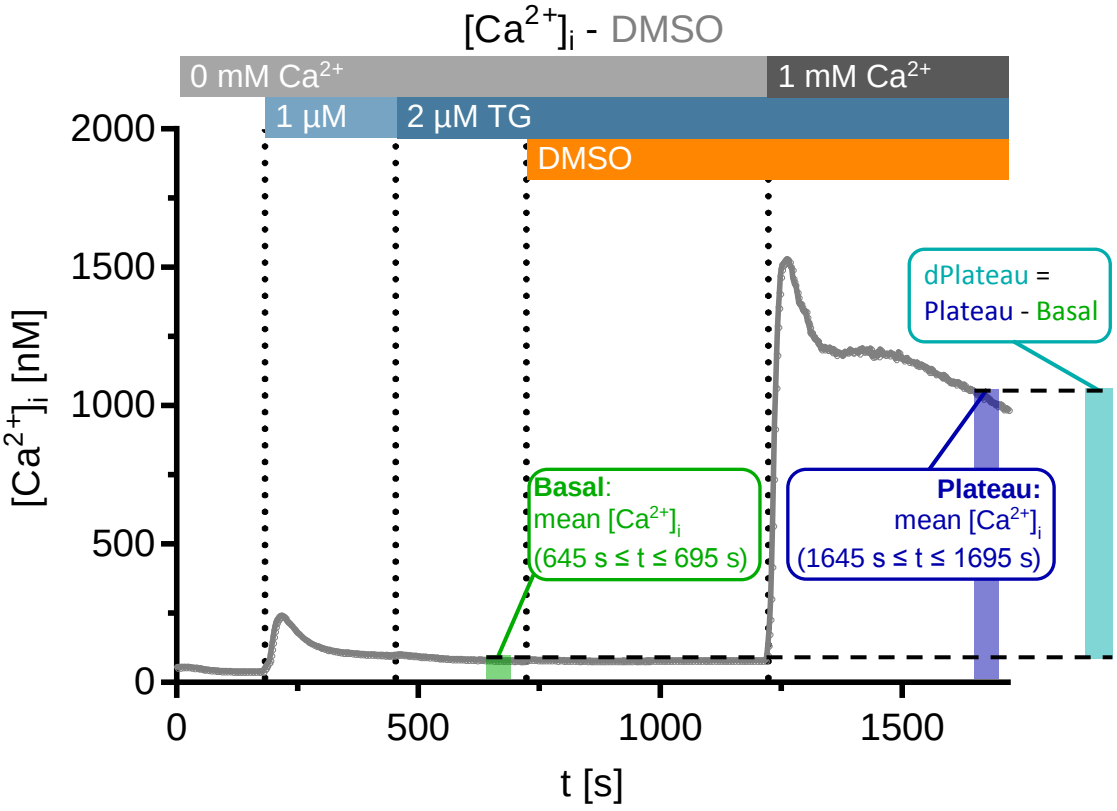

Figure 3: Calculation of dPlateau for quantitative analysis of concentration-response curves.

Mean Ca^{2+} measurement for DMSO (n = 15). dPlateau is calculated as the difference between plateau values and basal values. Plateau values are calculated as mean $[Ca^{2+}]_i$ between1645 and 1695 s which is 425 and 495 s after Ca^{2+} re-addition. Basal values are calculated as mean $[Ca^{2+}]_i$ between 645 and 695 s which is 25 and 75 s before compound addition. The compound in this measurement is DMSO.

3.5.2 Data analysis: Mn^{2+} quenching

For a quantitative analysis of Mn^{2+} quenching, initial slopes of fluorescence decrease after Mn^{2+} addition was determined using GraphPad Prism. Therefore, data after Mn^{2+} addition were fitted to an exponential one phase decay equation:

$$y = (y_0 - Plateau) * e^{(-K * X)} + Plateau \quad (2)$$

y_0 resembles the fluorescence at the start of the decay, Plateau is the theoretically fluorescence at the end of the decay at infinite times, K is the rate constant, and X is the time. The first derivative of this equation was used to calculate the slope at 1230 s:

$$y = (y_0 - Plateau) * (-K) * e^{(-K * X)} \quad (3)$$

The fluorescence gradually decreased before Mn^{2+} addition due to bleaching in every measurement. The fluorescence before Mn^{2+} addition was fitted to a straight line using the following equation:

$$y' = m * x + c \quad (4)$$

m is the slope, x is the time and c is the y-axis intercept. The slope of this linear fit was subtracted from the initial slope of the exponential decay to avoid overestimation of the initial slope. So, the initial slope (s_i) after Mn^{2+} addition was calculated using the following equation:

$$s_i = (y_0 - Plateau) * (-K) * e^{(-K * X)} - m \quad (5)$$

3.6 Live cell imaging

$5 * 10^4$ transfected Jurkat T lymphocytes were pelleted at 500 xg for 5 min at RT and were taken up in 50 µl nominal Ca^{2+} free buffer. Subsequently, cells were placed within a rubber O-ring fixed on slides via Korasilon silicon paste of medium viscosity (Kurt Obermeier GmbH & Co. KG, Bad Berleburg, D). Slides were coated before cell addition with 5 µl of 5 mg/ml bovine serum albumin (BSA) solution and 5 µl of 0.1 mg/ml PLL solution (70 000 – 150 000 g/mol). Cells were allowed to settle down for 5 min on one slide. Then, 50 µl nominal Ca^{2+} free buffer were added and the slide was placed and fixed by tape on the stage of an inverted Leica microscope (type DM IRBE, Leica

microsystems, Wetzlar, D). Successfully transfected and not pre-activated cells were identified by a ring-shaped fluorescence of low intensity in the rim of cells, considered as G-GECO1.2-Orai1 within the plasma membrane. These cells commonly showed an additional fluorescence within the cytosol considered as G-GECO1.2-Orai1 within the Golgi-apparatus on the way from translation to the plasma membrane.

The light of Xe short arc lamp was filtered by a 472/30 BrightLine HC filter (AHF Analysentechnik, Tübingen, D) and the excitation wavelength of 488 nm was directed to the sample via a beam splitter T 495 LPXR filter (AHF Analysentechnik, Tübingen, D) which separated the excitation wavelength from the emission light which was filtered by a 520/35 BrightLine HC filter and measured at 520 nm. Cells were illuminated every 2 s with an exposure time of 50 ms. The fluorescence was measured with a sensitivity of 160 using a Hamamatsu camera (model C9100-13, Hamamatsu Photonics K.K., Hamamatsu, Japan). Measurements were controlled and data were stored by Volocity (version 6.3, Perkin Elmar, Walthem, MA USA).

3.6.1 Data analysis: Live cell imaging

Cells were analysed using Fiji (ImageJ Version 1.51k). For analysis, a ring-shaped ROI was placed around each fluorescent cell which increased in fluorescence upon ionomycin treatment. For background correction, 2 to 4 round ROIs were placed in an area with no cells and mean fluorescence was measured in this area. The mean fluorescence of all background ROIs were calculated for every time point and the mean fluorescence of each cell was subtracted by this mean background fluorescence. To compensate for different amounts of fluorescent proteins in the plasma membrane, the fluorescence of each time point was divided by the fluorescence of the first time point (F/F0).

For quantitative analysis, basal fluorescence was subtracted from peak and plateau values for obtaining dPeak and dPlateau. Basal fluorescence was calculated as the mean F/F0 ratio between 75 s and 25 s before compound addition. The peak value is the maximal value which was reached within 100 s after Ca^{2+} addition. The plateau value is the mean relative fluorescence between 445 s and 495 s after Ca^{2+} addition.

3.7 Electrophysiology

35 mm cell culture dishes (Greiner bio-one, Kremsmünster, AT) were coated with 2 µg/ml high-molecular poly-L-lysine solution (150 000 – 300 000 g/mol) for at least 30 min. Afterwards, dishes were washed with high-purity water twice. After removing the solution, the dishes were dried for about an hour and subsequently stored at +4 °C for up to 7 days. Usually the dishes were used the day after preparation.

A RC-37W or RC-37F recording chamber (Warner Instruments, Hamden, CT USA) was placed into the dish to decrease the chamber volume. The bottom of the recording chamber was covered with silicone (Korasilon, Kurt Obermeier GmbH & Co. KG, Bad Berleburg, D) and attached to the cell culture dish immediately before placing cells in the cell culture dish. About $1.5 * 10^5$ cells were placed in the cell culture dish and were allowed to settle for 5 min. Cells were washed with ECB K_V or ECB K_{Ca} twice before covering the cells in the according ECB containing 200 nM TG and 0.2 % (v/v) DMSO and, in dependence of the experiment, STX-compounds or K^+ channel inhibitors. Dishes were mounted on a costumer build holder and placed on an inverted Zeiss AxioVert 100 microscope (Carl Zeiss Microscopy GmbH, Jena, D).

Up to one hour before the experiment, micropipettes were pulled and fire polished (Flaming/Brown micropipette puller P-97, Sutter instruments Co, Novato, CA USA) resulting in pipette resistances ranging from 2.7 to 5.1 MΩ (mean: 3.9 MΩ). Micropipettes was filled with 4 µl ICB covering 2 – 3 mm of the intracellular electrode. The intracellular electrode consisted of an Ag/AgCl wire which was gently sanded and covered with melted AgCl every day prior to the first experiment. The extracellular electrode was made of an Ag/AgCl barrel which was sanded every day before the first experiment and was exchanged if the offset potential differed for more than 10 mV from zero.

The intracellular electrode was connected to a HEKA EPC-10 amplifier (HEKA Elektronik Dr. Schulze GmbH, Lambrecht, D) and the currents were recorded using Patch Master (HEKA Elektronik Dr. Schulze GmbH, Lambrecht, D).

First, a medium sized cell with a relatively smooth surface was selected which was firmly attached to the bottom of the cell culture dish. Subsequently, a micropipette was filled with ICB and was attached to the pipette holder in the way that the intracellular electrode was covered for 2 – 3 mm by the ICB. The pipette holder was connected via tubing and a

three-way valve to a 5 ml syringe. Using this syringe, a positive pressure was applied by pushing the plunger for 1 ml before dipping of the micropipette tip into the ECB. For measuring K_{Ca} channels, the liquid junction potential was set to -13 mV (Fanger et al., 2001). Then, the micropipette was navigated in close proximity of the cell using a micromanipulator device (PatchMan NP2, Eppendorf AG, Hamburg, D). The tip was carefully narrowed to the cell surface until it showed a small indentation due to liquid jet emitting from the pipette tip. At this point, the three-way valve was opened to release pressure. In some cases, this release was efficient to form a tight connection between cell membrane and micropipette, a so-called gigaseal. This was observed as the resistance increased to a low gigaohm range. Cell membranes which did not seal immediately after removal of pressure, were carefully pulled to the micropipette by application of mild suction using the syringe plunger. After gigaseal formation, capacitative currents (c-fast) were compensated using Patch Master. By applying short pulses of strong suction, the cell membrane was ruptured and subsequently, capacitative currents (c-slow) were compensated. Within a few seconds, the holding potential was set to -60 mV and the voltage protocol was started. Before every sweep, c-slow and series resistance Rseries were automatically compensated by the protocol and corresponding values were recorded. Currents were recorded at a sampling rate of 20 kHz and were low-passed filtered at 1 kHz.

3.7.1 Recording and data analysis of K_V channels

For recording K_V channels, a step protocol was applied consisting of a voltage pulse of defined duration and amplitude. Every sweep started with application of the holding potential of -60 mV for 50 ms. Afterwards the stimulation voltage was applied for 100 ms which was +80 mV during the first sweep and was decreased by 10 mV after every sweep. The stimulation voltage of the last sweep was -80 mV. After the stimulation voltage, the holding potential of -60 mV was applied for another 50 ms. Between two sweeps, an intersweep interval was set to 30 s during which the holding potential of -60 mV was applied.

As a qualitative readout of the quality of the seal and recording, different parameters were carefully checked. Only cells were analysed which exhibited a leak current smaller than -30 pA. The leak current was calculated as the mean current between 40 ms and 10 ms before the start of the stimulation voltage. Furthermore, the Rseries

was calculated as a ratio between Rseries and micropipette resistance (Rpip) and had to be below a value of 4.2 (mean: 2.1).

For a quantitative readout, mean currents were calculated between 80 and 90 ms after beginning of the stimulation voltage. Furthermore, these currents were normalized to cell capacity.

3.7.2 Recording and data analysis of K_{Ca} channels

For recording K_{Ca} channels, a ramp protocol was used. This protocol started with the holding potential of -60 mV for 300 ms. Afterwards, the voltage was set to -120 mV for 50 ms. Then the voltage continuously changed during a ramp from -120 mV to +100 mV within 200 ms. Subsequently, the voltage was remained at +100 mV for another 50 ms before the potential was set to the holding potential for 300 ms again. Before every ramp, a voltage of +80 mV was applied for 500 ms to inactivate K_V channels. Between two sweeps, the holding potential of -60 mV was applied for 10 s.

Only data of measurements were analysed in which leak currents at the beginning of a sweep did not exceed -120 pA. Another criterion for data analysis was the relative Rseries which was below 5.25 (mean: 3.0).

3.8 Statistical analysis

Statistical analysis was performed with Prism (Version 6.07, GraphPad Prism Software Inc, San Diego, CA USA). Data sets were tested for normal distribution by Kolmogorov-Smirnov test with Dallal-Wilkinson-Lilliefor P value. If data sets did not significantly differ from normal distribution ($p > 0.05$) and if more than two groups were investigated, data were investigated for statistically significant differences by using a normal or a repeated measures ANOVA (analysis of variance) corrected for multiple testing with a Bonferroni correction. If the data were not normally distributed, a non-parametric Kruskal-Wallis test was performed with Dunn's correction for multiple testing. The latter was also performed if the number of experiments was too small to be checked for normality by Kolmogorov-Smirnov test.

4. Results

Different endogenous steroids as well as the E2 metabolite 2ME2 interfere with T lymphocyte activation (Correale et al., 1998; Duncan et al., 2012; Engler et al., 2017; Marzi et al., 1996; Stubelius et al., 2011; Wegmann et al., 1993). As Ca^{2+} signalling pathways are a crucial part of T lymphocyte activation (see section 1.2.1 “Activation of T lymphocytes”), I investigated the effects of different compounds by analysing Jurkat T lymphocytes and restimulated rat T_{MBP} lymphocytes. Results section is mainly separated into two parts.

In the first part, I investigated the impact of 2ME2 on Ca^{2+} signalling pathways. Further, I analysed if endogenous steroid hormones also interfere with Ca^{2+} signalling as endogenous steroid hormones are structurally similar to 2ME2. Additionally, I used 2ME2 derivatives to identify a compound more potent than 2ME2 as discussed in section 2 “Study aims”. In the second part, I investigated the target which is affected by these compounds.

4.1 Impact of steroids, 2ME2 and its derivatives on $[Ca^{2+}]_i$ increase

For investigating the impact of compounds on the Ca^{2+} signalling pathways, I stimulated Fura2- or Fluo4-loaded Jurkat T lymphocytes or T_{MBP} lymphocytes with thapsigargin and acutely treated the cells with the compounds in a Ca^{2+} free / Ca^{2+} re-addition protocol.

4.1.1 2ME2 inhibits Ca^{2+} entry in T lymphocytes after ER depletion

2ME2 inhibits the highly Ca^{2+} dependent NFAT translocation in T lymphocytes (Duncan et al., 2012) which suggests that 2ME2 might directly interfere with Ca^{2+} signalling pathways. Therefore, 2ME2 was investigated for its impact on influencing $[Ca^{2+}]_i$ after stimulation of the CRAC system by ER depletion via thapsigargin. After Ca^{2+}-depletion of the ER via TG in nominal Ca^{2+} free buffer, 2ME2 and 500 s later 1 mM Ca^{2+} were added to the cells and the fluorescence was monitored. As it is shown in Figure 4, 2ME2 inhibited the increase in $[Ca^{2+}]_i$ after Ca^{2+} re-addition in a concentration

dependent manner with half-maximal inhibition at 20 µM and an almost complete inhibition at 100 µM. Thus, 2ME2 interferes with Ca^{2+} signalling pathways by decreasing $[Ca^{2+}]_i$ after T lymphocyte stimulation.

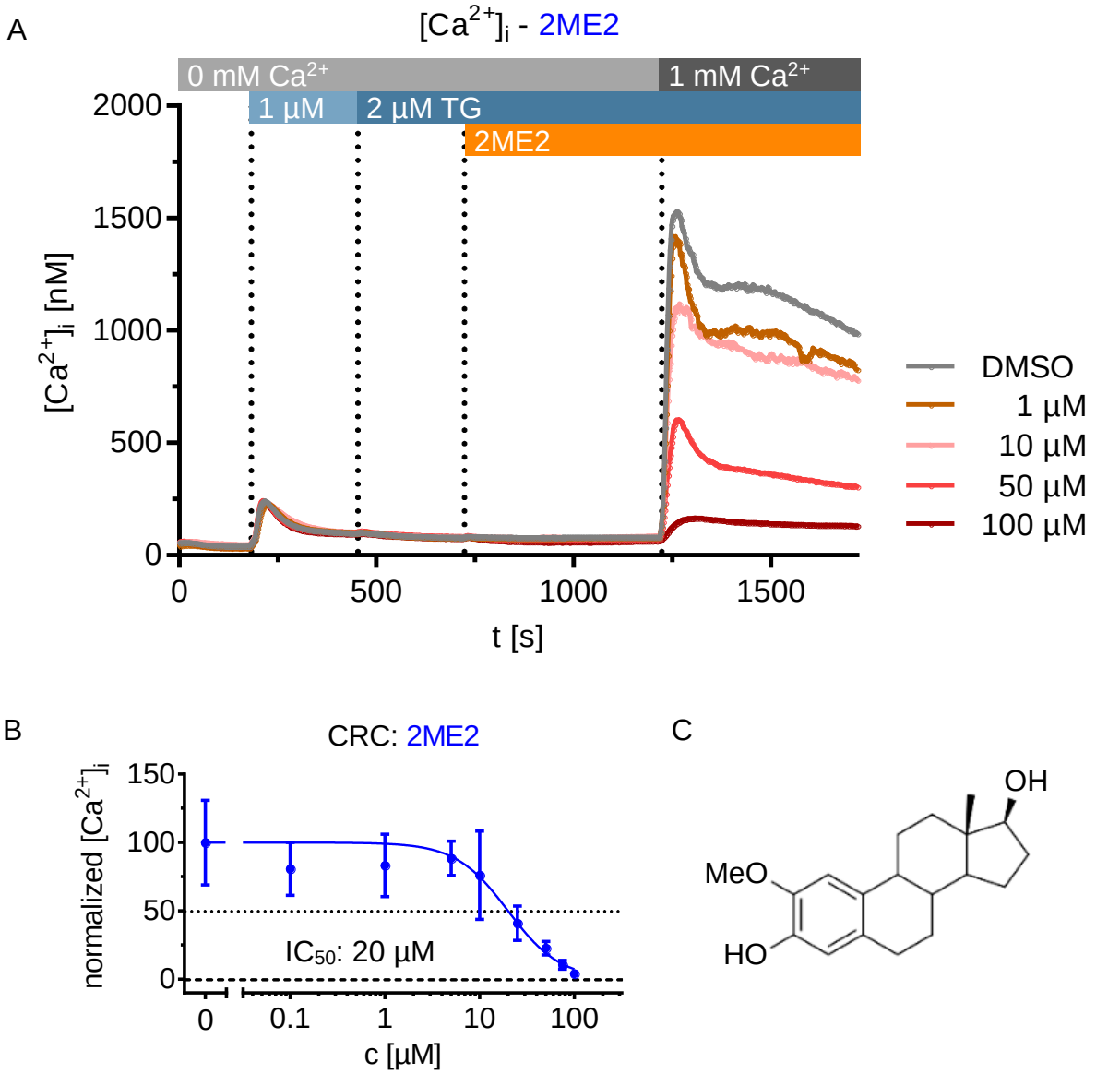

Figure 4: Impact of 2ME2 on $[Ca^{2+}]_i$.

2ME2 inhibits Ca^{2+} entry in Jurkat T lymphocytes. Fura2 loaded T lymphocytes were analysed by a Ca^{2+} free / Ca^{2+} re-addition protocol. A: Ca^{2+} tracing of T lymphocytes treated with 2ME2. Data represent mean values of 15 (DMSO), 4 (1 µM), 6 (10 µM), 7 (50 µM) and 12 (100 µM) measurements. B: Concentration-response curve (CRC) of 2ME2 calculated from A. For each measurement, dPlateau values were calculated as it is described in Figure 3. These values were normalized for 0.2 % (v/v) DMSO (100 %) and 50 µM STX49 (0 %; see Figure 6). Concentrations were log-transformed and dPlateau values were fitted via nonlinear regressions with variable slopes using least square fits. Data represent the mean ± SD of 4 (0.1, 1 µM), 6 (10 µM), 7 (5, 50 µM), 8 (25 µM), 12 (100 µM), 13 (75 µM) and 15 (DMSO) measurements. C: Chemical structure of 2ME2.

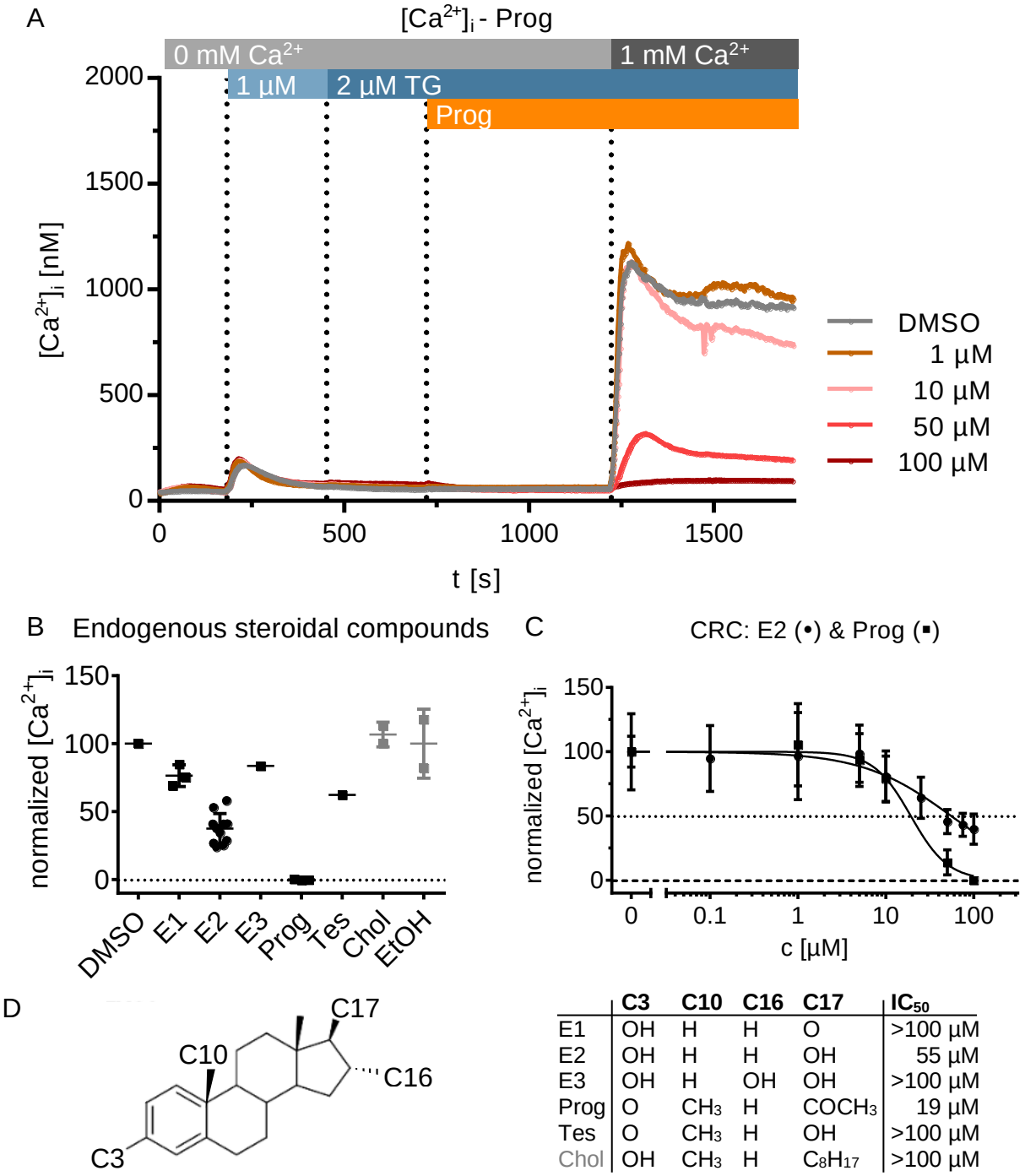

	C3	C10	C16	C17	IC_{50}
E1	OH	H	H	O	>100 µM
E2	OH	H	H	OH	55 µM
E3	OH	H	OH	OH	>100 µM
Prog	O	CH_3	H	$COCH_3$	19 µM
Tes	O	CH_3	H	OH	>100 µM
Chol	OH	CH_3	H	C_8H_{17}	>100 µM

Figure 5: Impact of endogenous steroidal compounds on $[Ca^{2+}]_i$.

A: Progesterone (Prog) was investigated for its impact on $[Ca^{2+}]_i$ increase. The tracing shows an almost complete inhibition of Ca^{2+} entry at 100 µM. Depicted are mean values of 3 measurements each. B: 100 µM estrone (E1; n = 3), estradiol (E2; n = 11), estriol (E3; n = 1), Prog (n = 3), testosterone (Tes; n = 1) and cholesterol (Chol; n = 2) were screened for their impact to inhibit $[Ca^{2+}]_i$ increase after ER depletion upon Ca^{2+} re-addition. The black squares resemble compounds which were measured with DMSO (n = 1) and the grey squares depict compounds which were dissolved in ethanol (EtOH; n = 2). Data points represent individual measurements. Lines resemble mean and SD. C: Concentration-response curves (CRC) for E2 & Prog. IC_{50} values are about 55 µM for E2 and 19 µM for Prog. Mean values ± SD are shown for 3 measurements for each concentration of Prog and 12 (DMSO), 7 (0.1 µM), 9 (1 µM), 3 (5 µM), 6 (10 µM), 4 (25 µM), 9 (75 µM) and 11 (100 µM) measurement for E2 concentrations. D: Chemical structures and IC_{50} of E1, E2, E3, Prog, Tes and Chol.

4.1.2 The impact of endogenous steroidal compounds on Ca^{2+} entry in Jurkat T lymphocytes after ER depletion

Next, the impact of endogenous steroid hormones, namely estrone (E1), E2, estriol (E3), progesterone (Prog) and testosterone (Tes) as well as cholesterol (Chol) on Ca^{2+} signalling was investigated. These experiments showed that 100 µM of neither E1, E3, Tes nor Chol inhibited SOCE (Figure 5B). Nonetheless, 100 µM E2 decreased $[Ca^{2+}]_i$ by 60 % compared to control measurements (Figure 5C). A concentration-response analysis revealed that E2 inhibits $[Ca^{2+}]_i$ increase with an IC_{50} of about 56 µM which is about three times higher compared to 2ME2.

The most potent endogenous steroidal compound was Prog. It almost completely inhibited the $[Ca^{2+}]_i$ increase at 100 µM (Figure 5A – C) and showed an IC_{50} of about 19 µM (Figure 5D) which is quite similar to 2ME2.

4.1.3 Synthetic 2ME2 derivatives inhibit Ca^{2+} entry even more potently

As 2ME2 was more potent than E2, differing only in the methoxy group at C2, a 2-methoxy groups seems to be important for inhibiting Ca^{2+} entry. How 2ME2 can be modified to further increase the potency was investigated in the next series of experiments.

3,17-Sulfamoyloxylated derivatives of 2ME2

First, 2ME2 derivatives were investigated which possessed sulfamoyloxy groups at either C3 or C17 or at both positions. These compounds were namely 3-sulfamoyloxy-2-methoxyestradiol (STX68), 17-sulfamoyloxy-2-methoxyestradiol (STX738), 3,17-bis-sulfamoyloxy-2-methoxyestradiol (STX140) and 3,17-bis-sulfamoyloxy-estradiol (STX49). These sulfamoyloxylated derivatives show a higher potency compared to 2ME2 in cancer studies (Ireson et al., 2004; Jourdan et al., 2010, 2011; Leese et al., 2006, 2008).

Surprisingly, STX140 concentration-dependently increased $[Ca^{2+}]_i$ of unstimulated T lymphocytes in nominal Ca^{2+} free buffer (Figure 7A). The increase starts shortly after STX140 addition and rises to 200 nM 80 s after 100 µM STX140 was added. $[Ca^{2+}]_i$

was sustained at this elevated concentration. In contrast to the STX140 mediated Ca^{2+} signal, OKT3 induces a transient increase in $[Ca^{2+}]_i$ which peaks at 240 nM 70 s after addition of OKT3. The maximal $[Ca^{2+}]_i$ in the vehicle control measurements is about 100 nM. However, the Ca^{2+} increase after Ca^{2+} re-addition is much smaller after treating cells with STX140 compared to treatment with OKT3. In these measurements, the $[Ca^{2+}]_i$ increased to a peak of 280 nM while $[Ca^{2+}]_i$ in cells treated with OKT3 rises above 1 µM.

If the ER is depleted before STX140 addition (Figure 7B), $[Ca^{2+}]_i$ increases to a lower extent. The $[Ca^{2+}]_i$ rises to 125 nM upon addition of 100 µM STX140 while $[Ca^{2+}]_i$ in the vehicle control measurement shows a maximal $[Ca^{2+}]_i$ of about 90 nM.

In the Ca^{2+} free / Ca^{2+} re-addition protocol using thapsigargin induced depletion of the ER, STX140 inhibited $[Ca^{2+}]_i$ with a potency comparable to 2ME2 (Figure 4B, Table 2). STX140 has an IC_{50} of about 20 µM and shows an almost complete inhibition of $[Ca^{2+}]_i$ increase after Ca^{2+} re-addition at 100 µM.

Further, the presence of just one sulfamoyloxy group either at C3 (STX68) or at C17 (STX738) does also not change the IC_{50} substantially (STX68: 25 µM, STX738: 20 µM, Table 2). Thus, the sulfamoyloxy groups at C3 and C17 do not seem to have an influence on the *in vitro* Ca^{2+} signalling pathways. But interestingly, the IC_{50} was decreased by half (about 10 µM) with the 3,17-bis-sulfamoyloxy-estradiol (STX49) as shown in Figure 6B and C.

These results show that sulfamoyloxy groups at C3 and / or C17 in combination with a 2-methoxy group do not change the potency of decreasing Ca^{2+} signalling *in vitro*. Interestingly, if a hydrogen is present at C2, the bis-sulfamoyloxy derivative (STX49, 10 µM) decreased the IC_{50} by a factor of 5 compared to the 3,17-hydroxy compound (E2, 55 µM). However, the relevance of sulfamoyloxy groups at C3 and / or C17 are considered to be rather unimportant for the inhibition of $[Ca^{2+}]_i$ increase in Jurkat T lymphocytes *in vitro* at least if the derivative also possesses a 2-methoxy group. Nonetheless, these compounds might be efficient in *in vivo* experiments due to their higher bioavailability.

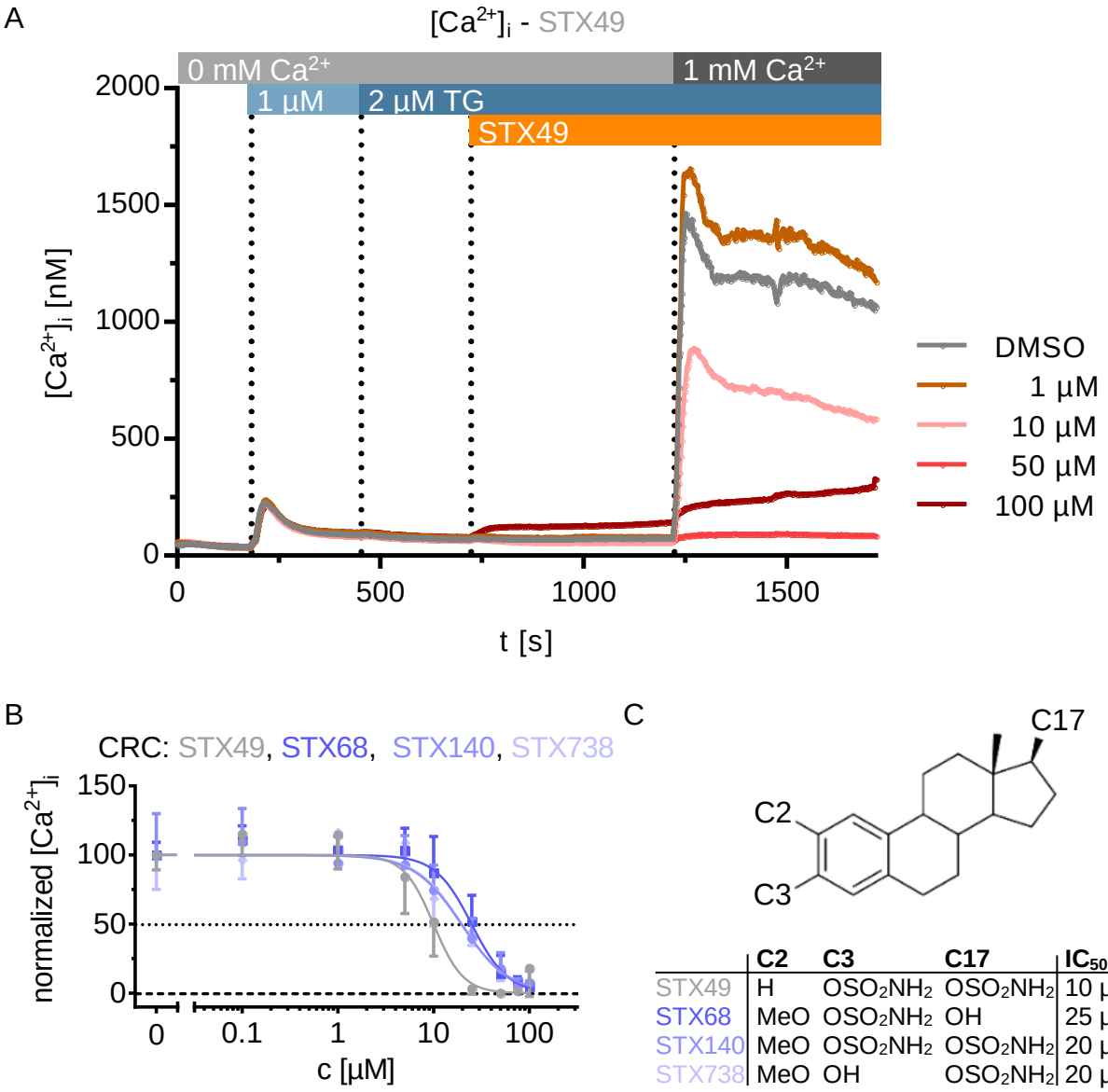

	C2	C3	C17	IC_{50}
STX49	H	OSO_2NH_2	OSO_2NH_2	10 µM
STX68	MeO	OSO_2NH_2	OH	25 µM
STX140	MeO	OSO_2NH_2	OSO_2NH_2	20 µM
STX738	MeO	OH	OSO_2NH_2	20 µM

Figure 6: Impact of 3,17-sulfamoyloxy derivatives on $[Ca^{2+}]_i$.

3,17-Bis-sulfamoyloxy-estradiol (STX49), 3-sulfamoyloxy-2-methoxyestradiol (STX68), 3,17-bis-sulfamoyloxy-2-methoxyestradiol (STX140) and 17-sulfamoyloxyl-2-methoxyestradiol (STX738) inhibit Ca^{2+} entry in Jurkat T lymphocytes. A: Ca^{2+} tracing of T lymphocytes treated with STX49 which showed the smallest IC_{50} among compounds depicted in this figure. Data represent mean values of 4 (DMSO, 1 µM, 10 µM), 3 (50 µM) and 7 (100 µM) measurements. B: Concentration-response curve (CRC) of STX49, STX68, STX140 and STX738 calculated from tracings as it shown for STX49 in A. The calculation was performed as it is described in Figure 4. Data represent the mean ± SD. Number of measurements for STX49 is 3 (0.1, 5, 50, 75 µM), 4 (DMSO, 1, 10, 25 µM) or 7 (100 µM), for STX68 3 (0.1 – 5 µM, 75 µM), 4 (25, 50 µM), 6 (100 µM) or 7 (DMSO, 10 µM), for STX140 4 (0.1, 1, 10 µM), 7 (5, 50 µM), 8 (25 µM), 13 (DMSO, 75 µM) or 14 (100 µM) and for STX738 3 (0.1 – 5, 50, 75 µM), 4 (25 µM), 5 (10 µM), 6 (100 µM), 7 (DMSO). C: Chemical structures and IC_{50} of STX49, STX68, STX140 and STX738.

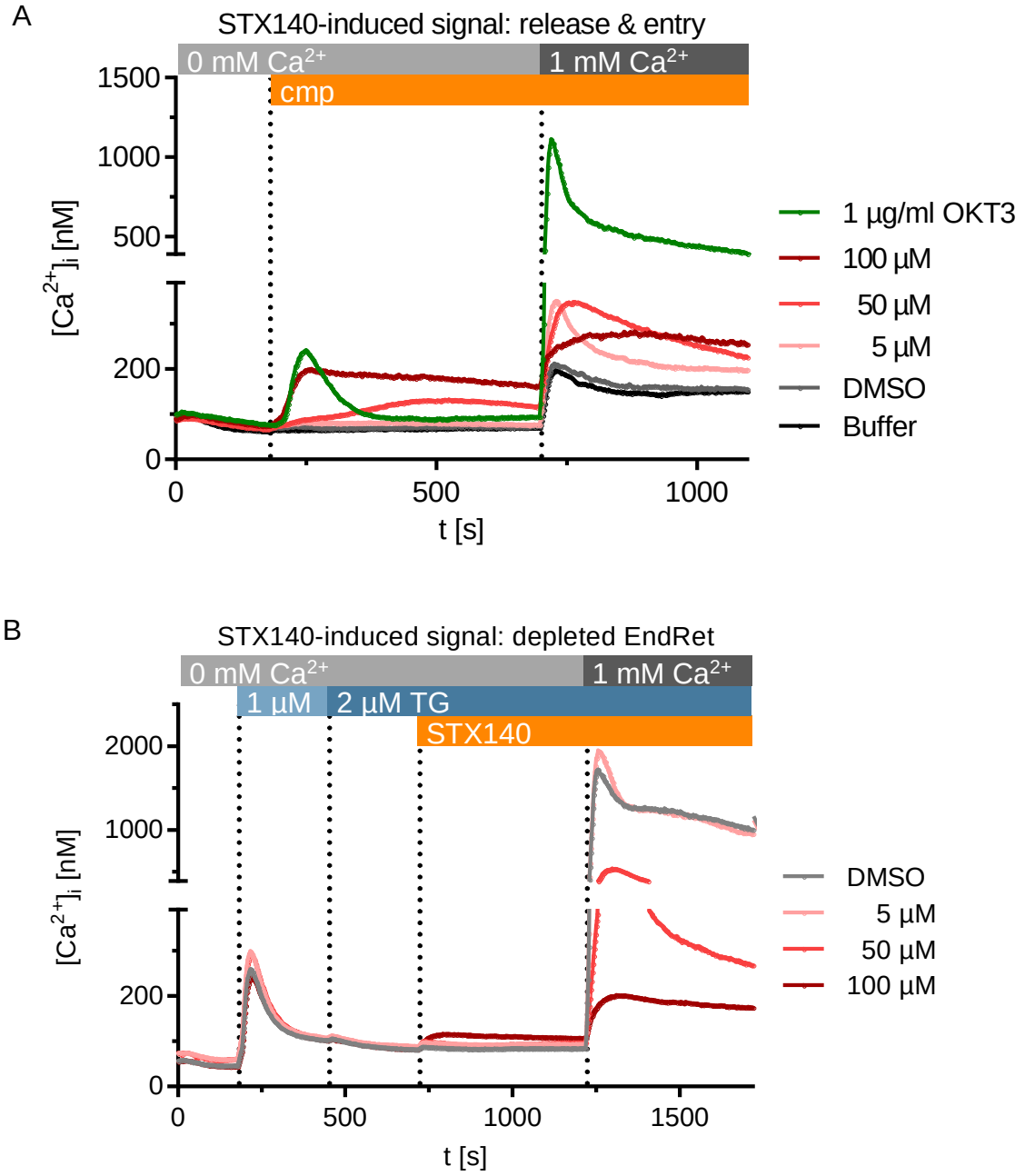

Figure 7: STX140 induces a Ca^{2+} release signal originating from the ER.

A: Upon addition of STX140 to Jurkat T lymphocytes in nominal Ca^{2+} free buffer, a sustained Ca^{2+} release is induced (A). OKT3 was added as a control for stimulation. 50 µM STX140 is efficient to mediate a clearly visible Ca^{2+} release signal which is not evoked by 5 µM STX140. STX140 was dissolved in DMSO and added to a final concentration of 0.2 % (v/v) DMSO. OKT3 was dissolved in buffer and therefore, buffer was added to the cells as a control for this measurement. Ca^{2+} entry is slightly increased compared to control measurements but is not efficient to evoke an increase in $[Ca^{2+}]_i$ comparable to the increase mediated by OKT3. Data represent mean values of 3 (OKT3), 6 (buffer, DMSO, 100 µM) or 7 (5, 50 µM) measurements. B: The Ca^{2+} release signal evoked by STX140 is diminished by previous ER depletion via thapsigargin. Data represent mean values of 7 (5, 50 µM), 13 (DMSO) or 14 (100 µM) measurements.

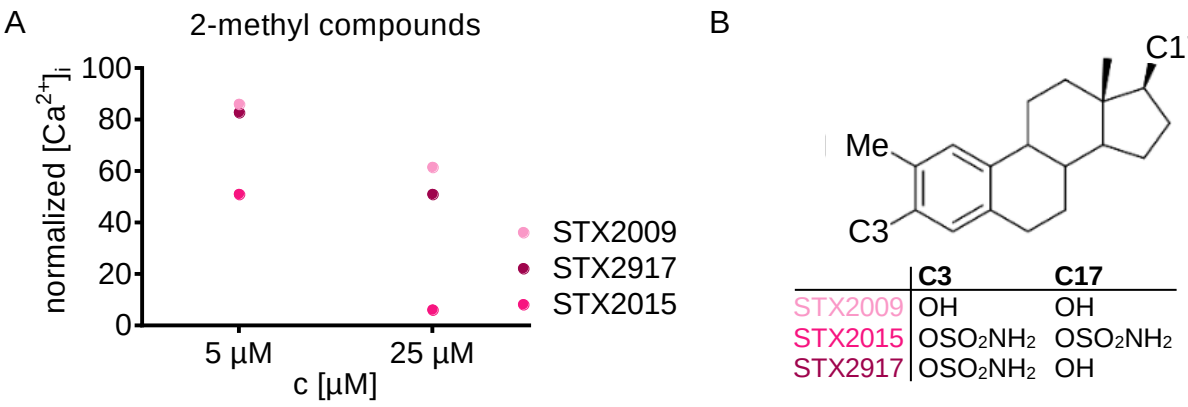

Figure 8: Impact of 2-methyl derivatives on $[Ca^{2+}]_i$.

2-Methylestradiol (STX2009), 2-methyl-3,17-bis-sulfamoyloxyl-estradiol (STX2015) and 2-methyl-3-sulfamoyloxyl-estradiol (STX2917) inhibit Ca^{2+} entry in Jurkat T lymphocytes. A: 2-Methyl compounds STX2009, STX2917 and STX2015 were screened for their impact on $[Ca^{2+}]_i$. These compounds showed a slight inhibition at 5 µM and STX2015 even an almost complete inhibition at 25 µM. Each compound was measured once per concentration. The $[Ca^{2+}]_i$ was normalized to the corresponding DMSO controls (100 %) measured at the same day and 50 µM STX49 (0 %) as measured in Figure 6. B: Chemical structures of 2-methyl derivatives of 2ME2.

2-Methyl derivatives

The effect of the oxygen in the methoxy group was investigated by replacement of the 2-methoxy group by a 2-methyl group. These compounds include 2-methylestradiol (STX2009), 2-methyl-3,17-bis-sulfamoyloxy-estradiol (STX2015) and 2-methyl-3-sulfamoyloxy-estradiol (STX2917; Figure 8). 25 µM STX2009 or STX2917 showed a small reduction in $[Ca^{2+}]_i$ compared to control measurements (62 % and 51 %, respectively). STX2015 decreased SOCE at 25 µM quite substantially (remaining $[Ca^{2+}]_i$: 6 %) and caused an almost half-maximally reduction at about 5 µM (51 %) compared to control measurements (Figure 8A). Thus, the 2-methyl group is only effective in the presence of 3,17-bis-sulfamoyloxy groups, but not if a sulfamoyloxy group is only present at C3 or not at all.

2-Ethyl derivatives

For investigating the effect of an ethyl group at C2, two compounds were analysed, namely 2-ethylestradiol (STX139) and 2-ethyl-3,17-bis-sulfamoyloxyl-estradiol (STX243; Figure 9B, C). These compounds showed quite a large decrease in the IC_{50} of decreasing $[Ca^{2+}]_i$ increase even with 3,17-bis-hydroxy groups. STX139 showed an IC_{50} value of about 10 µM which is halved compared to 2ME2 and is similar to STX49.

STX243 showed an IC_{50} of about 5 µM which is half as large as for STX139 and even 4-fold lower than the corresponding 2-methoxy compound (STX140). So, in contrast to 2-methoxy derivatives, the 3,17-bis-sulfamoyloxy compound shows an effect on reducing the IC_{50} and therefore it is more potent than the 3,17-hydroxyl-compound by a factor of two. These results show that an 2-ethyl group is more efficient in reducing the IC_{50} in vitro in Jurkat T lymphocytes after ER depletion.

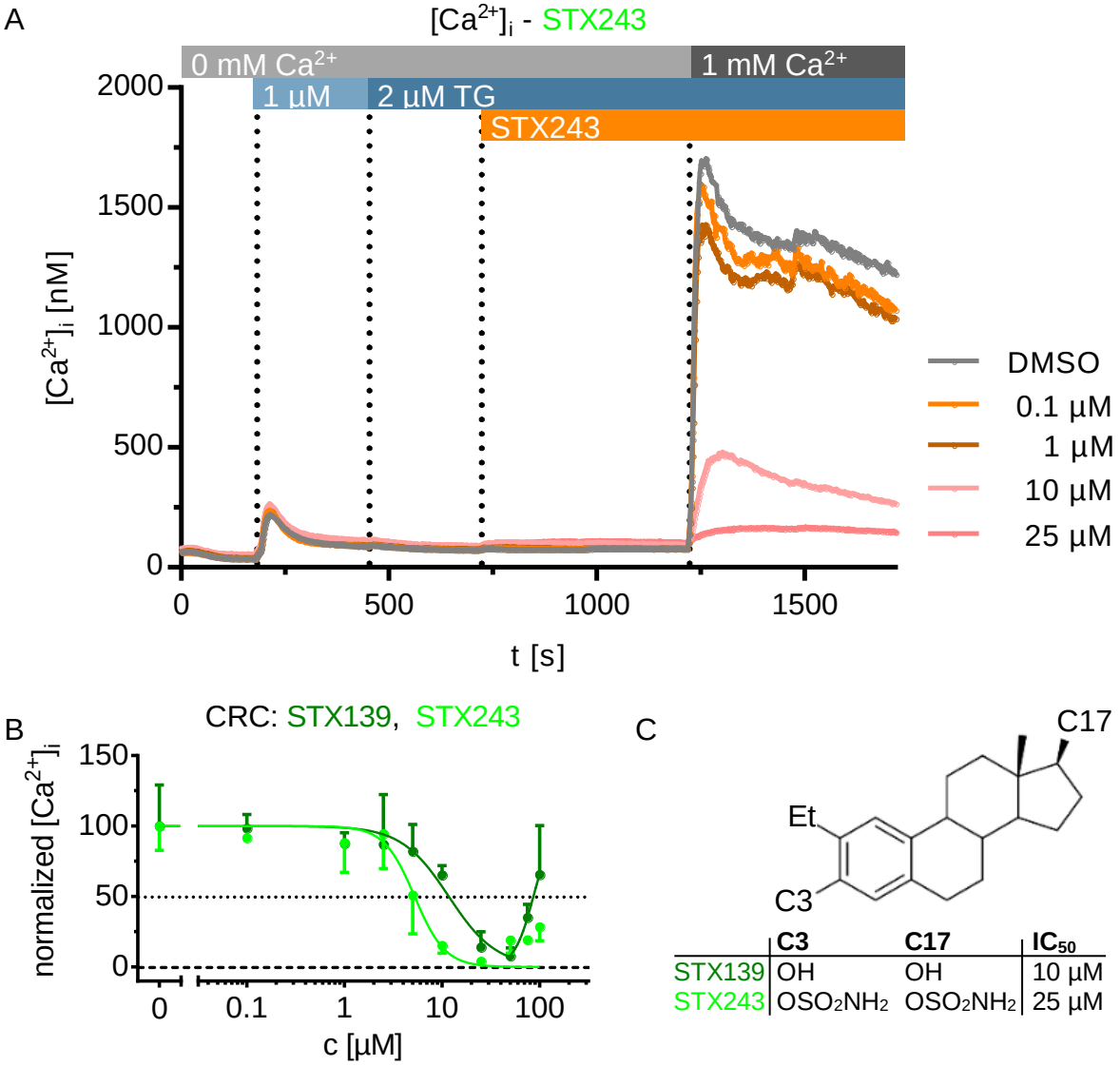

Figure 9: Impact of 2-ethyl derivatives on $[Ca^{2+}]_i$.

2-Ethylestradiol (STX139) and 2-ethyl-3,17-bis-sulfamoyloxyl-estradiol (STX243) inhibit Ca^{2+} entry in Jurkat T lymphocytes. A: Ca^{2+} tracing of T lymphocytes treated with STX243 which showed smaller IC_{50} than STX139. Data represent mean values of at least 4 measurements. B: Concentration-response curve (CRC) of STX139 and STX243 calculated from tracings as it shown for STX243 in A. Normalized $[Ca^{2+}]_i$ for STX139 and STX243 were fitted up to a concentration of 50 and 25 µM, respectively. The calculation was performed as it is described in Figure 4. Data represent the mean ± SD of 3 (0.1 µM), 4 (1, 10, 50, 75 µM), 5 (25 µM), 6 (2.5, 5 µM) or 7 (DMSO, 100 µM) for STX139 and 3 (0.1, 10, 50, 75 µM), 4 (1, 2.5, 25 µM), 5 (5 µM), 6 (100 µM) or 8 (DMSO) measurements. C: Chemical structures and IC_{50} of STX139 and STX243.

C17 Hydrogen bond acceptor derivatives

It has been shown in animal models studies for tumor growth that a hydrogen bond acceptor group at C17 increased the potency for inhibition of tumor growth (Jourdan et al., 2010, 2011; Leese et al., 2008). Thus, these compounds were analysed for their potential to inhibit $[Ca^{2+}]_i$ increase. The results are shown in Figure 10 – Figure 12 as well as in Table 2.

One such hydrogen bond acceptor is a cyanomethyl group. 2-Methoxy-3-hydroxy-17-cyanomethyl-estra-1,3,5(10)-triene (STX640) showed an IC_{50} of 2 µM which is 10 fold lower than the IC_{50} of 2ME2 (Figure 10 and Figure 4). Therefore this group is considered to be highly efficient in increasing the potency.

One compound which additionally possessed a 3-sulfamoyloxy group (2-methoxy-3-sulfamoyloxy-17-cyanomethyl-estra-1,3,5(10)-triene; STX641) inhibited the $[Ca^{2+}]_i$ increase with an IC_{50} of 1.7 µM, which is also about 10 fold smaller compared to the 17-hydroxylated (STX68) or 17-sulfamoyloxylated (STX140) compounds (Figure 10 and Figure 6). However, it did not differ markedly from its 3-hydroxylated compound (STX640) in the IC_{50} value (Figure 10). Therefore, the C17 cyanomethyl group highly increases the potency while the sulfamoyloxy group at C3 is not considered to be crucial for this activity.

2-Ethyl compounds of 2ME2 showed a decrease in IC_{50} value by a factor of 2 and 4, respectively (see 2-Ethyl derivatives). Therefore, I investigated if a 2-ethyl group is also efficient in combination with the highly effective 17-cyanomethyl group, namely 2-ethyl-3-hydroxy-17-cyanomethyl-estra-1,3,5(10)-triene (STX505) and 2-ethyl-3-sulfamoyloxy-17-cyanomethyl-estra-1,3,5(10)-triene (STX564). These compounds decreased the IC_{50} value further by 19 % (STX505) and 29 % (STX564) down to IC_{50} values of 1.7 and 1.2 compared to the 17-hydroxylated (STX139) or 17-sulfamoyloxylated (STX243) compounds, respectively (Figure 10 and Figure 9). Therefore, the 17-cyanomethyl group is more important than the 2-ethyl group in reducing the IC_{50} value but the 2-ethyl group additionally decreases the IC_{50} value compared to 2-methoxylated compounds.

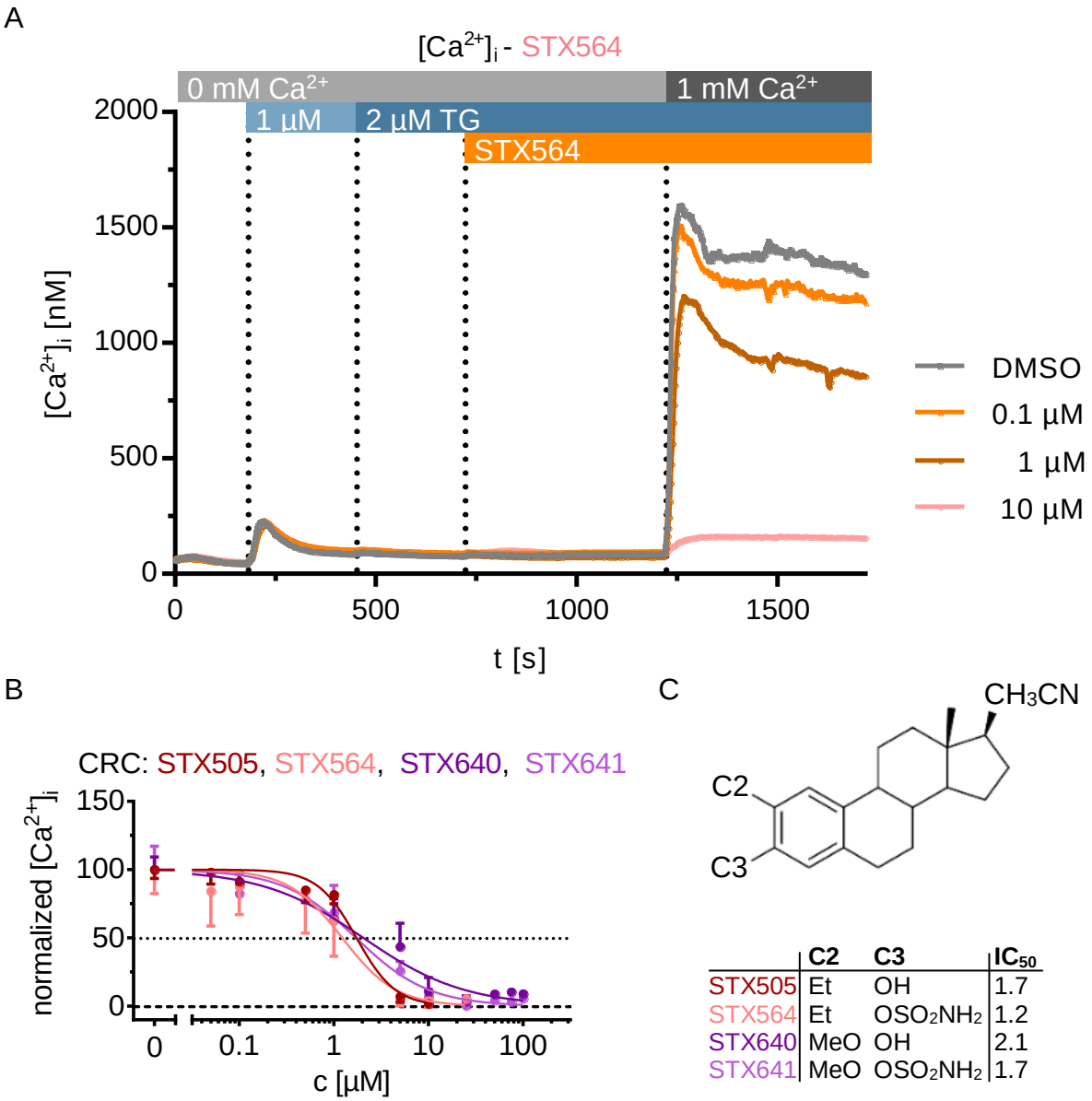

	C2	C3	IC_{50}
STX505	Et	OH	1.7
STX564	Et	OSO_2NH_2	1.2
STX640	MeO	OH	2.1
STX641	MeO	OSO_2NH_2	1.7

Figure 10: Impact of 17-cyanomethyl derivatives on $[Ca^{2+}]_i$.

2-Ethyl-3-hydroxy-17-cyanomethyl-estra-1,3,5(10)-triene (STX505), 2-ethyl-3-sulfamoyloxyl-17-cyanomethyl-estra-1,3,5(10)-triene (STX564), 2-methoxy-3-hydroxy-17-cyanomethyl-estra-1,3,5(10)-triene (STX640) and 2-methoxy-3-sulfamoyloxy-17-cyanomethyl-estra-1,3,5(10)-triene (STX641) inhibit Ca^{2+} entry in Jurkat T lymphocytes. A: Ca^{2+} tracing of T lymphocytes treated with STX564 which showed the smallest IC_{50} among compounds depicted in this figure. Data represent mean values of 5 (0.1, 1, 10 µM) or 6 (DMSO, 0.05, 0.5, 5 µM) measurements. B: Concentration-response curve (CRC) of STX505, STX564, STX640 and STX641 calculated from tracings as it shown for STX564 in A. The calculation was performed as it is described in Figure 4. Data represent the mean ± SD of 3 (0.1, 1, 10 µM) or 4 (DMSO, 0.05, 0.5, 5 µM) measurements for STX505, 5 (0.1, 1, 10 µM) or 6 (DMSO, 0.05, 0.5, 5 µM) measurements for STX564, 4 (DMSO, 0.1 – 10, 50, 75 µM), 5 (25 µM) or 7 (100 µM) measurements for STX640 and 3 (0.1 – 1, 50, 75 µM), 4 (10 µM) or 5 (DMSO, 25, 100 µM) measurements for STX641. C: Chemical structures and IC_{50} of STX505, STX564, STX640 and STX641.

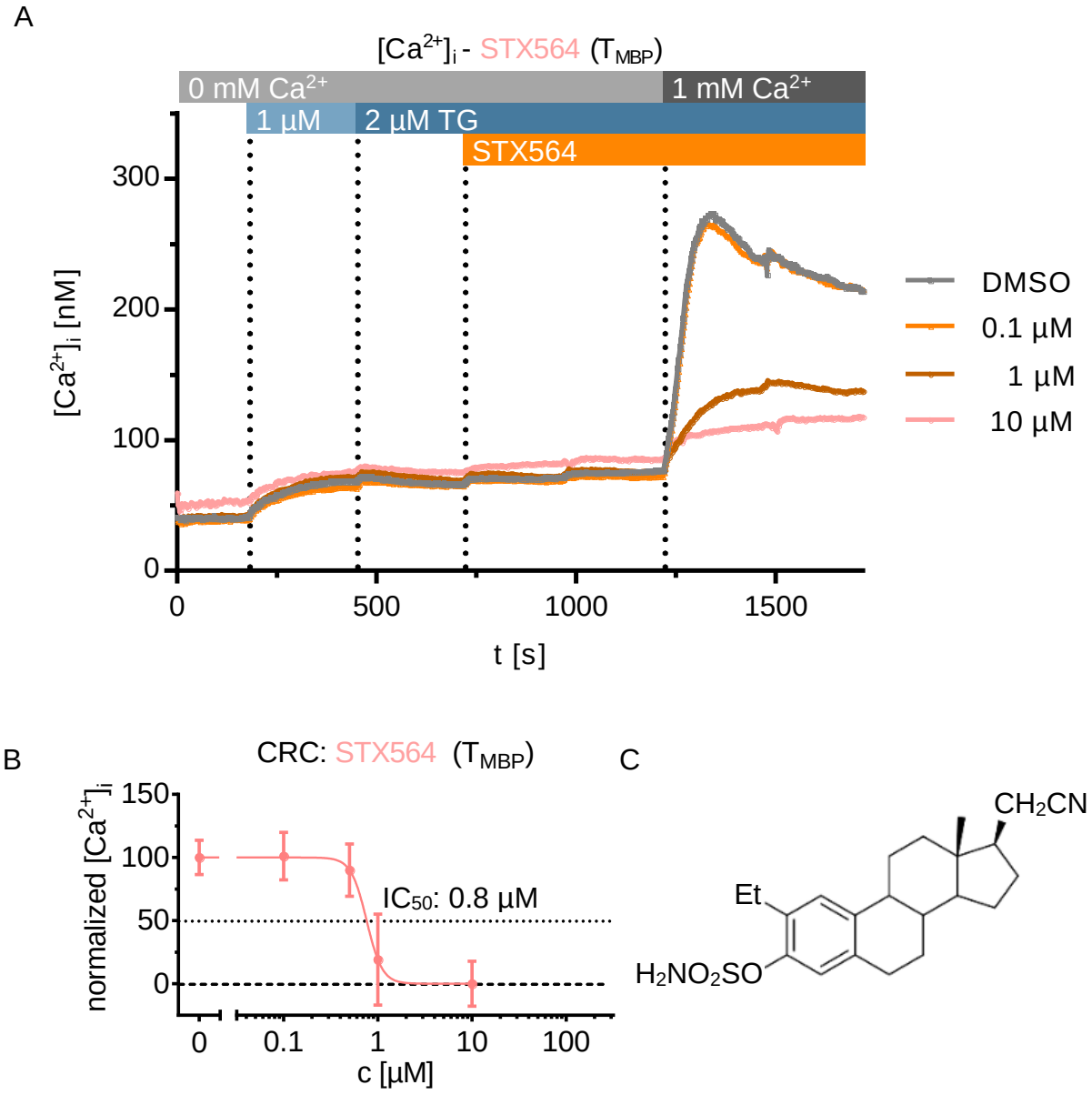

Figure 11: STX564 inhibits Ca^{2+} entry in T_{MBP} lymphocytes from rats.

Restimulated, MBP specific rat T lymphocytes (T_{MBP}) were treated like the Jurkat T lymphocytes described in Figure 4. A: $[Ca^{2+}]_i$ tracings. Data represent mean data of 3 (10 µM), 4 (0.1, 1 µM) or 5 (DMSO) measurements. B: Concentration-response curve of STX564 in T_{MBP}s. Data represent the mean data ± SD of 3 (0.5, 10 µM), 4 (0.1, 1 µM) or 5 (DMSO) measurements. The dPlateau values were normalized to 0.2 % (v/v) DMSO (100 %) and 10 µM STX564 (0 %) which showed the smallest $[Ca^{2+}]_i$ after Ca^{2+} re-addition. Subsequently, the compound concentrations were log-transformed and the concentration-response curves were fitted via a nonlinear regression with variable slope using the least squares fit. C: Chemical structure of STX564.

STX564 was additionally investigated in T_{MBP} lymphocytes which were kindly provided by Dr. Dmitri Lodygin from the laboratory of Prof. Alexander Flügel (Department of Neuroimmunology, University Medical Center, Göttingen, D). In general, T_{MBP}

lymphocytes showed a smaller increase in $[Ca^{2+}]_i$ compared to Jurkat T lymphocytes (Figure 11A). This increase was also concentration-dependently prevented by addition of STX564 leading to a similar IC_{50} as STX564 did in Jurkat T lymphocytes (Figure 11B, Table 2). Thus, the mechanism of action is not limited to Jurkat T lymphocytes but STX564 is also able to prevent $[Ca^{2+}]_i$ increase in restimulated T lymphocytes from rats.

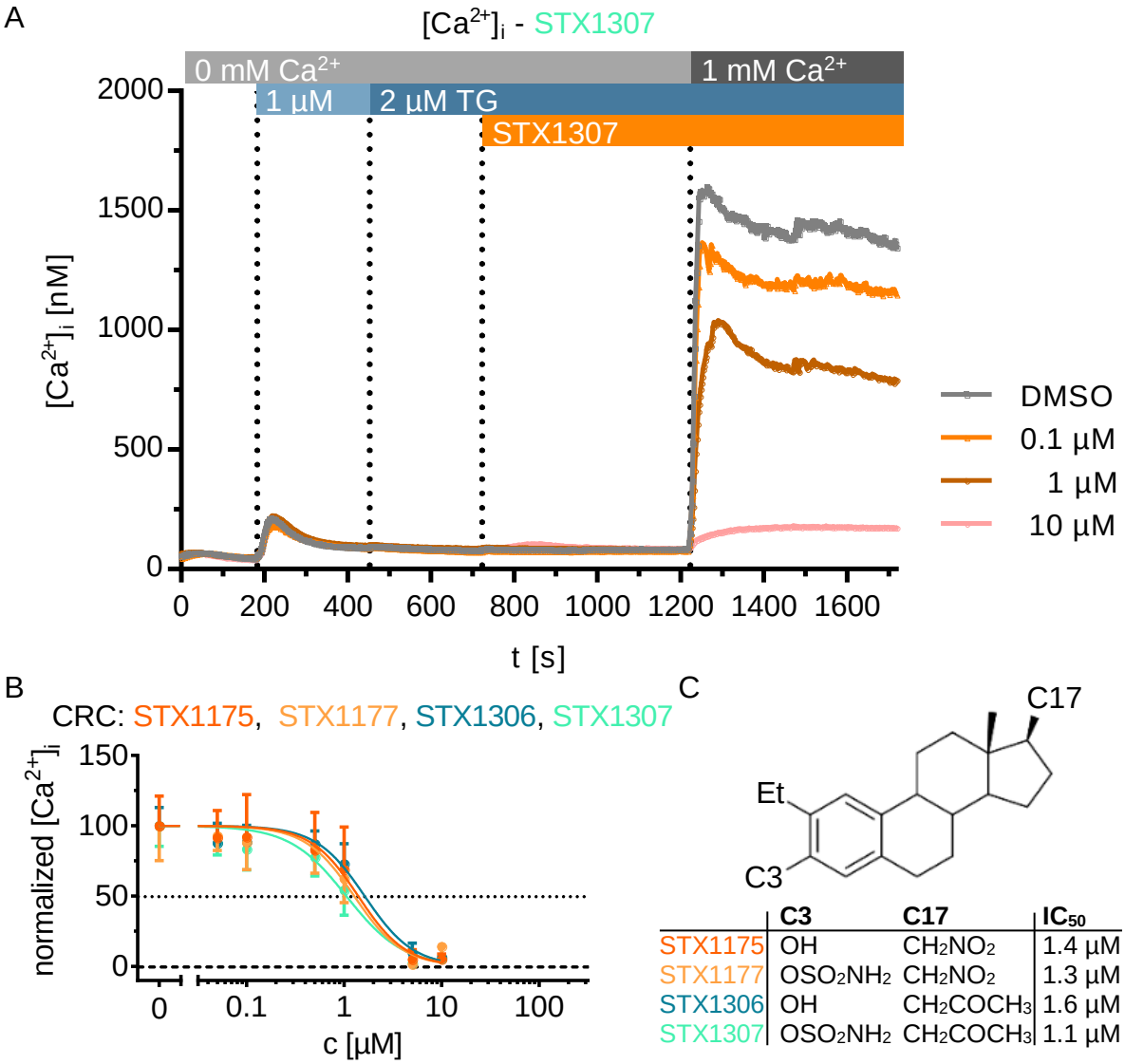

Figure 12: Impact of derivatives with hydrogen bond acceptor at C17 on $[Ca^{2+}]_i$.

2-Ethyl-3-hydroxy-17-nitromethylestra-1,3,5(10)-triene (STX1175), 2-ethyl-3-sulfamoyloxy-17-nitromethylestra-1,3,5(10)-triene (STX1177), 2-ethyl-3-hydroxy-17-oxopropylestra-1,3,5(10)-triene (STX1306) and 2-ethyl-3-sulfamoyloxy-17-oxopropyl-estra-1,3,5(10)-triene (STX1307) inhibit Ca^{2+} entry in Jurkat T lymphocytes. A: Ca^{2+} tracing of T lymphocytes treated with STXSTX1307 which showed the smallest IC_{50} among compounds depicted in this figure. Data represent mean values of 3 (0.1, 1, 10 µM) or 5 (DMSO) measurements. B: Concentration-response curve (CRC) of STX1175, STX1177, STX1306 and STX1307 calculated from tracings as it shown for STX1307 in A. The calculation was performed as it is described in Figure 4. Data represent the mean ± SD of 4 (0.1, 1, 10 µM) or 5 (DMSO, 0.05, 0.5, 5 µM) for STX1175 and STX1177 and 3 (0.1, 1, 10 µM) and 4 (DMSO, 0.05, 0.5, 5 µM) for STX1306 and STX1307. C: Chemical structures and IC_{50} of STX1175, STX1177, STX1306 and STX1307.

Further hydrogen bond acceptor groups at C17 like 17-nitromethyl (3-hydroxy: STX1175; 3-sulfamoyloxy: STX1177) and 17-oxopropyl (3-hydroxy: STX1306; 3-sulfamoyloxy: STX1307) combined with a 2-ethyl group revealed similar IC_{50} values compared to 2-ethyl derivatives with a 17-cyanomethyl group (STX1175: 1.4 µM, STX1177: 1.3 µM, STX1306: 1.6 µM, STX1307: 1.1 µM) as it is shown in Figure 12.

In summary, a hydrogen bond acceptor at C17, irrespective of whether this group is a cyanomethyl, a nitromethyl or an oxopropyl group, is highly efficient to decrease the IC_{50} value and therefore increases the potency. Also the presence of a 2-ethyl group is efficient for this purpose whereas a 3-sulfamoyloxy group does not change the IC_{50} value significantly.

Table 2: Side groups and IC_{50} values of compounds tested in Jurkat T lymphocytes as well as in T_{MBP} lymphocytes.

Data are summarized from Figure 4 to Figure 6 and from Figure 9 to Figure 12. The number in brackets at STX564 indicates the IC_{50} of this compound measured in T_{MBP} lymphocytes.

compound	C2	C3	C17	IC_{50} JMP (IC_{50} T_{MBP}) [µM]
E2	H	OH	OH	55
2ME2	MeO	OH	OH	20
STX49	H	OSO_2NH_2	OSO_2NH_2	10
STX68	MeO	OSO_2NH_2	OH	25
STX140	MeO	OSO_2NH_2	OSO_2NH_2	20
STX738	MeO	OH	OSO_2NH_2	20
STX139	Et	OH	OH	12
STX243	Et	OSO_2NH_2	OSO_2NH_2	5.2
STX505	Et	OH	CH_2CN	1.7
STX564	Et	OSO_2NH_2	CH_2CN	1.2 (0.8)
STX640	MeO	OH	CH_2CN	2.1
STX641	MeO	OSO_2NH_2	CH_2CN	1.7
STX1175	Et	OH	CH_2NO_2	1.4
STX1177	Et	OSO_2NH_2	CH_2NO_2	1.3
STX1306	Et	OH	CH_2COCH_3	1.6
STX1307	Et	OSO_2NH_2	CH_2COCH_3	1.1

A

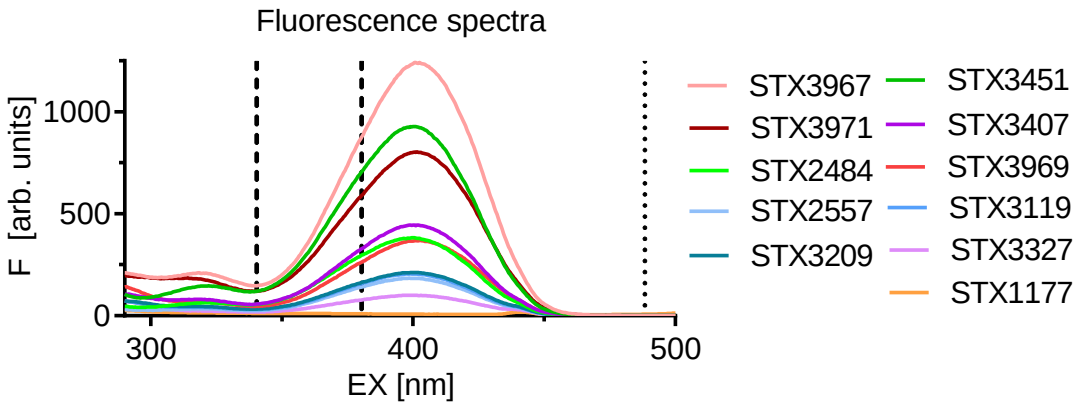

B

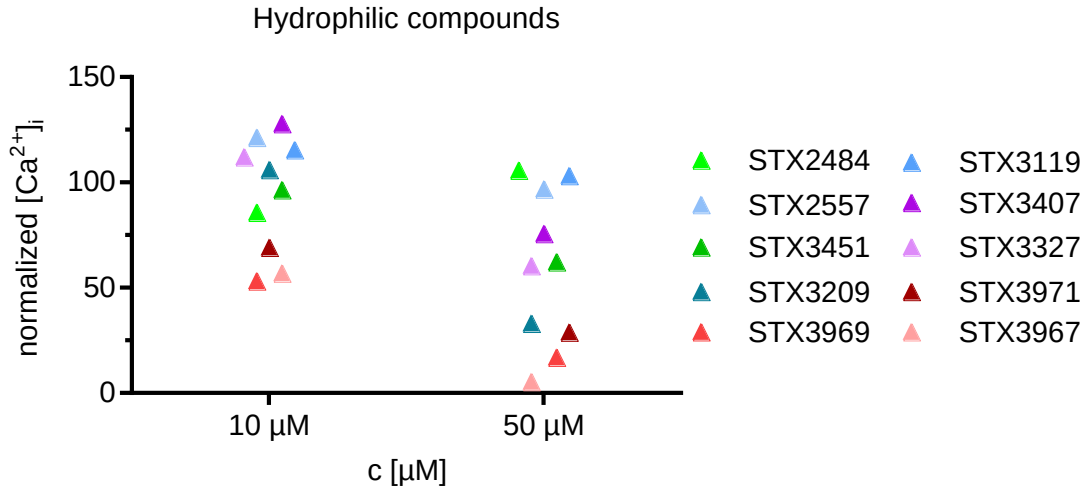

C

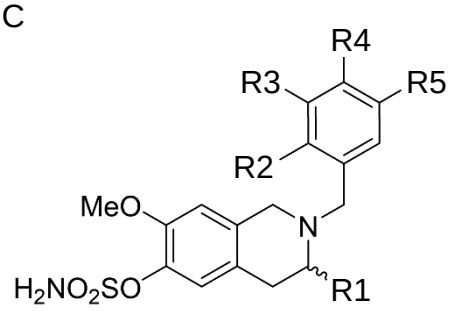

	R1	R2	R3	R4	R5
STX2484	H	H	MeO	MeO	MeO
STX2557	Me	H	H	H	MeO
STX3119	Me	F	H	H	MeO
STX3209	Me	Cl	H	H	MeO
STX3327	Me	Cl	H	H	H
STX3407	Me	H	H	H	Cl
STX3451	H	H	MeO	MeO	Br
STX3967	Me	Cl	Cl	H	H
STX3969	Me	Cl	H	Cl	H
STX3971	Me	Cl	H	H	Cl

Figure 13: Impact of hydrophilic compounds on $[Ca^{2+}]_i$.

More hydrophilic compounds that are structurally related to 2ME2 were analysed for their impact on $[Ca^{2+}]_i$. A: 10 µM of the compounds are fluorescent at the excitation wavelengths which are used for exciting Fura2 (340 nm and 380 nm, dashed lines) but not at the excitation wavelength of Fluo4 (488 nm, dotted line). The fluorescence was measured at an emission wavelength of 520 nm. STX1177 was measured as a control compound which is not fluorescent. Data represent fluorescence of single measurements. B: Compounds were tested at 10 and 50 µM in the Ca^{2+} free / Ca^{2+} re-addition protocol which was also performed before. Data points resemble normalized $[Ca^{2+}]_i$ of single measurements. STX3209, STX3971, STX3969 and STX3967 showed a large reduction in $[Ca^{2+}]_i$ compared to control measurements of which STX3967 almost completely inhibited $[Ca^{2+}]_i$ increase at 50 µM. However, these compounds were not as potent as the best lipophilic compounds and therefore they were not investigated further. The values were normalized to the corresponding DMSO control measurements of the same day (100 %) and to 50 µM STX49 which was measured with Fura2 (0 %). C: Chemical structures of the hydrophilic compounds analysed.

Hydrophilic compounds

The compounds tested so far are quite lipophilic with cLogP values ranging from 2.2 (STX140) to 5.8 (STX1306, Figure 14A). It has been shown in tumor cell studies that hydrophilic compounds are also efficient in increasing compounds' potencies (Dohle et al., 2014a, 2014b; Leese et al., 2010). These compounds were designed by pharmacophore translation from STX140. The basal structure of most compounds are a 7-methoxy-3-methyl-6-sulfamoyloxy-1,2,3,4-tetrahydroisoquinoline but STX2484 and STX3451 had a basal structure of 7-methoxy-6-sulfamoyloxy-1,2,3,4-tetrahydroisoquinoline. In addition, hydrogens at position 2 were substituted by 3,4,5-tetramethoxybenzyl (STX2484), 3-methoxybenzyl (STX2557), 2-fluoro-5-methoxybenzyl (STX3119), 2-chloro-5-methoxybenzyl (STX3209), 3-chlorobenzyl (STX3327), 2-chlorobenzyl (STX3407), 3-bromo-4,5-dimethoxybenzyl (STX3451), 2,3-dichlorobenzyl (STX3967), 2,4-dichlorobenzyl (STX3969), 2,5-dichlorobenzyl (STX3971). Their structures are depicted in Figure 13A.

As these compounds were highly fluorescent at excitation wavelengths of 340 nm and 380 nm which are used for Ca^{2+} measurement with Fura2 (Figure 13B), T lymphocytes treated with hydrophilic compounds were loaded with Fluo4-AM which is excited at 488 nm. At this wavelength, none of the compounds was fluorescent. The emission was measured at 520 nm.

STX2557 and STX2484 showed only a minor reduction in $[Ca^{2+}]_i$ increase at 100 µM whereas STX3451 and STX3971 showed a reduction by about 50 % at 50 µM. cLogP values for STX3451 and STX3971 are 2.7 and 4.3, respectively. As 2ME2 derivatives of similar cLogP values showed IC_{50} values around 20 µM (Figure 14A), the hydrophilic compounds are less potent compared to lipophilic compounds with similar cLogP values. These results indicate that hydrophilic compounds are not as efficient as 2ME2 derivatives. Therefore, hydrophilic compounds were not further investigated. Additionally, these compounds showed similar tPSA values as the sulfamoyloxy compounds tested before (Figure 14B), indicating that not the size but the overall structure of the molecules is crucial for their action.

None of the hydrophilic compounds showed a marked inhibition of $[Ca^{2+}]_i$ increase after ER depletion at 100 µM although all of these compounds possessed 2-methoxy and 3-sulfamoyloxy groups. This observation suggests that the other side groups are too

large for an efficient binding and thereby sterically hinder an interaction with the target. Further, the interaction of the compounds with their target might rely on a hydrophobic interaction. These compounds will possess a charged nitrogen at physiological pH. Therefore, the interaction between lipophilicity and the compounds' potency were investigated further.

Lipophilic compounds inhibit Ca^{2+} entry

Since the hydrophilic compounds STX2484, STX2557, STX3451, and STX3971 did not decrease SOCE after ER depletion in contrast to the more lipophilic compounds which were analysed before (Figure 13, Figure 4 – 6, Figure 9, Figure 10, Figure 12), one could argue that the effect on the $[Ca^{2+}]_i$ might only depend on the compound's lipophilicity. It is also possible that for efficient action a certain degree of lipophilicity is required. Lipophilicity might facilitate the compound's diffusion across the plasma membrane enabling binding to intracellular targets. Furthermore, lipophilicity might cause the compounds to remain within the plasma membrane and sterically decrease its fluidity hindering rearrangement and recruitment of proteins, including the interaction between STIM and Orai.

Therefore, the IC_{50} values were correlated with the cLogP values of the compounds (Figure 14A). This analysis shows a significant correlation (Pearson, $r^2 = 0.256$, $p = 0.038$) indicating that increased cLogP values result in smaller IC_{50} values. Although the most lipophilic compounds are those with the lowest IC_{50} values, this correlation is quite weak and there are some compounds which show a great deviation from the correlation line. These include STX49 and STX641 which show a much smaller IC_{50} value and E2 which shows a much higher IC_{50} than would be expected from their cLogP value. Therefore, a certain degree of lipophilicity seems to be necessary for a reduction in $[Ca^{2+}]_i$ increase but is not crucial for their overall action.

Further, the size of the compounds does not correlate with the IC_{50} values (Figure 14B; Pearson, $r^2 = 0.0213$, $p = 0.590$). Therefore, it is considered that the general structure and the side groups are more important for the effects of the compounds than the resulting lipophilicity or hydrophilicity or the size of the compounds.

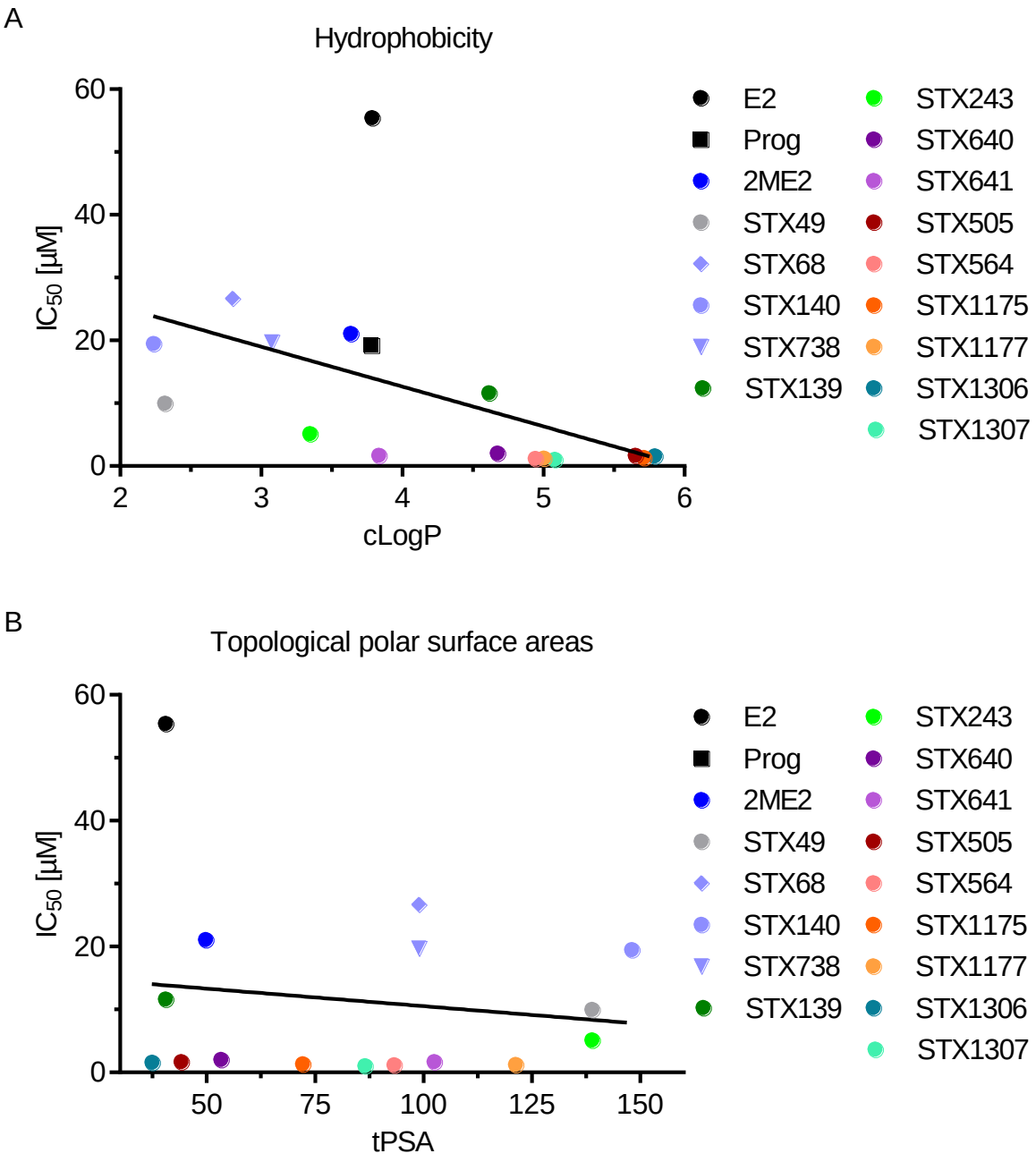

Figure 14: Correlation between hydrophobicity and topological polar surface areas with IC_{50} values.

The most promising compounds which were investigated before were analysed for putative unspecific effects of which two are hydrophobicity and the surface area of polar side groups. A: The cLogP values of the compounds significantly correlates with the IC_{50} values shown in Table 2 (Pearson: $r^2 = 0.2560$, $p = 0.0383$). This correlation suggests that a compound's potency on its hydrophobicity. B: The topological polar surface area (tPSA) did not correlate with the IC_{50} value (Pearson: $r^2 = 0.0213$, $p = 0.590$).

In summary, the endogenous E2 metabolite 2ME2 inhibited SOCE *in vitro* in Jurkat T lymphocytes. A reduction in $[Ca^{2+}]_i$ increase was also evoked by E2 and Prog but not by other steroid hormones like E1, E3, Tes or Chol. Prog showed a similar IC_{50} values compared to 2ME2 whereas E2 was less potent. By derivatisation of 2ME2, the potency of the compounds was even increased leading to a reduction in the IC_{50} value by a factor of 15-18 to the most potent compounds which are STX564, STX1177 and STX1307. In general, a methoxy or an ethyl group at C2 is efficient in reducing the IC_{50}, especially in combination with a hydrogen bound acceptor at C17. A sulfamoyloxy group at C3 and / or C17 did not change the IC_{50} greatly in *in vitro* experiments. Nonetheless, these groups were efficient in *in vivo* experiments due to an increased bioavailability. Additionally, STX564 was efficient to prevent $[Ca^{2+}]_i$ increase after ER depletion not only in human Jurkat T lymphocytes but also in T_{MBP} lymphocytes from rats indicating that the mechanism is species independent.

In general, $[Ca^{2+}]_i$ signalling in T lymphocytes is highly regulated and requires the activation of several ion channels and pumps as described in section 1.2.1 “Activation of T lymphocytes”. Which of these potential targets are influenced by the compounds was investigated further and is described in detail in the next section.

4.2 Mechanism of inhibiting $[Ca^{2+}]_i$ increase

In the previous experiments, 2ME2, endogenous steroids and 2ME2 derivatives were shown to prevent SOCE in Jurkat T lymphocytes and T_{MBP} lymphocytes. Next, the underlying mechanism of action was investigated. It is possible that the compounds act by modulating protein expression levels, e.g. by changing the activity of transcription factors. It may also be that the compounds directly interfere with certain targets, e.g. by binding to certain proteins or by interfering with the fluidity of the plasma membrane and thereby disturbing the binding of STIM and Orai. Besides the mode of action, the possible targets may also be very diverse. In principle, $[Ca^{2+}]_i$ may be decreased, among others, by activation of Ca^{2+} clearance which decrease $[Ca^{2+}]_i$. Ca^{2+} clearance include (i) Ca^{2+} extrusion to the extracellular space by PMCAs, (ii) Ca^{2+} reuptake into the ER by SERCAs, and (iii) Ca^{2+} uptake into mitochondria by MCUs. Other potential mechanisms include inhibition of (i) Ca^{2+} increasing mechanisms like

Ca^{2+} entry via CRAC channels / STIM and Orai, (ii) Ca^{2+} release from the ER by RyR or IP_3R or (iii) K^+ currents which counteract the decrease in driving force for Ca^{2+} entry by depolarization of the plasma membrane. The kinetics of the inhibition were analysed to consider how fast the action takes place and whether the compounds influence the expression levels of proteins.

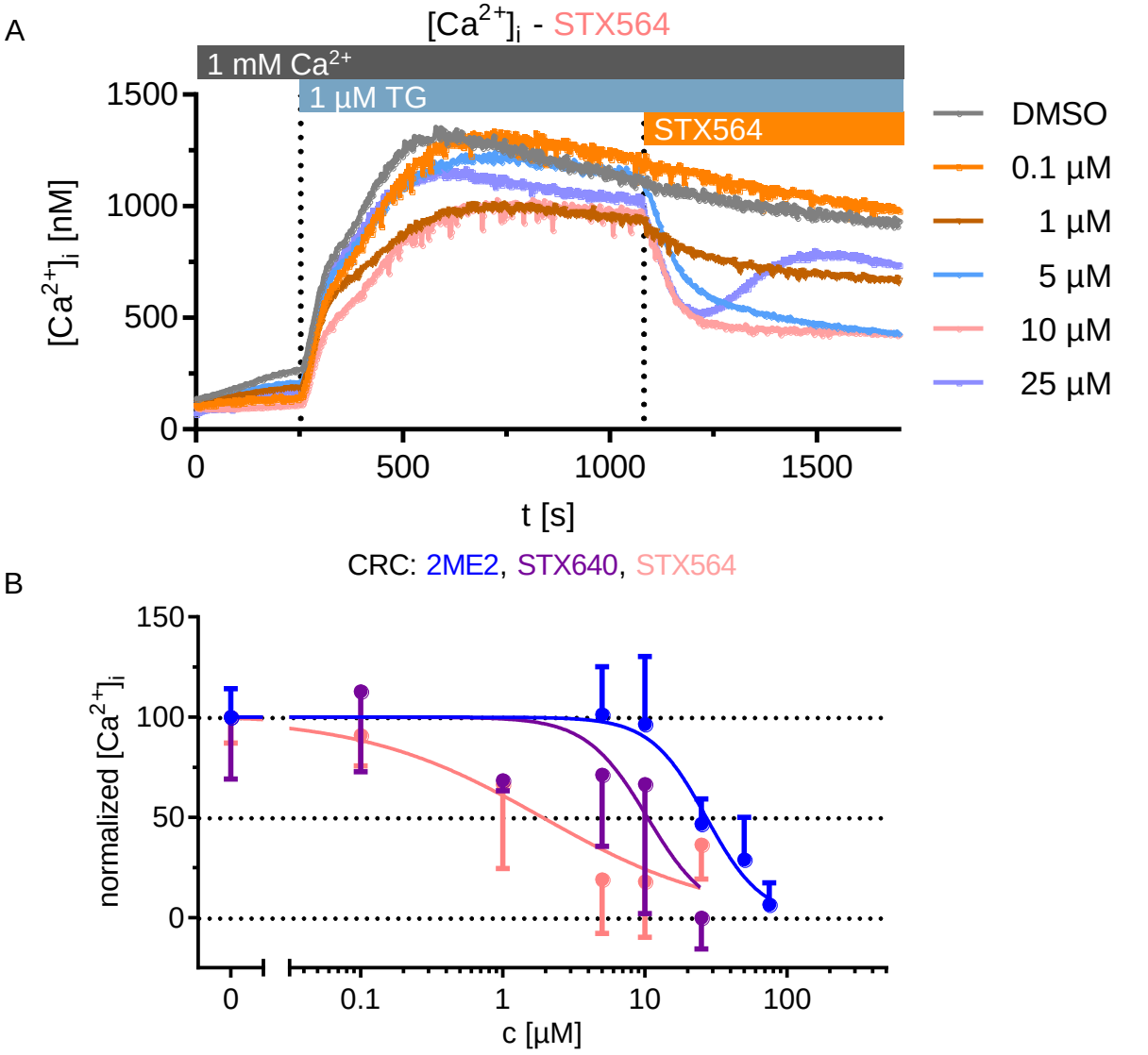

Figure 15: Rapid decrease in $[Ca^{2+}]_i$ after compound addition.

Jurkat T lymphocytes were analysed in Ca^{2+} measurement buffer with continuous, slow stirring. A: $[Ca^{2+}]_i$ tracings of T lymphocytes treated with STX564. Data represent mean values of 3 measurements except for 0.1 µM (n = 4). B: Concentration-response curve (CRC) of data shown in A and of T lymphocytes treated with 2ME2 and STX640. The ratio between plateau $[Ca^{2+}]_i$ after TG stimulation (mean 1005 – 1055 s) and minimal $[Ca^{2+}]_i$ after compound addition (mean 1625 – 1675 s) was calculated. Data represent the mean ± SD of 3 measurements except for 5 µM 2ME2 (n = 4), 0.1 µM STX564 (n = 4) and DMSO for STX640 (n = 5). Concentrations were log transformed and data was normalized to the DMSO control (100 %) and 25 µM STX640 (0 %) because this condition showed the smallest $[Ca^{2+}]_i$. IC_{50} values are 27 µM for 2ME2, 10 µM for STX640 and 1.9 µM for STX564. These experiments were performed by the medical student Sissy-Alina Waschkowski under my supervision.

4.2.1 2ME2 and its derivatives decrease elevated $[Ca^{2+}]_i$ very rapidly

In the previous experiments, the compounds were allowed to incubate for more than 8 min before the Ca^{2+} was re-added. To analyse how fast the action really takes place, Jurkat T lymphocytes were stimulated with TG in Ca^{2+} containing buffer and subsequently a compound was added. These experiments were performed by Sissy-Alina Waschkowski under my supervision.

Upon addition of 2ME2, STX640 or STX564, $[Ca^{2+}]_i$ immediately decreased in a concentration-dependent manner (Figure 15). The IC_{50} values are slightly increased (2ME2: 27 µM, STX640: 10 µM, STX564: 1.9 µM) compared to the results of the Ca^{2+} free / Ca^{2+} re-addition protocol (2ME2: 20 µM, STX640: 2.1 µM, STX564: 1.2 µM, Table 2). These results indicate that the efficiency is slightly decreased upon the presence of Ca^{2+} within the buffer. This finding makes it unlikely that changes in the expression level are the underlying mechanism as the protein transcription usually takes more time than several seconds. Next, the impact on Ca^{2+} decreasing and Ca^{2+} increasing mechanisms was analysed.

4.2.2 2ME2 and its derivatives prevent Ca^{2+} from entering cells

To investigate if 2ME2 and its derivatives stimulate Ca^{2+} increasing mechanisms or inhibit Ca^{2+} clearance mechanisms, Jurkat T lymphocytes were analysed in nominal Ca^{2+} free buffer as in the experiments described in section 4.1 “Impact of steroids, 2ME2 and its derivatives on $[Ca^{2+}]_i$ increase”. But instead of adding Ca^{2+}, Mn^{2+} was added. Mn^{2+} can enter the cells via similar mechanisms as Ca^{2+} and is able to quench the fluorescence of Fura2 (Grynkiewicz et al., 1985). Thus, Mn^{2+} entering into cells would result in a decreased fluorescence which was measured at its isosbestic point because the fluorescence at this point does not change Ca^{2+} dependently.

Fura2 Fluorescence rapidly decreases in the control experiments (0.2 % (v/v) DMSO) whereas the fluorescence is only slightly affected if 100 µM 2ME2, 100 µM STX140 or 10 µM STX564 were added beforehand, as it is shown in Figure 16A. These observations were also made with addition of 1 or 10 µM Synta66, a known CRAC inhibitor (Tian et al., 2016). Analysis of the initial slope of fluorescence decrease after Mn^{2+} addition revealed that the initial slope was significantly decreased upon addition of 1 or 10 µM

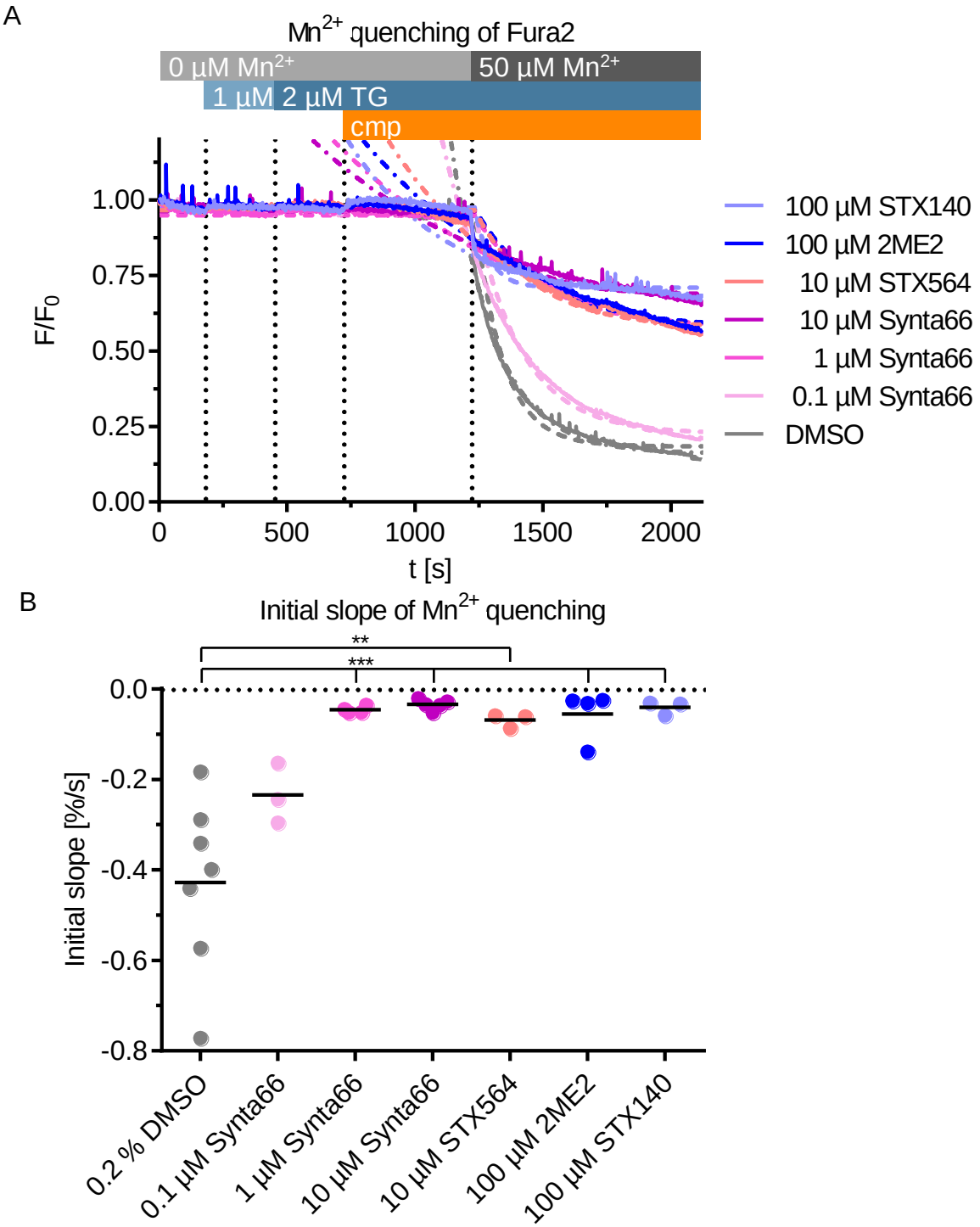

Figure 16: Mn^{2+} quenching of Fura2 in Jurkat T lymphocytes.

Jurkat T lymphocytes were measured in nominal Ca^{2+} free buffer and were continuously stirred during measurements. A: Mean tracings of Mn^{2+} quenching. Fura2 was excited at 357 nm and emission was measured at 495 nm. Tracings before Mn^{2+} addition were fitted to a straight line and the slope of this line was assumed to represent decrease in fluorescence due to bleaching. All tracings showed a fast drop in fluorescence after Mn^{2+} addition. Data after this drop were fitted to an exponential one phase decay equation (dashed lines). B: Initial slopes were calculated from the exponential curve fit shown in A and were subtracted by the slope of the linear curve fit before Mn^{2+} addition. Initial slopes were analysed for significant differences by an ordinary ANOVA with a Bonferroni correction for multiple testing. **: $0.001 < p \leq 0.01$; ***: $p < 0.001$. Dots represent individual experiments and lines symbolize mean values of 3 (STX564, STX140, 0.1 µM Synta66), 4 (2ME2, 1 µM Synta66), 5 (10 µM Synta66) or 7 (DMSO) measurements.

Synta66 as well as 100 µM 2ME2, 100 µM STX140 or 10 µM STX564 compared to DMSO control measurements (Figure 16B).

These results indicate that 2ME2 and its derivatives prevent divalent ions from entering cells and thereby decrease the Ca^{2+} increasing mechanisms rather than activation the Ca^{2+} clearance mechanisms as latter would require a Ca^{2+} entry first.

4.2.3 2ME2 and its derivatives do not inhibit K^+ channels

The previous experiments showed that divalent cations are prevented from entering Jurkat T lymphocytes. In principle, continuous Ca^{2+} entry is maintained by K^+ efflux. The cell depolarizes upon Ca^{2+} entry which breaks down the electrical and chemical gradient and prevents further Ca^{2+} from entering the cells. Thus, if K^+ channels would be inhibited by the compounds, the electrical gradient diminishes. In general, two different kinds of K^+ channels are involved in maintaining the gradient: voltage-gated K_V channels and Ca^{2+}-dependent K_{Ca} channels.

As shown in Figure 17A, Jurkat T lymphocytes were stimulated with a voltage step protocol ranging from +80 mV to -80 mV to activate K_V channels. The resulting currents were characterized by outward currents which are activated at voltages between -30 and +80 mV. During one voltage step, the current decreases slightly over time.

Upon the addition of 250 nM of the specific $K_V1.3$ inhibitor ShK-Dap22, this large outward current was almost completely abolished which pinpoints to the fact that this current is largely if not completely carried by K^+ ion flowing through $K_V1.3$ channels.

This current is not significantly changed upon the treatment with 10 µM STX564 (Kruskal-Wallis-Test, Bonferroni corrected, $p = 0.331$) compared to DMSO treated cells. This suggests that STX564 does not inhibit $[Ca^{2+}]_i$ increase by inhibiting K_V channels.

Besides K_V 1.3 channels, K_{Ca} channels were investigated (Figure 18). These channels open upon an increased $[Ca^{2+}]_i$. K_{Ca} channels are inward rectifier channels and thus were investigated with an increased $[K^+]$ in the extracellular buffer. These currents were not inhibited by 10 nM of the specific $K_{Ca}2$ channel blocker UCL1684. Furthermore, 10 µM STX564 which showed an almost complete reduction in $[Ca^{2+}]_i$ increase in Ca^{2+} measurements (see Figure 10), did not show a reduction in the currents.

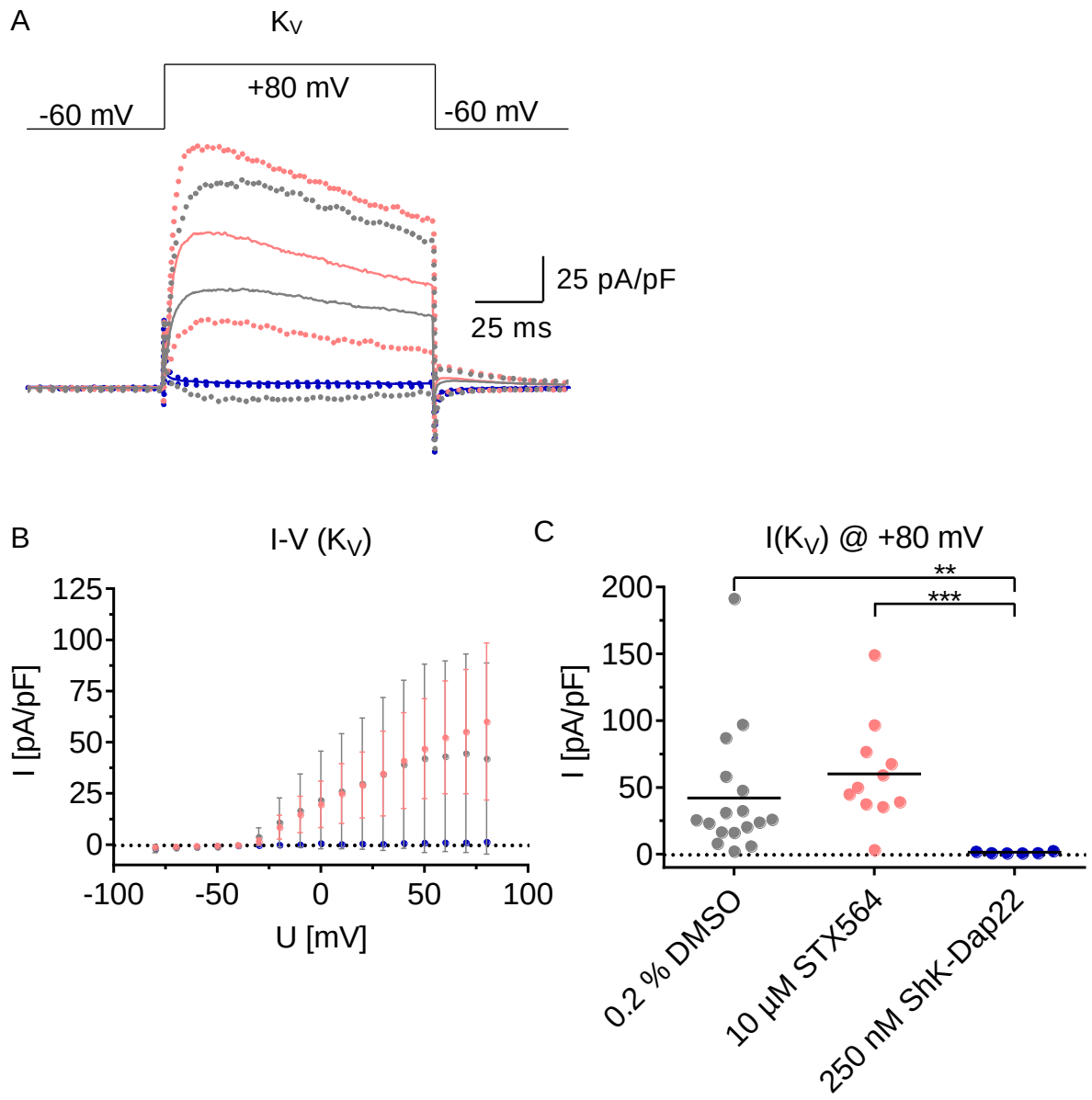

Figure 17: Whole-cell patch clamp analysis of K_V channels in Jurkat T lymphocytes.

A: Step protocol and mean currents (line) ± SD (dots) of K_V currents. The application protocol was set to the holding potential of -60 mV for 50 ms. Then, the stimulus voltage was applied for 100 ms which was set to +80 mV in this case. Afterwards, the holding potential was applied again for 50 ms. B: Current-voltage relationship for K_V currents are depicted. The stimulus voltage started at +80 mV and was decreased by 10 mV after every step until it reached -80 mV. The intersweep interval was set to 30 s. Currents were calculated as the mean between 80 and 90 ms after the start of the stimulus voltage. Data represent mean ± SD of 17 (DMSO), 11 (STX564) and 6 cells (ShK-Dap22). C: Currents of single cells of K_V currents at +80 mV. Leak currents were calculated as the mean between 10 and 40 ms prior to the start of a step voltage. At this point of time, the holding potential was applied to the cells. The leak current is a criterion for the tightness of the seal and was smaller than -30 pA (mean -4 pA) throughout the whole recording time. The current at voltage stimulation was measured as the mean between 80 and 90 ms after the start of the stimulation to measure sustained currents. Currents were normalized to cell capacity c-slow which ranged from 2.4 to 7.5 pF (mean: 5 pF). Currents of DMSO control measurements do not differ significantly from currents of cells treated with 10 µM STX564 (Kruskal-Wallis-Test, Bonferroni corrected, $p = 0.311$). Currents recorded from ShK-Dap22 treated cells differed significantly from DMSO treated cells (Kruskal-Wallis-Test, Bonferroni corrected, $p = 0.007$) as well as STX564 treated cells (Kruskal-Wallis-Test, Bonferroni corrected, $p < 0.001$).

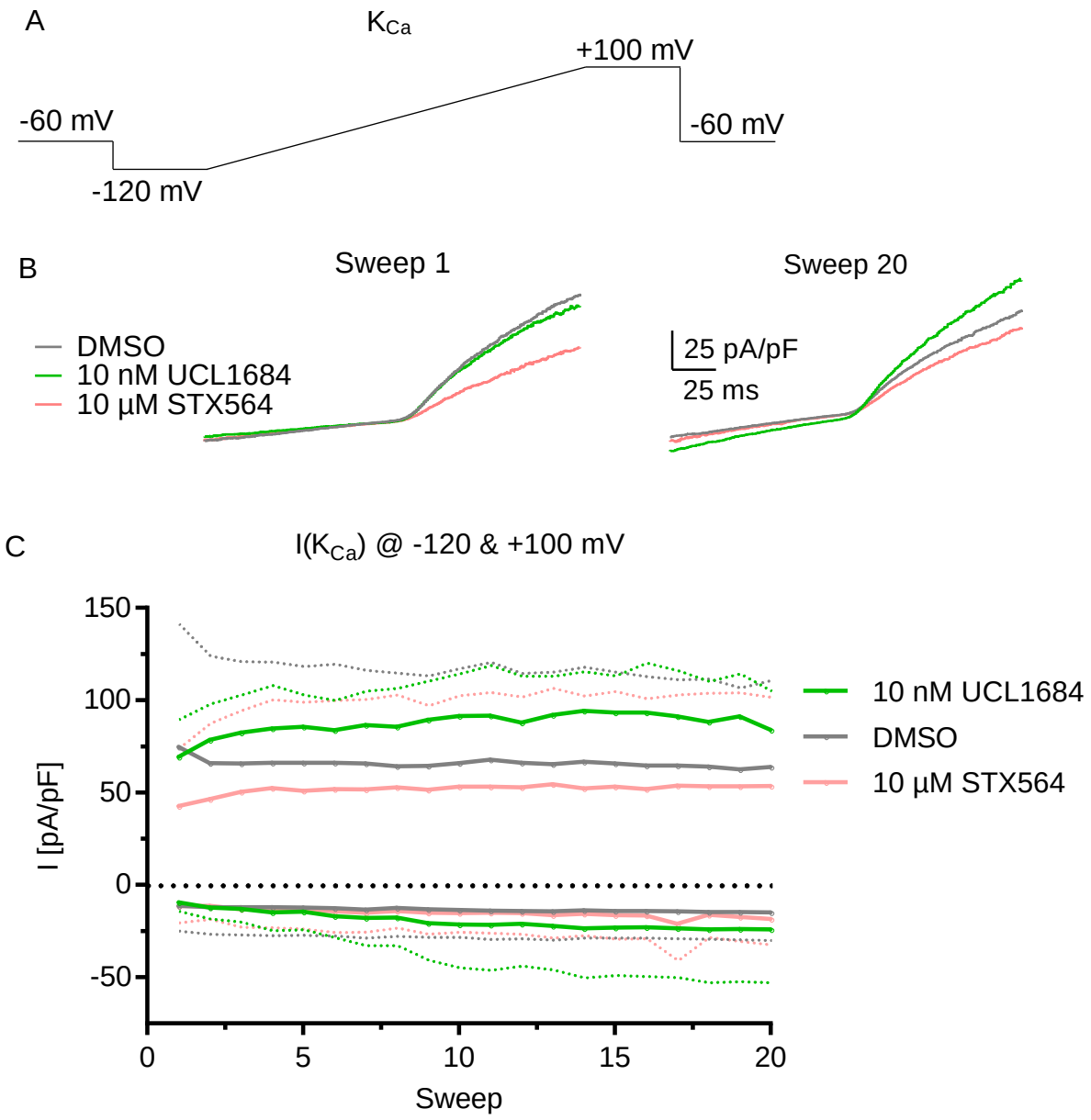

Figure 18: Whole-cell patch clamp analysis of K_{Ca} channels in Jurkat T lymphocytes.

A: Ramp protocol and mean currents of currents measured with K_{Ca} buffers. Stimulation potentials were corrected for a liquid junction potential of -13 mV. The ramp protocol was set to the holding potential of -60 mV for 300 ms. Then the voltage was set to -120 mV for 50 ms and subsequently raised to +100 mV during a time period of 200 ms. At the end of the ramp, +100 mV was applied for another 50 ms and then the voltage was returned to the holding potential of -60 mV. The intersweep interval was set to be 10 s. Before every ramp, a voltage of +80 mV was applied for 500 ms to inactivate K_V channels. B: Normalized currents obtained from these ramps are depicted. Currents were normalized to the cell capacity c-slow which ranged from 3.3 to 13 pF (mean 6.9 pF). Cells were analysed with a relative series resistance below 5 (mean 3). Data represent mean currents of 4 (UCL1684, STX564) or 7 (DMSO) measurements. C: Mean currents (lines) ± SD (dots) at -120 and +100 mV are shown. These currents were measured as mean currents over a time period 25 ms before the start (-120 mV) or 25 ms after the end of the ramp (+100 mV). Mean currents were calculated of 4 (UCL1684, STX564) or 7 (DMSO) measurements.

Therefore, it is highly suspected if the corresponding currents are really mediated by $K_{Ca}2$ channels. As a protocol was used which was used by other groups to measure K_{Ca} channels, one reasonable explanation would be that something was wrong in preparing the buffers (e.g. that the $[Ca^{2+}]_i$ was too low to activate K_{Ca} channels). Another possibility would be that those cells which were measured, did not express K_{Ca} channels.

4.2.4 2ME2 and its derivatives decrease local Ca^{2+} concentration around Orai1 channels

To further characterize the target of the steroidal compounds, Jurkat T lymphocytes were transiently transfected with GECO1.2-Orai1 vectors. The transfected cells express Orai1 proteins covalently bound to genetically encoded Ca^{2+} indicators derived from GFP.

Upon activation by ER depletion in Jurkat T lymphocytes, GECO fluorescence highly increased (Figure 19A). This increase was almost completely diminished by either 10 µM STX564 or 10 µM Synta66. These compounds significantly decreased the amplitude of the peak signal (Kruskal-Wallis test, Dunn's corrected, Synta66: $p = 0.002$, STX564: $p = 0.012$) as well as the fluorescence intensity at the plateau phase (Kruskal-Wallis test, Dunn's corrected, Synta66: $p = 0.003$, STX564: $p < 0.001$). These results show that STX564 is able to decrease local Ca^{2+} concentrations around Orai channels, indicating that Ca^{2+} entry mediated by Orai channels is the main target of inhibiting $[Ca^{2+}]_i$ increase.

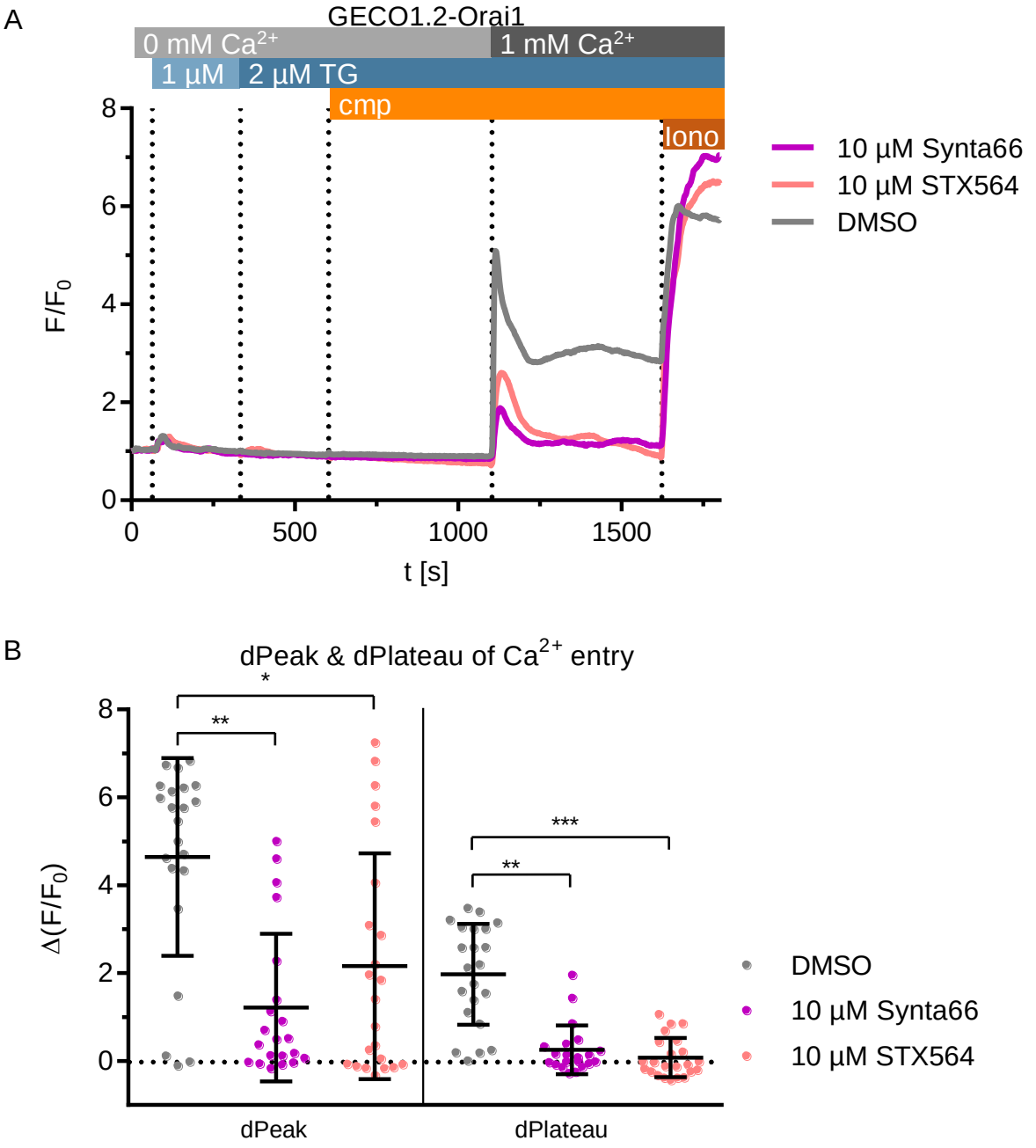

Figure 19: Analysis of Ca^{2+} entry via G-GECO1.2-Orai1 fluorescence.

Jurkat T lymphocytes transfected with GECO1.2-Orai1 were analysed 17 to 22 hours after transfection via life cell imaging. Cells were taken up in nominal Ca^{2+} free buffer and stimulated with thapsigargin. At the end of every measurement, 5 µM ionomycin (Iono) was added. A Mean tracings of transfected cells. Fluorescence intensities were normalized to the fluorescence intensity at the beginning of each measurement. B: Quantitative analysis of data shown in A. Basal values were calculated as mean values between 525 and 575 s. Peak values were calculated as maximum fluorescence after Ca^{2+} re-addition. dPeak is the basal value subtracted from Peak values. Similarly, dPlateau is the basal value subtracted from the Plateau value which is calculated as the mean between 1545 and 1595 s. Data points represent individual cells and the mean ± SD is indicated by lines. Data was collected from 7 independent transfections which resulted in 21 (Synta66), 22 (DMSO) or 23 (STX564) measured cells. dPeak is significantly decreased in cells treated with 10 µM Synta66 (Kruskal Wallis test, Dunn's correction, $p < 0.002$) or 10 µM STX564 ($p = 0.012$) compared to DMSO controls. Additionally, dPlateau is significantly decreased in cells treated with 10 µM Synta66 ($p < 0.003$) or 10 µM STX564 ($p < 0.001$).

5. Discussion

In this study, the impact of 2ME2, endogenous steroid hormones and synthetic 2ME2 derivatives on SOCE as well as the underlying mechanisms were investigated. 2ME2 as well as several steroid hormones were shown before to inhibit the proliferation of immune cells as well as tumor cells (Duncan et al., 2012; Seegers et al., 1989). One important mechanism which suppresses T lymphocyte proliferation involves NFAT translocation (Duncan et al., 2012) which is essentially dependent on Ca^{2+} signalling (Kar et al., 2016). However, it has not yet been revealed how endogenous steroid hormones or 2ME2 interferes with Ca^{2+} signalling in the dependence of inhibiting T lymphocyte proliferation. This study identified that 2ME2, E2, Prog and 2ME2 derivatives decrease Ca^{2+} entry in T lymphocytes by inhibition of the STIM / Orai system.

5.1 Methods to measure free cytosolic Ca^{2+} concentrations

Different methods were used to determine $[Ca^{2+}]_i$. Fluorescence spectrophotometry was used to analyse cell suspensions, loaded with Fluo4-AM or Fura2-AM of which the latter is a ratiometric dye. Alternatively, cells were transfected with a genetically encoded Ca^{2+} indicator (GECO) and individual, transfected cells were analysed by live cell imaging. The results of either method are discussed in this section.

5.1.1 Instruments to measure free cytosolic Ca^{2+} concentrations

Fluorescence spectrophotometry allows for the determination of $[Ca^{2+}]_i$ in cell suspension. Results from few measurements obtained by this method show little variability compared to single cell recordings which are more variable than a signal averaged from several thousand cells.

In theory, one million cells were measured in one measurement as ten million cells were loaded and are finally used for ten measurements. But it is considered that several cells were lost, e.g. by several washing steps during dye loading. Some cells are certainly lost during washing steps either because they underwent cell death or

because they were not tightly attached to the pellet. Thus, the number of recorded cells is presumably slightly less than one million. Furthermore, cells equally distribute in the cuvette's volume. As the light path only detects a small area of the cuvette, the amount of cells measured at each time point is even lower and estimated to be roughly 10.000 to 100.000 cells. However, these cell numbers are still suitable to measure well averaged Ca^{2+} signals. Additionally, this method is quite sensitive and therefore suitable to detect low fluorescence intensities.

However, measuring cell suspensions is not efficient to resolve local Ca^{2+} concentrations around Orai channels. These results were measured in single cells using live cell imaging. This method provides the distinction of dye localized in different subcellular compartments, e.g. dye at the plasma membrane or centrally localized dye. This distinction was important for measuring genetically encoded GECO-Orai because cells frequently showed fluorescence at the inner part. This fluorescence resembles functional GECO which has not been transferred to the plasma membrane yet. By analysing single cells at subcellular levels, this inner fluorescence was not analysed.

Using either method, namely measuring $[Ca^{2+}]_i$ in cell suspensions or via live cell imaging, rather long measurements were performed which commonly exceeded 30 min. To prevent marked dye loss due to bleaching (Tsien et al., 1985), dyes were excited every two seconds. As rather slow changes in $[Ca^{2+}]_i$ were analysed, this method is sufficient to reduce dye loss and to obtain a good time resolution.

5.1.2 Ca^{2+}-sensitive dyes

Within cells, $[Ca^{2+}]_i$ can be measured by using different Ca^{2+}-sensitive dyes. Cells can either be loaded with cell permeant dyes, like Fura2-AM or Fluo4-AM, or cells can be transfected with a vector genetically encoding a Ca^{2+}-sensitive dye, like GECO.

Ratiometric measurement of $[Ca^{2+}]_i$ with Fura2

For measuring $[Ca^{2+}]_i$, Jurkat T lymphocytes were loaded with Fura2-AM or Fluo4-AM. Fura2 was used as a Ca^{2+}-sensitive dye in most of the experiments and therefore this

dye is discussed in more detail in this section. However, many of the aspects discussed for Fura2 are also true for Fluo4.

AM-esters are acetoxy-methyl esters of the respective free acid forms. As the ester form masks the carboxy groups, the esterified dyes are lipophilic and can freely diffuse across the cell membrane (Grynkiewicz et al., 1985). Within the cytosol, endohydrolases hydrolyse the esters and cause the dye to be present in the highly negatively charged acidic form at physiological pH. As de-esterified dyes are hydrophilic, they cannot diffuse across cell membranes and therefore accumulate within cells.

Esterified dyes cannot just diffuse across plasma membranes, but they are also able to pass intracellular membranes if they are not de-esterified fast enough. Further, dyes can be transferred into cellular compartments by endo- or pinocytotic events as these frequently take place within a cell (Roe et al., 1990). Esterases in these compartments de-esterify the dyes leading to an accumulation of dye in the compartments as it has been shown for hepatocytic mitochondria (Gunter et al., 1988). The presence of Ca^{2+}-sensitive Fura2 in mitochondria was shown by Quintana & Hoth (2004) who claim that Fura2 trapped inside mitochondria is responsible for subcellular differences in the Ca^{2+} concentration. As I have just measured global mean $[Ca^{2+}]_i$, I can only speculate on the amount of Fura2 present in mitochondria. Mitochondria are considered to act as Ca^{2+} buffers preventing Ca^{2+}-dependent inactivation of Orai channels and thus mediate a sustained Ca^{2+} entry necessary for T lymphocyte activation (Hoth et al., 2000). As mitochondria take up Ca^{2+} after stimulation resulting in an increased luminal Ca^{2+} concentration, this event is indistinguishable from $[Ca^{2+}]_i$ increase upon stimulation. To acquire a substantial amount of Fura2 present in mitochondria, mitochondria have to be in close proximity to the plasma membrane. Additionally, cytosolic endohydrolases have to be slow enough that Fura2-AM can diffuse across the plasma membrane as well as across the mitochondrial membranes before ester groups are hydrolysed. As Fura2 loading was performed at 37 °C, de-esterification by endohydrolases is considered to be sufficiently fast. Furthermore, it has been shown that mitochondria translocate to the plasma membrane after T lymphocyte stimulation with antibody coated beads (Quintana et al., 2007). Thus, in resting state, most mitochondria should not be in close proximity to the plasma membrane facilitating cytosolic hydrolysis of Fura2-AM. Therefore, the

amount of Fura2 within mitochondria is considered to be rather low although its exact amount and the impact on Ca^{2+} signalling was not determined.

Another problem with loading cells with Fura2-AM arises from de-esterification. Incomplete de-esterification of Fura2-AM results in a fluorescent but Ca^{2+}-insensitive compound which interferes especially with the calibration method (Scanlon et al., 1987). Thus, this compound might result in a large difference between calculated $[Ca^{2+}]_i$ and actual $[Ca^{2+}]_i$. As the fluorescence in my study shows a large dynamic range and the minimum fluorescence at F380 during Rmax is very low compared to F340 during Rmax, this possibility is also considered to not largely, if at all, affect $[Ca^{2+}]_i$.

While Fura2-AM is not Ca^{2+}-sensitive, ester hydrolysis cause Fura2 to become Ca^{2+}-sensitive. Upon Ca^{2+} binding, the excitation maximum shifts from about 360 nm to about 340 nm while the emission maximum stays nearly the same around 510 nm (Grynkiewicz et al., 1985). The excitation was measured at 495 nm in this study as this is the wavelength at which the instruments show maximum emission when measuring Fura2 (data not shown). Interestingly, the fluorescence intensity at the excitation wavelength of around 360 nm stays the same upon different Ca^{2+} concentrations. This wavelength is called the isosbestic point. The fluorescence intensity at the isosbestic point directly correlates with the amount of dye within cells, while intensities at other wavelengths also depend on $[Ca^{2+}]_i$. To measure a good ratio between wavelengths at which the fluorescence dynamically changes upon changes in $[Ca^{2+}]_i$, Fura2 was excited at 340 and 380 nm.

As Fluo4 was only measured at one excitation and one emission wavelength each and does not have an isosbestic point, calibration of Fluo4 is sensitive to intracellular dye concentration. Decreases in fluorescence can commonly occur by Ca^{2+} independent events. These events include dye loss due to bleaching or to fewer cells measured during one measurement (Grynkiewicz et al., 1985). The latter event might also account for differences in fluorescence intensities between several individual measurements. In single cells, a decrease in fluorescence intensity might also resemble a loss of dye by extrusion. However, in fluorescence spectrophotometry this event would cause an increase in fluorescence as the dye binds to extracellular Ca^{2+}. Furthermore, differences in fluorescence in single cells might be the result of either different amounts of dye within cells or different $[Ca^{2+}]_i$ but cannot be told apart.

These Ca^{2+} independent changes in fluorescence are prevented by measuring $[Ca^{2+}]_i$ ratiometrically. However, Ca^{2+} independent changes in fluorescence can also occur with this method. These changes include the binding of other divalent ions like Mg^{2+}, Zn^{2+}, Mn^{2+} and Fe^{2+} (Grynkiewicz et al., 1985). If Fura2 binds to Mg^{2+}, its fluorescence properties are only very little affected (Grynkiewicz et al., 1985) but Mg^{2+} bound Fura2 is not available for binding Ca^{2+}. Thus, Fura2 is then blocked to bind Ca^{2+} and thereby affects fluorescence properties resulting in a lower $[Ca^{2+}]_i$.

Fura2 binds Zn^{2+} with a higher affinity of 2 nM compared to Ca^{2+} resulting in a similar shift in the spectrum like Ca^{2+}. If Fura2 binds Zn^{2+}, $[Ca^{2+}]_i$ would be overestimated (Grynkiewicz et al., 1985). In contrast to this, Fe^{2+} binds to Fura2 3 to 10 fold more strongly and thereby causing a quenching of the dye which is also true for Mn^{2+} (Grynkiewicz et al., 1985). These ions can get into the buffer by contamination. Putative sources for contamination include water or the chemicals both of which are used to prepare the buffers. As high-purity water was used for buffer preparation, the possibility of these ions coming from water is considered to be unlikely. Nonetheless, the chemicals might be contaminated. According to the specification of the chemicals, KCl contains a maximum of 20 µg/g Mg^{2+} and 3 µg/g Fe^{2+}. $MgSO_4$ includes up to 5 µg/g Mn^{2+} and up to 1 µg/g Fe^{2+}. The amount of Fe^{2+} in NaH_2PO_4 is equal to or below 5 µg/g which is also the amount of Fe^{2+} present in HEPES which also contains up to 5 µg/g Mg^{2+}. Assuming that the chemicals are contaminated with the highest amount of these ions, the amount of these ions sums up to 110 nM Mg^{2+}, 121 nM Fe^{2+} and 5 nM Mn^{2+}. As these ions are within the extracellular buffer, they first have to enter cells before they can interfere with the fluorescence of Fura2 which is considered to take place only to a minor extent. Furthermore, these concentrations are at least about 4 orders of magnitude smaller than the extracellular Ca^{2+} concentration and therefore just plays a minor role in interfering with the fluorescence of Fura2 and changes in fluorescence intensities should take place in dependence of Ca^{2+} binding.

Further, these ions might be within the cytosol of the cells beforehand. In this case, the concentration of these ions is considered to not increase during Ca^{2+} measurements as the concentration in the extracellular buffer is rather small and the entry of these ions is considered to be unlikely. Thus, the interference of the ions with Fura2 should stay nearly the same during one measurement.

Additionally, if these ions should indeed interfere with the fluorescence of Fura2, this interference is considered to be nearly the same in all experiments as the same buffer was used for several experiments and the same chemicals were used every time a new buffer was made. However, one possibility to prevent the binding of these ions to Fura2 is the addition of small amounts EGTA as this compound binds Zn^{2+}, Mn^{2+} and Fe^{2+} with higher affinities compared to Ca^{2+} (Grynkiewicz et al., 1985). But EGTA was not added to the extracellular buffer because the interference of these ions with Fura2 is considered to be rather low due to the arguments just mentioned above.

Another problem provided by loading cells with a cell permeant dye arises from dye loss e.g. by dye extrusion via the organic anion transporter or via cell lysis due to cell death. One the one hand, this would lead to a lower fluorescence within cells and on the other hand, the amount of $[Ca^{2+}]_i$ would be overestimated as extruded Fura2 binds to the extracellular high Ca^{2+} concentration. As in most experiments, I exchanged the extracellular buffer just before the start of a measurement with nominal Ca^{2+}-free buffer, the amount of extracellular Fura2 is considered to take not into account as the amount of Fura2 as well as the Ca^{2+} concentration in the extracellular buffer are very low. However, the experiments performed with 1 mM Ca^{2+} in the extracellular buffer (see Figure 15) showed a high increase in the ratio after TG addition, resembling that most of the Fura2 was still present within cells. Also in these experiments, the buffer was not exchanged immediately before the start of each measurement, resulting in a slightly increased basal $[Ca^{2+}]_i$ compared to measurements using nominal Ca^{2+} free buffer. An increased basal $[Ca^{2+}]_i$ is most probably due to Fura2 binding to the extracellular Ca^{2+} resulting in a higher concentration of Fura2 bound to Ca^{2+}. Extracellular Fura2 could have been removed by an exchange of extracellular buffer by fresh buffer. But basal $[Ca^{2+}]_i$ are just slightly increased in comparison to $[Ca^{2+}]_i$ increase in $[Ca^{2+}]_i$ after TG addition, indicating that major amounts of Fura2 remain within cells. Furthermore, decreased Fura2 concentration within cells is also not considered to influence the calculated $[Ca^{2+}]_i$ as the fluorescence was ratiometrically measured to exclude changes due to differences in dye concentrations.

Calibration of fluorescence ratios using Fura2 to obtain $[Ca^{2+}]_i$

The calibration was performed to obtain the $[Ca^{2+}]_i$ from the measured light intensities (Grynkiewicz et al., 1985). This method is suitable to exclude differences concerning light intensities between different cells and different instruments.

By measuring cell suspensions, cells are lysed by Triton X-100 which is a mild detergent keeping proteins intact (Tiller et al., 1984). Thereby, intracellular Fura2 can bind to an extracellular high Ca^{2+} concentration and thus Fura2 is Ca^{2+} saturated, meaning that all Fura2 molecules are in the Ca^{2+} bound state and the ratio reaches a maximal value. Afterwards, Ca^{2+} is dissociated from Fura2 by addition of EGTA resulting in the ratio reaching a minimal value.

As the dissociation constant Kd of EGTA and Fura2 as well as the light intensity of Fura2 highly depends on the ionic strength, the temperature and particularly the pH (Tsien & Pozzan, 1989), the solution was additionally buffered by Tris. The additional buffering is required as every Ca^{2+} bound EGTA molecule produces two molecules of H^+ (Bers et al., 2010). Differences concerning ionic strength and temperature are considered to be of minor relevance as all experiments were performed at RT using the same buffers in every experiment.

One big disadvantage by using Triton X-100 for cell lysis is its auto-fluorescence at excitation and emission wavelengths used for measuring Fura2 (Tiller et al., 1984). By using Triton X-100, fluorescence intensities for calculating Rmax and Rmin during calibration are influenced by this compound and thereby slightly change the value of $[Ca^{2+}]_i$. Thus, the fluorescence intensities at maximal and minimal ratios but not during the measurement before are influenced by this detergent and thereby slightly changes the absolute value of $[Ca^{2+}]_i$. Triton's auto-fluorescence creates a systemic error which is the same in every measurement and can be neglected if measurements are compared which also uses Triton X-100 for calibration.

Alternatively to Triton X-100, Rmax could also be obtained by using ionomycin (Tsien & Pozzan, 1989). This compound is a Ca^{2+} ionophor mediating a Ca^{2+} entry into cells without cell lysis. Possibly, this compound would lead to lower Ca^{2+} concentrations in close proximity to Fura2 as the electrochemical gradient for Ca^{2+} might break down before Fura2 reaches Ca^{2+} saturation. Thereby, Rmax would be underestimated resulting in an overestimation of $[Ca^{2+}]_i$.

Rmax and Rmin were calculated using equation (1) according to Grynkiewicz et al. (1985). Therefore, Rmax and Rmin were determined by finding the maximal and the minimal ratio among all ratios determined. Ratios were calculated for each time point by dividing F340 by F380. Determination of Rmax and Rmin could have also been performed by the data acquisition software FLSolutions. But this software determines the maximal and minimal fluorescence intensities of F340 and F380 and divides the maximal F340 by the minimal F380 for Rmax ($Rmax = F340_{max} / F380_{min}$) and the minimal F340 by the maximal F380 for Rmin ($Rmin = F340_{min} / F380_{max}$).

Usually, one would consider that the minimal and maximal fluorescence is measured during the calibration and correspond to the minimal and maximal ratio. Nonetheless, the experiments showed that the maximal fluorescence at 340 nm as well as at 380 nm commonly was lower during calibration compared to measurements before which is considered to be due to bleaching.

Particularly, maximal fluorescence intensities were often not measured during calibration but during the actual measurement while minimal fluorescence intensities of both wavelengths were measured during calibration. Thus, the maximal fluorescence intensity is reached at the beginning of the measurement for F380 and at the maximal Ca^{2+} concentration after stimulation for F340. Thereby, the maximal and minimal ratios calculated by the fluorescence intensities are measured at different time points. This calculation results in an overestimation of Rmax while Rmin is underestimated compared to the ratio values calculated from the fluorescence intensities measured at the same time points resulting in an overall underestimation of $[Ca^{2+}]_i$. (Grynkiewicz et al., 1985) do not take this aspect into account in their paper. As I used only one dye, the bleaching might affect both wavelengths equally (but see Bassnett et al., 1990). Therefore, Rmax and Rmin values calculated with intensities reached during calibration is considered to differ less from unbleached values than these values differ from Rmax and Rmin calculated by the actual maximal and minimal fluorescence intensities.

Single wavelength measurement of $[Ca^{2+}]_i$ by using G-GECO1.2

Disadvantages of cell permeant esterified Ca^{2+}-sensitive dyes can be circumvented by using a genetically encoded Ca^{2+}-sensitive dye like G-GECO (Dynes et al., 2016).

During this method, cells are transfected with a vector which encodes the G-GECO-protein covalently bound to an Orai channel. This method provides an additional advantage as this dye can detect local changes in Ca^{2+} concentrations in close proximity to Orai channels. Nonetheless, the fluorescence can change independently of Ca^{2+} which flows across the plasma membrane as during transcriptional protein synthesis, the dye is present in subcellular compartments like the ER or Golgi apparatus. If the channel is functional in this state but has not been transferred to the plasma membrane yet, a change in Ca^{2+} concentrations within these compartments would also change the fluorescence of G-GECO which does not resemble local Ca^{2+} concentrations near Orai channels in the plasma membrane. However, this possibility was largely ruled out as the fluorescence was only analysed in the outer rim of a cell.

Calibration of the fluorescence using live cell imaging

Live cell imaging by using GECO1.2-Orai1 channels mainly provides information about changes in $[Ca^{2+}]_i$ rather than the actual value of $[Ca^{2+}]_i$ because the fluorescence is measured at just one excitation and one emission wavelength with one dye. Thereby, differences in the fluorescence intensity between individual cells might either be due to differences in $[Ca^{2+}]_i$ or, unspecifically, due to variation in the amount of fluorescent molecules expressed. According to (Grynkiewicz et al., 1985), single wavelength dyes can also be calibrated. But in this study, the G-GECO dye was analysed by live cell imaging. Calibration of this method is usually performed by permeabilizing the cells with the Ca^{2+} ionophor ionomycin to obtain Rmax and subsequent Ca^{2+} chelation with EGTA to obtain Rmin. Usually, this is performed in two independent steps as the cells often undergo cell death after several minutes of ionomycin treatment. But this prolonged incubation is required as some cells take minutes to reach the maximal fluorescence while others already underwent cell death. Therefore, only a few cells which show the highest fluorescence or ratio can be used for Rmax determination. Minimal ratios are usually obtained by a short-term incubation with ionomycin followed by EGTA addition. Some cells might not have reached the maximum in fluorescence at EGTA addition. Nonetheless, EGTA instantly chelates Ca^{2+} from the cytosol through pores which ionomycin built. Therefore, the minimum is reached after some time, although the maximum in fluorescence intensity was not reached before and the mean

value of all cells can be used to calculate the minimum fluorescence or ratio. Thus, this method is inappropriate to determine the $[Ca^{2+}]_i$ in individual cells using only one dye which is not used in a ratiometric method.

Instead of calibrating the fluorescence for calculating $[Ca^{2+}]_i$, the fluorescence intensity of every time point was divided by the fluorescence intensity at the first time point measured (F/F0). Thus, all cells start at an F/F0 ratio of 1 and differences according to unequal dye loading are compensated. However, this method is vulnerable for pre-stimulated cells. These are cells which show an increased $[Ca^{2+}]_i$ from the beginning of the experiment on, even before the actual stimulation. As this situation cannot be distinguished from a cell which expresses a high amount of dye, this normalization might lead to smaller ratios after stimulation if the increased fluorescence from the beginning only rises to a smaller relative amount compared to not pre-stimulated cells. However, by acquiring several measurements, this discrepancy should be balanced out.

Thus, the ratiometric measurement of $[Ca^{2+}]_i$ using a cell permeant dye as well as the expression of a genetically encoded Ca^{2+}-sensitive dye provide specific advantages and disadvantages. Nonetheless, both methods provide a good readout in their specification. However, there are further consideration in measuring $[Ca^{2+}]_i$ arising from the measurement protocol which are discussed in the next section.

5.1.3 Ca^{2+} contamination within nominal Ca^{2+} free buffers

2ME2 addition to Jurkat T lymphocytes in nominal Ca^{2+} free buffer induced a very tiny reduction in $[Ca^{2+}]_i$, as it can be seen in Figure 4A. On the one hand, this might be due to a reduction in resting $[Ca^{2+}]_i$. As even under resting conditions Ca^{2+} flows from the ER into the cytosol by Ca^{2+} leakage and back by Ca^{2+} reuptake, 2ME2 might interfere with this signalling pathway. On the other hand, small amounts of Ca^{2+} might be present in nominal Ca^{2+} free measurement buffer which might enter cells by STIM activated Orai channels in response to thapsigargin induced ER depletion. Thus, 2ME2 might also interfere with this pathway. Ca^{2+} contaminations within nominal Ca^{2+} free measurement buffer might arise from high-purity water solving Ca^{2+} out of bottles and

cylinders or arise from chemicals used for preparing buffers (Bers et al., 2010). Ca^{2+} concentrations of nominal Ca^{2+} free buffers are considered to range from 1 to 3 µM (Bers et al., 2010).

Bottles and cylinders used for buffer preparation were made of plastic. Furthermore, buffers were prepared with fresh high-purity water to minimize the amount of Ca^{2+} present (Bers et al., 2010). Thus, the amount of Ca^{2+} contamination by these mechanisms should be negligible.

According to the specification sheets, $MgSO_4$ as well as NaH_2PO_4 contain less than 50 µg/g Ca^{2+} each and KCl contains a maximum of 10 µg/g Ca^{2+}. As the buffer consists of 5 mM KCl, 1 mM $MgSO_4$ and 1 mM NaH_2PO_4, the overall Ca^{2+} contamination would sum up to 150 nM if the maximum values are considered to be the actual amount of Ca^{2+} present in the chemicals. As $[Ca^{2+}]_i$ is measured to be about 80 nM right before compound addition, there is a little concentration gradient which might in principle result in a small Ca^{2+} entry.

The more likely source for Ca^{2+} in the nominal Ca^{2+} free buffer does not originate from the chemicals but from the procedure of extracellular buffer exchange. During Fura2 loading, the extracellular buffer contains Ca^{2+} which is exchanged directly before starting the measurement by nominal Ca^{2+} free buffer. Therefore, cells were pelleted and Ca^{2+} measurement buffer was carefully removed via an Eppendorf pipette. This removal was a trade-off between discarding the Ca^{2+} containing extracellular buffer as completely as possible and not rupturing the cell pellet. A remaining volume of 10 µl of Ca^{2+} measurement buffer would result in an extracellular Ca^{2+} concentration of about 10 µM which might be sufficient for Ca^{2+} entry after ER depletion via thapsigargin. Nevertheless, the resulting $[Ca^{2+}]_i$ would only be slightly elevated compared to the increase after Ca^{2+} re-addition. To avoid Ca^{2+} contamination, cells could have been washed once in nominal Ca^{2+} free measurement buffer before measurements were started. This would have decreased free Ca^{2+} concentrations to 100 nM by calculating with the same values as above. This amount would just be slightly above the resting $[Ca^{2+}]_i$ in Jurkat T lymphocytes which is thought not to be sufficient for a substantial Ca^{2+} entry via CRAC channels. Nevertheless, this washing step was not performed as only 2ME2 addition showed a decrease in $[Ca^{2+}]_i$ while its derivatives showed a similar inhibition of Ca^{2+} entry after Ca^{2+} re-addition assuming that Ca^{2+} concentrations in nominal Ca^{2+} free measurement buffer is too small to evoke a substantial Ca^{2+} entry.

Furthermore, the washing step was not performed to not harm the cells too much as some cells would always be removed or lysed during centrifugation leading to cell loss.

Substantial amounts of extracellular Ca^{2+} would have also been seen in an increased $[Ca^{2+}]_i$ after thapsigargin addition and before compound addition. $[Ca^{2+}]_i$ after thapsigargin addition transiently increased and almost completely returned to $[Ca^{2+}]_i$ obtained before thapsigargin addition. This small increase might be due to a small amount of Ca^{2+} entry. The more likely source is a higher $[Ca^{2+}]_i$ due to decreased Ca^{2+} clearance.

As only 2ME2 decreased $[Ca^{2+}]_i$ immediately after compound addition, this observation might also point to an additional effect of 2ME2 compared to other compounds. This could be an enhanced removal of $[Ca^{2+}]_i$ by an increased Ca^{2+} uptake into mitochondria by MCUs or via an enhanced Ca^{2+} extrusion to the extracellular space by PMCAs. As an increased permeation rate per se is not very likely, 2ME2 might decrease the amount of inhibition or shift the conditions of activation of these channels. 2ME2 might shift this activation of the MCU towards concentrations below the resting $[Ca^{2+}]_i$ in Jurkat T lymphocytes which was measured to be about 80 nM. Further studies would be necessary to validate this hypothesis.

5.2 Steroids and non-steroidal compounds inhibit Ca^{2+} entry

The object of this study was to investigate the role of 2ME2, steroidal hormones as well as 2ME2 derivatives concerning their impact on Ca^{2+} signalling pathways. As 2ME2 inhibits Ca^{2+} dependent NFAT translocation in T lymphocytes (Duncan et al., 2012), it is likely that 2ME2 directly interferes with Ca^{2+} signalling pathways. 2ME2 is an endogenous E2 metabolite which like E2 as well as other steroid hormones interferes with T lymphocyte activation (e.g. (Duncan et al., 2012; Engler et al., 2017; Paavonen et al., 1981). Therefore, I also investigated the impact of E2, E1, E3, Prog and Tes as well as Chol on Ca^{2+} signalling in T lymphocytes. 2ME2 was further shown before to interfere with tumor cell growth (Leese et al., 2005). Its potency might be increased by derivatisation (Bubert et al., 2007; Dohle et al., 2014a, 2014b; Jourdan et al., 2010, 2011; Leese et al., 2006, 2008, 2010). Thus, I also investigated the impact

of synthetic 2ME2 derivatives in Ca^{2+} signalling. Furthermore, I unravelled the underlying mechanism.

5.2.1 Prog and E2 inhibit Ca^{2+} entry in T lymphocytes

E2, E1, E3, Prog and Tes influence cytokine production by T_{eff} lymphocytes (Correale et al., 1998; Matejuk et al., 2001; McMurray et al., 2001; reviewed in Khan & Ahmed, 2016) which can be modulated by Ca^{2+} signals (for details, see section 1.2.1 “Activation of T lymphocytes”). Furthermore, E2, Prog and Tes have been shown before to influence Ca^{2+} signalling in T lymphocytes (Azenabor & Hoffman-Goetz, 2001; Benten et al., 1997, 1999; Ehring et al., 1998) as well as in STIM and Orai transfected HEK cells (Sheridan et al., 2013). Thus, I investigated the impact of these endogenous steroids on Ca^{2+} signalling in T lymphocytes.

Only Prog and E2 affected the $[Ca^{2+}]_i$ increase after T lymphocyte stimulation in Jurkat T lymphocytes, which is shown in Figure 5. Interestingly, Tes did not influence Ca^{2+} signalling pathways investigated in this study. This was a surprising result as Benten et al. (1997, 1999) demonstrated a rapid activation of Ca^{2+} entry in T lymphocytes after Tes addition. However, this was not confirmed in the current study. This discrepancy is most probably due to differences in the protocol. I used a protocol in which I added the compounds after ER depletion in nominal Ca^{2+} free buffer. Thus, Tes specific Ca^{2+} entry was not demonstrated by my measurement protocol as an increase in $[Ca^{2+}]_i$ after Ca^{2+} re-addition might either arise from compounds tested for their impact on Ca^{2+} entry or from ER depletion by thapsigargin. However, Tes does not increase $[Ca^{2+}]_i$ after Ca^{2+} re-addition compared to DMSO measurements.

Inhibition of Ca^{2+} entry in T lymphocytes by E2 has not been shown before. However, E2 was shown to inhibit STIM1 phosphorylation leading to impaired Ca^{2+} signalling which was shown in STIM and Orai transfected HEK293 cells (Sheridan et al., 2013). Further, Prog was just recently shown to protect mice from EAE symptoms and increased T_{reg} lymphocyte population in cells cultured for 48 h at 1 µM (Engler et al., 2017). This observation is most likely explained by inhibition of T_{eff} lymphocytes which

were suppressed by a glucocorticoid dependent pathway resulting in a relative increase in T_{reg} lymphocyte population. But as Ca^{2+} signalling plays a crucial role in T lymphocyte activation and proliferation, my results point to a downregulation of T_{eff} lymphocytes by inhibiting Ca^{2+} signalling pathways. These are more important in T_{eff} than in T_{reg} lymphocytes which is shown by natural T_{reg} lymphocytes being less affected by CRAC inhibition (Jin et al., 2013).

E1, E3 and Tes have also been shown to inhibit T_{eff} lymphocytes and influence Ca^{2+} signalling as well as cytokine production (Correale et al., 1998; Lieberherr & Grosse, 1994) although the effect mediated by Tes might be mediated after the conversion to E2 as it was suggested by Behl & Holsboer (1999). However, my results suggest that these steroid hormones in addition to Chol do not influence Ca^{2+} entry.

Although E2 is known to inhibit ion channels in many cell types including Ca^{2+} channels (e.g. Ruehlmann et al., 1998; Zhang et al., 1999), it has not been shown yet to inhibit Ca^{2+} entry in T lymphocytes. Thus, my study provides new information on a possible mechanism by which at least E2 and Prog might inhibit T lymphocyte activation.

5.2.2 2ME2 and its derivatives inhibit Ca^{2+} entry in T lymphocytes

One metabolite of E2 is 2ME2 which inhibits NFAT translocation in human T lymphocytes (Duncan et al., 2012). As NFAT translocation highly depends on an increased $[Ca^{2+}]_i$ (for details see section 1.2.1 “Activation of T lymphocytes”), 2ME2 might interfere with Ca^{2+} signalling pathways in T lymphocytes.

Figure 4 clearly shows an inhibition of 2ME2 on Ca^{2+} entry in T lymphocytes which has not been described before. 2ME2 inhibited Ca^{2+} entry in T lymphocytes with an IC_{50} of 20 µM which is almost 3 fold lower compared to E2.

As it is known from cancer studies, 2ME2 inhibits cancer cell proliferation (Fotsis et al., 1994; Leese et al., 2005). Further studies investigated the impact and the potency of 2ME2 derivatives which were also shown to inhibit cell proliferation more potently compared to 2ME2 (Bubert et al., 2007; Dohle et al., 2014a, 2014b; Jourdan et al., 2010, 2011; Leese et al., 2006, 2008, 2010). Some of these compounds were tested in the current study for their impact on Ca^{2+} signalling pathways in Jurkat T

lymphocytes. The most potent compounds showed IC_{50} values of about 1 µM. STX564, one of the most potent compounds, was also effective in inhibiting Ca^{2+} entry T_{MBP} lymphocytes from rats which differ from Jurkat T lymphocytes e.g. in the expression certain ion channels like K^+ channels. It is known from human T lymphocytes that $K_{Ca}3.1$ is expressed in primary T lymphocytes while $K_{Ca}2.2$ is expressed in Jurkat T lymphocytes (Jäger et al., 2000; Logsdon et al., 1997). STX564 inhibited SOCE in rat as well as in Jurkat T lymphocytes, indicating that this mechanisms is not specific to one of these K^+ channel subtypes.

5.2.3 Relevance of 2ME2's modifications

Among all 2ME2 derivatives analysed in this study, the most potent compounds possessed an ethyl group at C2 in combination with a hydrogen bond acceptor group at C17 which is different from a sulfamoyloxy group. The hydrogen acceptor group includes either an oxopropyl, a cyanomethyl or a nitromethyl group. The modification of 2ME2 derivatives are considered to inhibit Ca^{2+} entry specifically because 2ME2 derivatives inhibited Ca^{2+} entry more potently. Further, this effect does not arise from insertion of the compounds into the plasma membrane which is known for cholesterol by forming lipid rafts (reviewed in Pani & Singh, 2009).

Slightly less efficient than the ethyl group is a methoxy group at C2, pointing towards a lipophilic alkyl group being more efficiently than a hydrophilic ether group. However, a 2-methoxy group is more potent than a hydrogen at C2. One exception is STX49 which is more potent than the corresponding 2-methoxy compound STX140. Maybe, in this particular case, sulfamoyloxy groups at C3 and C17 are important for the increased potency. All other compounds do not tremendously change IC_{50} values in dependence of sulfamoyloxy groups (e.g. see Figure 6B, C). However, sulfamoyloxy groups are more hydrophilic and might therefore be advantageous in increasing the bioavailability as it has been shown for STX140 in rat and mouse models of cancer because, in contrast to 2ME2, it is not metabolised (Ireson et al., 2004). They showed that STX140 possessed a bioavailability of 85 % whereas 2ME2 was taken up to a very much lesser extent (<1 %). The higher bioavailability makes a compound more

suitable as a potential new drug, as less compound is required to obtain the same effect compared to a compound with lower bioavailability.

A methoxy group covalently bound to an aromatic ring was also shown to increase potencies of other compounds inhibiting Ca^{2+} entry (Djillani et al., 2014; Ng et al., 2008). One of these compounds is 2-aminoethyl diphenylborinate (2-APB). 2-APB shows a biphasic effect on Ca^{2+} entry which is evoked after ER depletion resulting in a potentiation of Ca^{2+} entry at 5 µM and an inhibition at 30 µM (Djillani et al., 2014). Although 2-APB in general looks quite different from 2ME2 and its derivatives, the presence of one or two methoxy groups decreases the potentiation at 5 µM, although these side groups do not change the concentration of maximal inhibition (Djillani et al., 2014). Thus, the 2-position at the 2ME2 derivatives is considered to be important for the interaction of the compounds with their target. Furthermore, Synta66 is a well-known inhibitor for CRAC channels although the exact mechanism of inhibition is not revealed by now (Ng et al., 2008). This compound possesses two methoxy groups covalently bound to a terminal aromatic ring (Ng et al., 2008). However, 2-APB as well as Synta66 have been described to possess a low specificity as well as a high toxicity, preventing them from being used in clinical studies (Tian et al., 2016).

A hydrogen bond acceptor at C17 is highly efficient irrespective of which group exactly it is, suggesting that this group stabilizes the binding between the compound and its target and thereby increases the specificity. A positive effect of this group was also shown in the context of cancer treatment. In these experiments, compounds which possess a hydrogen bond acceptor at C17 were more potent than compounds with hydrogen groups at this position (Jourdan et al., 2010, 2011; Leese et al., 2008). However, studies performed with cancer cells revealed that the hydrogen bond acceptor property of a sulfamoyloxy group at C17 is the striking effect of this group. In my study, derivatives with sulfamoyloxy groups were almost equally potent as hydroxyl derivatives. This observation suggests that the overall mechanism seems to differ between cancer cells and T lymphocytes.

Thus, the effects of the side groups are quite ambiguous except for compounds with the hydrogen bond acceptor at C17 different from a sulfamoyloxy group, indicating that this class of groups is the most specific and the most important group for reducing Ca^{2+}

entry. However, as addition of oxopropyl, nitromethyl or cyanomethyl groups highly increase lipophilicity (see Figure 14A) as well as the compound's size, these features might be more important for interference with Ca^{2+} entry than the side group itself. Particularly lipophilicity might facilitate compounds crossing plasma membranes to reach intracellular targets. Furthermore, interaction with the target might require a hydrophobic interaction.

Although the compounds' potencies correlate with their lipophilicity (see Figure 14A), there is also a clear effect of the side groups. If the compound's potency would solely depend on its lipophilicity, E2 would be expected to be more potent compared to 2ME2. But instead, the IC_{50} values shown in Table 2 indicate that 2ME2 is more potent which is shown by the decreased IC_{50} value. Furthermore, Chol should have strong effects on the prevention of Ca^{2+} entry as this compound has a cLogP value of about 9.5 (Achrem-Achremowicz et al., 2010). Thus, Chol is much more lipophilic than all other compounds tested in this study but did not interfere with Ca^{2+} entry at concentrations up to 100 µM.

5.2.4 Compound concentrations

Relevance of side groups also resembles the specificity of binding which is important for a low concentration range of action. However, IC_{50} values of 2ME2, E2 and some other compounds are quite high and thus in a concentration range which is considered unspecific according to Falkenstein and colleagues who claim that an action is assumed to be unspecific at concentrations above 10 µM (Falkenstein et al., 2000). Nonetheless, the most potent compounds show IC_{50} values at about 1 µM or even below which can be considered specific. But these concentrations are still quite beyond physiological concentrations. The physiological concentration for E2 ranges between approximately 200 pM (Bebo et al., 2001; Pozzilli et al., 1999) and below 300 nM (Elenkov et al., 2001) in females and rises to values above 5 µM during pregnancy (Elenkov et al., 2001). The serum level of 2-methoxyestrogens range from 30 pM in adult males and peaks in the last trimester of pregnancy at about 1 nM (Shen et al., 2014; reviewed in D'Amato et al., 1994). One further hormone which showed a substantial inhibition of Ca^{2+} entry in this study is Prog whose physiological

concentration ranges between 10 and 25 nM in non-pregnant women (Bansil et al., 1999; Elenkov et al., 2001; Pozzilli et al., 1999) and rises to 300 nM (Cahalan et al., 2001) or above 450 nM (Elenkov et al., 2001) during pregnancy. Notably, these concentrations are peripheral concentrations. This means that local concentrations, e.g. at the place of production, are probably higher, maybe even in the range of the IC_{50} values I measured for Ca^{2+} entry inhibition as it was assumed for Prog by Cahalan and colleagues (Cahalan et al., 2001). This would suggest a decreased Ca^{2+} entry in T lymphocytes by these compounds might be a very local effect which only takes place in close proximity to the placenta, an event which might favour the feto-maternal immunotolerance (reviewed in Arck & Hecher, 2013).

Besides these local effects of high concentrations, it is further likely that the compounds cause further effects after hours to days after application like modulating protein expression levels. The latter effects might be present at lower compound concentrations as it has been described before, for example for 2ME2 (Attalla et al., 1996; Josefsson & Tarkowski, 1997) and E2 (McMurray et al., 2001). E2 supress IL-2 production at high concentrations in a short-term assay and at a low concentration upon long-term incubation by decreasing IL-2 transcription factors NF-κB and AP1 and also by downregulating IL-2 receptor (McMurray et al., 2001). Furthermore, proliferation of Jurkat T lymphocytes can be inhibited by 1 µM 2ME2 noticeably after 2 h of treatment (Attalla et al., 1996).

In this study, I investigated the acute effects which take place within seconds to minutes after compound application which most likely resemble direct effects on ion channels or pumps rather than changes in protein expression levels. Upon a long term incubation of the compounds, they might be effective at lower concentrations in an assay which resembles more an *in vivo* treatment. However, the concentration of the compounds given as a treatment may be lower at the target because they are either diluted with body fluids, like blood or lymph, or they are filtered by the liver or the kidneys. Kulke et al. (2011) have shown that patients suffering from cancer who received an oral dose of 1 g Panzem® NCD every six hours developed a steady-state maximal concentration of 210 nM in the periphery. Panzem® NCD is the nanocrystalline form of 2ME2 which was shown to increase the bioavailability of 2ME2 (Matei et al., 2009). However, this concentration is still beyond the physiological

concentration of 2ME2 pointing to the possibility that there might be locally higher concentrations which convey antitumor effects.

5.3 Target for decreasing Ca^{2+} entry in T lymphocytes

As Ca^{2+} signals are modulated by many pathways, there are several possible targets by which the compounds might act. These targets encompass estrogen receptors as the compounds are metabolites or derivatives of estradiol. Furthermore, Ca^{2+} release, Ca^{2+} clearance and Ca^{2+} entry mediating ion channels and pumps might be valid targets. These mechanisms were described in detail in section 1.2.1 “Activation of T lymphocytes”, were intensively investigated in the results section and are discussed in this section which starts with the discussion of the engagements of estrogen receptors.

5.3.1 Estrogen receptors

Steroid hormones and their derivatives were investigated in this study making estrogen receptors a valid target (Danel et al., 1983; reviewed in Khan & Ahmed, 2016). Classical estrogen receptors are transcription factors which bind estrogens in the cytosol, translocate to the nucleus and modulate gene expression levels. Estrogen receptors are divided into two subtypes, namely ERα and ERβ, both of which are expressed in T lymphocytes and are considered to mediate pro- as well as anti-inflammatory responses (Danel et al., 1983; Maselli et al., 2016). Modulation of gene expression involves the synthesis and modification of mRNA, the formation of proteins as well as the transport of the proteins to their target compartment. This process takes about 7.5 to 30 min (reviewed in Wehling, 1997). Estrogens are believed to affect innate immune cells in general by involving estrogen receptors (Kovats, 2015) and signalling by ERα is required for the anti-inflammatory effects of E2 in EAE (Lélu et al., 2011). Actions evoked by E2 include downregulation of IL-2 receptor expression in murine thymocytes (Azenabor & Hoffman-Goetz, 2001; McMurray et al., 2001), modulation of secretion of IFN-γ in Th1 lymphocytes and IL-4 in Th2 lymphocytes but also TNF-α and IL-17 secretion (Azenabor & Hoffman-Goetz, 2001; McMurray et al.,

2001; controversially discussed in Khan & Ahmed 2016). Furthermore, engagement of ERα by E2 is considered to stimulate T_{reg} lymphocytes (Polanczyk et al., 2004).

As the engagement of estrogen receptors usually takes several minutes (Wehling, 1997) and Ca^{2+} entry is inhibited within seconds after compound addition (see Figure 15), engagement of classical estrogen receptors and a change in gene expression levels are unlikely to be involved in decreasing Ca^{2+} entry. Additionally, Garidou et al. (2004) found that the protective effect of E2 in the context of EAE was mediated to a negligible degree by the ERα. Also 2ME2 was found to inhibit the proliferation and activation of microglia by an estrogen receptor independent mechanism (Schaufelberger et al., 2016). Furthermore, 2ME2 was shown in this study to be 2.5 fold more potent than E2 but does not evoke any sex hormone effect (Josefsson & Tarkowski, 1997) and binds to the ERα 500 fold and to the ERβ 3200 fold less affine (LaVallee et al., 2002). Furthermore, 2ME2 was shown to not induce uterine growth (Martucci & Fishman, 1979) and thereby is considered to be non-estrogenic. However, Lee and colleagues claim that 2ME2 indeed binds to and activates estrogen receptors, but also decrease the level of ERα expressed (Lee et al., 2015).

However, if the decrease of Ca^{2+} entry in the current study would be mediated solely by binding of 2ME2 and its derivatives to estrogen receptors, one would expect that steroidal compounds, like E2, are more effective than its non-steroidal metabolite 2ME2 or its derivatives as it binds the estrogen receptors much more specific (LaVallee et al., 2002). In fact, the results showed that 2ME2 is even more potent than E2 (see Figure 4 and Figure 5) which points towards a mechanism which does not involve a genomic action of the classical estrogen receptors. Therefore, 2ME2 and also its derivatives are considered to inhibit Ca^{2+} entry without the involvement of classical estrogen receptors.

Besides classical estrogen receptors, there are also G protein-coupled estrogen receptors (GPER, GPR30) which bind E2 and mediate rapid non-genomic estrogen signalling (Yates et al., 2010; reviewed in Prossnitz & Barton, 2014). These rapid non-genomic events evoked by hormones take place within some seconds up to a few minutes and are most likely mediated by the engagement of proteinlipase C, phosphoinositide turnover, changes in the intracellular pH and $[Ca^{2+}]_i$ as well as

proteinkinase C and tyrosine activity most of which actions are considered to be specific (reviewed in Wehling, 1997). Thus, an engagement of GPER might be more plausible than engagement of the classical estrogen receptors. Nonetheless, E2 would be expected to show a higher potency compared to 2ME2 if GPER are the main target for Ca^{2+} entry inhibition. But as 2ME2 is more potent than E2, an involvement of GPER seems not to be the main target if at all.

5.3.2 Ca^{2+} release channels

I focussed on the mechanisms which directly modulate Ca^{2+} signalling because classical as well as the G protein-coupled estrogen receptors likely do not account for Ca^{2+} entry inhibition. As steroids can also directly bind and modulate ion channels conductivity, they are a putative target (reviewed in Miller, 2010). One plausible mechanism would involve inhibition of Ca^{2+} release channels like IP_3R and RyR or decreased formation of their ligands. This would be a new mechanism for steroid hormones which was not described before. However, the opposite effect, namely the stimulation of Ca^{2+} release channels by steroid hormones, has been described several times (Marino et al., 1998; Morley et al., 1992).

In general, after TCR engagement, second messengers are formed after several phosphorylation steps as it is described in detail in section 1.2.1 “Activation of T lymphocytes”, part “Second messenger formation”. If second messenger formation is inhibited, neither Ca^{2+} release by IP_3R and RyR nor Ca^{2+} entry would be evoked. Therefore, $[Ca^{2+}]_i$ would not increase upon TCR stimulation. The same would be true if the compounds directly inhibit Ca^{2+} release channels IP_3R and RyR.

However, inhibiting Ca^{2+} release by 2ME2 and its derivatives as the main target for decreasing Ca^{2+} entry in T lymphocytes can be excluded due to the experimental protocol (see e.g. Figure 4A). Thapsigargin evokes SOCE by inhibition of SERCA pumps and thus prevent Ca^{2+} reuptake into the ER (Lytton et al., 1991). As Ca^{2+} continuously leaks out of the ER, the ER depletes of Ca^{2+} over time leading to SOCE activation. Thus, the stimulation of cells by TG provides a measurement of $[Ca^{2+}]_i$ increase independently of second messenger formation and phosphorylation steps required for this formation. However, TG was added several minutes before compound

addition resulting in a complete ER depletion when the compounds were added. If the primary mechanism of action was Ca^{2+} release inhibition, the Ca^{2+} entry would not be affected with stores depleted before. Thus, the inhibition of IP_3R and RyR or formation of their ligands are not considered to be the main target in T lymphocytes.

Nonetheless, several groups have described that steroidal compounds like E2 or Tes to induce Ca^{2+} release and thereby also evoke SOCE (Benten et al., 1998, 1997, 1999; Fiorelli et al., 1996; Lieberherr & Grosse, 1994). In the current study, an increased Ca^{2+} release was not observed with E2 but with STX140 (see Figure 7). STX140 induces a sustained Ca^{2+} release event in nominal Ca^{2+} free buffer which shows a different temporal modulation than a Ca^{2+} release evoked by the αCD3 antibody OKT3. By OKT3 addition, TCR is engaged resulting in second messenger formation causing a Ca^{2+} release from the ER (for details see section 1.2.1 “Activation of T lymphocytes”). This Ca^{2+} release leads to a transient Ca^{2+} signal while STX140 induces a sustained increased $[Ca^{2+}]_i$. As $[Ca^{2+}]_i$ increase by STX140 is decreased upon ER depletion (see Figure 7B), the main source of Ca^{2+} is thought to derive from the ER. However, STX140 as well as STX49, STX139 and STX243 induce an increase in $[Ca^{2+}]_i$ at high concentrations even if the ER is depleted (Figure 6 and Figure 9). This Ca^{2+} most likely arises from further intracellular Ca^{2+} stores like mitochondria or lysosomes because the cells were measured in nominally Ca^{2+} free measurement buffer and the ER was Ca^{2+} depleted by thapsigargin before. As no or very low amounts of Ca^{2+} are present in the ER or in the extracellular space, these sources can be excluded as for Ca^{2+} originating from. Compound mediated Ca^{2+} release from the ER might either arise from an increased sensitivity of IP_3R or RyR in the ER for their ligands or an induced ligand formation. The latter effect was shown for E2 and T (Lieberherr & Grosse, 1994; Marino et al., 1998). However, the exact source of Ca^{2+} as well as the mechanism underlying this observation remains the object of future studies.

5.3.3 Ca^{2+} clearance mediating ion channels and pumps

Besides Ca^{2+} release channels, Ca^{2+} clearance mediating ion channels and pumps are a possible target for decreasing Ca^{2+} entry. These channels include (i) PMCAs mediating Ca^{2+} extrusion to the extracellular space, (ii) SERCAs pumping Ca^{2+} back

into the ER (so-called Ca^{2+} reuptake) and (iii) MCUs mediating Ca^{2+} uptake into mitochondria (for details see section 1.2.1 “Activation of T lymphocytes”, part “Ca^{2+} signalling pathways”). As Gorska-Ponikowska et al. (2018) showed, 2ME2 affects biogenesis of mitochondria in osteosarcoma cells, however, a direct effect of 2ME2 on MCUs, PMCAs or SERCAs has not been published yet.

Theoretically, an inhibition as well as an activation of these channels results in a decreased $[Ca^{2+}]_i$. If these channels and pumps are inhibited, they would not buffer Ca^{2+} in close proximity to Orai channels upon Ca^{2+} entry and thereby inhibit Orai channels resulting in a decreased Ca^{2+} entry (Hoth et al., 2000). Furthermore, if Ca^{2+} clearance pathways are activated, they would clear the cytoplasm more efficiently which would also result in decreased $[Ca^{2+}]_i$ given that Ca^{2+} clearance would be more efficiently than Ca^{2+} entry. However, these mechanisms include an initial Ca^{2+} entry. But the compounds analysed prevent divalent ions from entering lymphocytes (see Figure 16). Upon addition of Mn^{2+} to the extracellular buffer instead of Ca^{2+}, Mn^{2+} enters the cells and quenches Fura2 (Grynkiewicz et al., 1985; Sage et al., 1989). Quenching is blocked by addition of 2ME2 and its derivatives. Therefore, the inhibitory mechanism is Ca^{2+} dependent. The possibility that Orai channels are inhibited by an increased local Ca^{2+} concentration due to insufficiently cleared Ca^{2+} ions is excluded. Furthermore, an increased Ca^{2+} clearance mechanism can also be excluded as this mechanism would also require Ca^{2+} entry first. Thus, decreasing Ca^{2+} entry by 2ME2 and its derivatives directly involves Orai channels mediating Ca^{2+} entry or K^+ channels maintaining Ca^{2+} entry.

5.3.4 Ca^{2+} entry channels and K^+ channels

Ion channels and pumps mediating Ca^{2+} release as well as Ca^{2+} clearance were excluded as main targets for decreasing Ca^{2+} entry as discussed before. In this section, I address Ca^{2+} entry channels and K^+ channels.

Ca^{2+} entry maintaining K^+ channels

Ion channels maintaining Ca^{2+} entry include K^+ channels of which the $K_V1.3$ as well as the $K_{Ca}3.1$ ($K_{Ca}4$, IK1, primary T lymphocytes) and the $K_{Ca}2.2$ (SK2, Jurkat T lymphocytes) are expressed in human T lymphocytes (Chandy et al., 1990; Jäger et al., 2000; Logsdon et al., 1997). K_V channels mainly maintain the resting potential while K_{Ca} channels are activated upon an increase in $[Ca^{2+}]_i$ and are highly upregulated upon mitogen stimulation (Grissmer et al., 1993; reviewed in Lewis & Cahalan, 1995). K^+ channels maintain the electrical gradient for Ca^{2+} by a K^+ efflux and are necessary for a sustained Ca^{2+} entry and T lymphocyte activation (Beeton et al., 2001a). K_V channels activate by a change in membrane potential whereas K_{Ca} channels open upon an increased $[Ca^{2+}]_i$ (reviewed in Cahalan et al., 2001). The importance of these channels in T lymphocytes activation is indicated by inhibition of $K_V1.3$ channels ameliorating EAE symptoms and inhibiting T lymphocytes activation (Beeton et al., 2001a, 2001b). Furthermore, 2ME2 was shown to inhibit K_{Ca} channels in human vascular endothelial cells (Chiang & Wu, 2001). Additionally, 2ME2 as well as other steroids like E2 and Prog inhibit the K^+ driving force (Kitazawa et al., 1997).

I investigated the impact of the compounds on K^+ channels via patch clamp recordings. The main outward current is mediated by $K_V1.3$ channels which was inhibited by the specific $K_V1.3$ blocker ShK-Dap22 (see Figure 17). Currents evoked by $K_V1.3$ channels were not affected by addition of 10 µM STX564 which efficiently blocked Ca^{2+} entry. Therefore, STX564 does not inhibit $K_V1.3$ channels in Jurkat T lymphocytes.

Addition of 1 µM free cytosolic Ca^{2+} activates K_{Ca} channels (Grissmer et al., 1992). The currents which were recorded under these conditions did not differ largely from the measurements without Ca^{2+} in the intracellular buffer (see Figure 17 and Figure 18). These results were surprising because K_V channels usually undergo use-dependent inactivation which is counteracted by rather long intersweep intervals at voltages below -40 mV when measuring $K_V1.3$ channels. There are different explanations for these results which are discussed below.

On the one hand, the concentration of ShK-Dap22 might have been too high which might also inhibit other ion channels, like K_{Ca} channels. This possibility is considered to be rather unlikely because $K_{Ca}2.2$ channel was shown to be not inhibited at 250 nM ShK-Dap22 in Jurkat T lymphocytes (Fanger et al., 2001).

On the other hand, the free Ca^{2+} concentration in the buffer might differ from the calculated one (see also section 5.1.3 “Ca2+ contamination within nominal Ca2+ free buffers”). This might on the one hand include a free Ca^{2+} concentration in the ICB K_{Ca} far below 400 nM which resembles the IC_{50} concentration for $K_{Ca}2.2$ activation (Grissmer et al., 1992). On the other hand, the free Ca^{2+} concentration in the ICB K_V might have been above 400 nM which might also activate K_{Ca} channels and might be reached as the cells were stimulated with TG for several minutes. The latter possibility is considered to be unlikely because the ICB K_V buffer included the Ca^{2+} chelator BAPTA. Thus, even Ca^{2+} entry during thapsigargin stimulation should not activate K_{Ca} channels efficiently. A free Ca^{2+} concentration below 400 nM in the ICB K_{Ca} buffer is also considered to be rather unlikely as there are other research groups which used this technique to calculate free Ca^{2+} concentrations and they were able to record K_{Ca} channels (e.g. Fanger et al., 2001).

Although preparation of ICB K_{Ca} was performed carefully, one further mistake might arise from the pH electrode and pH adjustment. If the ionic strength of the buffer differs largely from the ionic strength of calibration solutions used for pH meter calibration, the measured pH in the buffer might largely differ from the solution’s actual pH (Bers et al., 2010). This ionic strength difference might result in a divergence of free Ca^{2+} concentrations by a factor of two to three from the calculated and the actual Ca^{2+} concentration (Bers et al., 2010). However, if one considers a free Ca^{2+} concentration of 1 µM, a threefold lower Ca^{2+} concentration would result in roughly 300 nM which is just below the IC_{50} concentration for activation of the channels (Grissmer et al., 1992). But as the buffer contains commonly used ion concentrations (Fanger et al., 2001), this possibility is thought to be also rather unlikely although the ionic strength of the calibration solutions is not indicated. One possible method to determine free Ca^{2+} concentrations within buffers would require the measurement with a Ca^{2+} electrode or the addition of Ca^{2+}-sensitive dyes which convey problems on their own (Bers et al., 2010).

One further explanation is a low K_{Ca} expression, if at all, and too small currents to be relevant for K^+ currents measured. This thesis is further supported by the observation that 10 nM of the specific K_{Ca} blocker UCL1684 had no effect on the currents measured which was efficient to block K_{Ca} currents in other studies (Fanger et al., 2001). Although Fanger and colleagues measured K_{Ca} channels in Jurkat T lymphocytes (Fanger et al., 2001), it has been shown that different T lymphocyte subsets express different levels

of K_{Ca} channels. For example, Th1 lymphocytes convey larger K_{Ca} currents in combination with little Ca^{2+} extrusion resulting in increased Ca^{2+} entry compared to Th2 lymphocytes (Fanger et al., 2000). Although Grissmer and colleagues suggest that Jurkat T lymphocytes express about 400 K_{Ca} channels (Grissmer et al., 1992). K_{Ca}2.2 channels are characterized by a small conductivity of 4 – 7 pS in 170 mM extracellular K^+, 400 K_{Ca} channels would evoke a current of -190 to -340 pA at -120 mV. These currents were not seen in this study most likely due to lower extracellular K^+ concentrations (40 mM). However, Fanger et al. (2001) report about -50 pA currents at -100 mV in Jurkat T lymphocytes measured with 40 mM extracellular K^+. These currents were inhibited by 10 nM UCL1684 (Fanger et al., 2001). Currents in the current study were not inhibited by 10 nM UCL1684, indicating that K_{Ca} channels are not expressed in the cells used in this study.

Furthermore, expression of ion channels underlies cell cycle dynamics (Cahalan et al., 2001). Thus, the most likely explanation for the absence of K_{Ca} currents in the current study is that the T lymphocytes measured in the current study do not express K_{Ca} channels at an efficient amount. As Beeton et al. (2001b) demonstrated, inhibition of K_{Ca}3.1 channels expressed in primary rat T lymphocytes, do not ameliorate EAE symptoms, indicating that K_{Ca} channels might not be important in downregulating T cells in this disease.

Ca^{2+} entry channels

Finally, CRAC channels were investigated by transfecting Jurkat T lymphocytes with genetically encoded Ca^{2+} indicators which were covalently bound to Orai channels. This method allows detection of local Ca^{2+} concentrations in close proximity to Orai channels (Dynes et al., 2016). These experiments showed that GECO's fluorescence was highly decreased upon compound addition compared to control experiments (see Figure 19). Fluorescence intensities directly correlate with the amount of Ca^{2+} bound to the indicator which increases upon an increased local Ca^{2+} concentration (Dynes et al., 2016). These experiments show that 2ME2 and its derivatives inhibit Ca^{2+} entry mediated by Orai channels. These results indicate that other channels are not affected which can be activated by STIM upon a depleted ER, like transient receptor potential (TRP) channels (Huang et al., 2006; but see DeHaven et al., 2009).

It cannot be elucidated by these experiments whether the compounds directly bind to Orai channels or to which other specific target they bind and thus, this aspect stays as a subject of future investigations. Possible mechanisms would be a direct binding to Orai channels, an inhibition of STIM or an integration of the compounds into the plasma membrane which might result in a sterically hindered rearrangement of plasma membrane and integrated ion channels. It has been shown for Prog to integrate into plasma membranes of human spermatozoa and thereby decreasing membrane fluidity (Shivaji & Jagannadham, 1992). This possibility would be in line with experiments showing that lipophilicity correlate with an increased potency for inhibiting Ca^{2+} entry (see Figure 13). But it is more likely, that hydrophilic compounds do not bind to the target as specifically as lipophilic compounds due to different structures compared to 2ME2 and its derivatives. Assuming that rather lipophilic compounds bind to the target, this target might be located intracellularly and these compounds are too hydrophilic to enter cells. However, these hydrophilic compounds were shown in studies investigating cancer cell proliferation and are hypothesized to act on the same targets as steroidal compounds (Dohle et al., 2014b). The target of steroidal compounds in cancer cell studies is the steroid sulfatase which is located intracellularly requiring compounds passing the plasma membrane (Leese et al., 2008). Irreversible inhibition of the steroid sulfatase is dependent upon the presence of a sulfamoyloxy group (reviewed in Potter, 2018; Reed et al., 2005).

One further possible mechanism of 2ME2 and its derivatives encompass inhibition of Ca^{2+} entry by interfering binding of STIM and Orai. One mechanism might include a direct inhibition of STIM, e.g. by inhibiting phosphorylation as it has been shown for E2 (Sheridan et al., 2013). However, this inhibition takes several minutes and is therefore considered to be unlikely mediating the rapid inhibition of Ca^{2+} entry shown in the current study (see Figure 15).

Another target might also include disruption of tubulin polymerization which is required for movements within cells and which was shown to be part of the mechanism in cancer cells (Leese et al., 2008). But this process is Ca^{2+} dependent on its own. Therefore, it cannot be specified by these experiments if tubulin is ruptured by a decreased Ca^{2+} entry or if Ca^{2+} entry is inhibited by a ruptured tubulin. However, the results in the current study point to an initial Ca^{2+} entry inhibition as the entry can be rapidly inhibited even if Ca^{2+} entry is established before compound addition (see Figure 15).

This study revealed that 2ME2, a non-steroidal endogenous E2 metabolite, and its derivatives inhibit SOCE in Jurkat T lymphocytes after thapsigargin stimulation by inhibiting the STIM / Orai system of Ca^{2+} entry and thus resembles a new generation of CRAC inhibitors. Ca^{2+} entry inhibition is considered to be the main mechanism for previously described downstream effects like inhibition of NFAT translocation, induction of cell-cycle arrest and inhibition of immune cell proliferation and their mediated immune responses (Duncan et al., 2012).

5.3.5 Further putative targets

Although the results of my study do not hint to further targets, many more targets have been described to which E2, 2ME2 or its derivatives bind. In general, these can be distinguished (i) in targets involving cell architecture by interfering with microtubule assembly or causing a cell cycle arrest in general and (ii) in ion channels as targets.

Many of the compounds analysed in this study were also analysed before in the context of cancer cell inhibition (Foster et al., 2007; Leese et al., 2008). One of these studies showed that the compounds inhibit steroid sulfatase as well as disrupt the polymerization of microtubules (Leese et al., 2008; reviewed in Potter, 2018; Reed et al., 2005). Interestingly, some compounds like STX139, STX505 and STX1306 were less potent than 2ME2 in the cancer cell line MCF-7 while these belong to the most potent compounds in the current study (Bubert et al., 2007; Jourdan et al., 2011; Leese et al., 2008). In contrast to this, hydrophilic compounds like STX2484 where more potent in the cancer cell line DU-145 compared to 2ME2 while this compound did not decreased Ca^{2+} entry in T lymphocytes at concentrations up to 50 µM (Leese et al., 2010). This divergence pinpoints towards different targets in T lymphocytes and tumor cells. The compounds inhibit Orai channels in T lymphocytes as this study has shown while they downregulate steroid sulfatase activity and microtubule polymerisation in cancer cells (Leese et al., 2008; reviewed in Potter, 2018; Reed et al., 2005). One mechanism by which 2ME2 arrests cells in the cell cycle is by binding to the colchicine binding site of tubulin with an IC_{50} of 22 µM and thereby depolymerising it (D'Amato et al., 1994). Furthermore, a pharmacological rupture of microtubules also abolished Ca^{2+} signalling in murine fibroblasts and epithelial cells from pigs (Tombes & Borisy, 1989). They also

showed that transition from metaphase to anaphase requires a sustained increase in $[Ca^{2+}]_i$ which were inhibited by nominal Ca^{2+} free extracellular medium supplemented with Ca^{2+} chelators (Tombes & Borisy, 1989). These studies indicate that 2ME2 and its derivatives might diminish Ca^{2+} entry by interfering with tubulin assembly. But, Attalla and colleagues argue that 2ME2 arrests cells in mitosis without tubulin rupture (Attalla et al., 1996). They mention that the transition from metaphase to anaphase is CaM-dependent and that 2ME2 inhibit CaM activity. Although they claim that 2ME2 does not interfere with Ca^{2+} entry (Attalla et al., 1996), the concentration range of CaM inactivation is comparable to concentrations at which 2ME2 inhibits Ca^{2+} entry in Jurkat T lymphocytes in the current study (see Figure 4A and B). They observe a small CaM inhibition at 1 µM after 5 min and a complete inhibition at 100 µM after 80 s. Nonetheless, an inhibition of Ca^{2+} entry would not activate CaM because its activation depends on an increased $[Ca^{2+}]_i$ (reviewed in Cahalan et al., 2001). Additionally, Attalla and colleagues claim that inhibition of CaM activity resulting in cell cycle arrest is independent of estrogen receptors because this effect was neither interfered by the anti-estrogenic drug toremifen nor could the effect be evoked by E2 (Attalla et al., 1996), being in line with my results (see section 5.3.1 “Estrogen receptors”).

Inhibition of Ca^{2+} signalling pathways and cell cycle arrest might also account for inhibiting proliferation which was shown for up to 100 µM in smooth muscle cells as well as in endothelial cells and splenic cells (Josefsson & Tarkowski, 1997; Nishigaki et al., 1995). These groups also found that 2ME2 is more potent than E2 which was also seen in the current study.

Furthermore, endogenous steroids can directly interfere with ion channels. Possible targets include ATP-dependent Ca^{2+} channels in endothelial cells by E2 and Tes (Hutchison et al., 1997) and L-type Ca^{2+} channels in smooth muscle cells inhibited by E2, 2ME2, E1, Tes or Prog (Cairrão et al., 2012; Kitazawa et al., 1997). T-type Ca^{2+} channels were also shown to be effected by steroids as well as L-type Ca^{2+} channels, voltage-gated Na^+ channels or ATP-dependent K^+ channels of which the latter is decreased upon E2 treatment in whole islets of Langerhans (Hill et al., 2010; Ropero et al., 1999; reviewed in Melcangi et al., 2016).

Besides these multiple targets which were shown to be influenced by steroid hormones as well as 2ME2 and its derivatives, my study provides an additional target for these compounds in Jurkat T lymphocytes as well as in primary rat T lymphocytes which are Orai channels activated by STIM. This mechanism might be the striking mechanism by which 2ME2 ameliorates the symptoms of EAE or pregnancy decreases relapse rates in MS patients. Thus, these compounds provide a new series of CRAC inhibitors which were generated on the basis of endogenous hormones without evoking steroid hormone specific events. Maybe one day, these compounds might be used in generating new drugs for downregulating the immune system which would be efficient for patients suffering from autoimmune diseases like MS.

5.4 Solved and unsolved questions

My thesis clearly shows that 2ME2 and its derivatives inhibit Ca^{2+} entry via the STIM / Orai system in T lymphocytes. Other targets like Ca^{2+} release channels, Ca^{2+} clearance channels and pumps as well as K^+ channels can be excluded as targets for Ca^{2+} entry inhibition. However, it remains unresolved if the compounds interact directly with STIM or Orai channels and how this interaction takes place (Figure 20). One method to measure a potential binding of the compounds to Orai channels would be isothermal titration calorimetry (ITC; reviewed in Krell et al., 2014). This method uses the changes in the enthalpy and entropy which occur upon ligand binding to the protein and manifests in a change of the energy which can be monitored as an endothermal or exothermal binding.

As Sheridan et al. (2013) suggested, E2 inhibits Ca^{2+} entry by interfering with STIM phosphorylation. They showed that this effect takes several minutes while my study clearly demonstrates that Ca^{2+} entry inhibition is an immediate effect. Therefore, it is unlikely that a decreased phosphorylation of STIM resembles the underlying mechanisms. However, to check this possibility, STIM's phosphorylation state can be investigated by purification of 2ME2 treated and stimulated T lymphocytes and analyse the protein via phosphorylation sensitive antibodies or by Phos-tag™ acrylamide gels. The matrix of these gels includes zinc complexes which bind phosphate groups with a high selectivity (Kinoshita et al., 2004). Thus, phosphorylated proteins take longer time

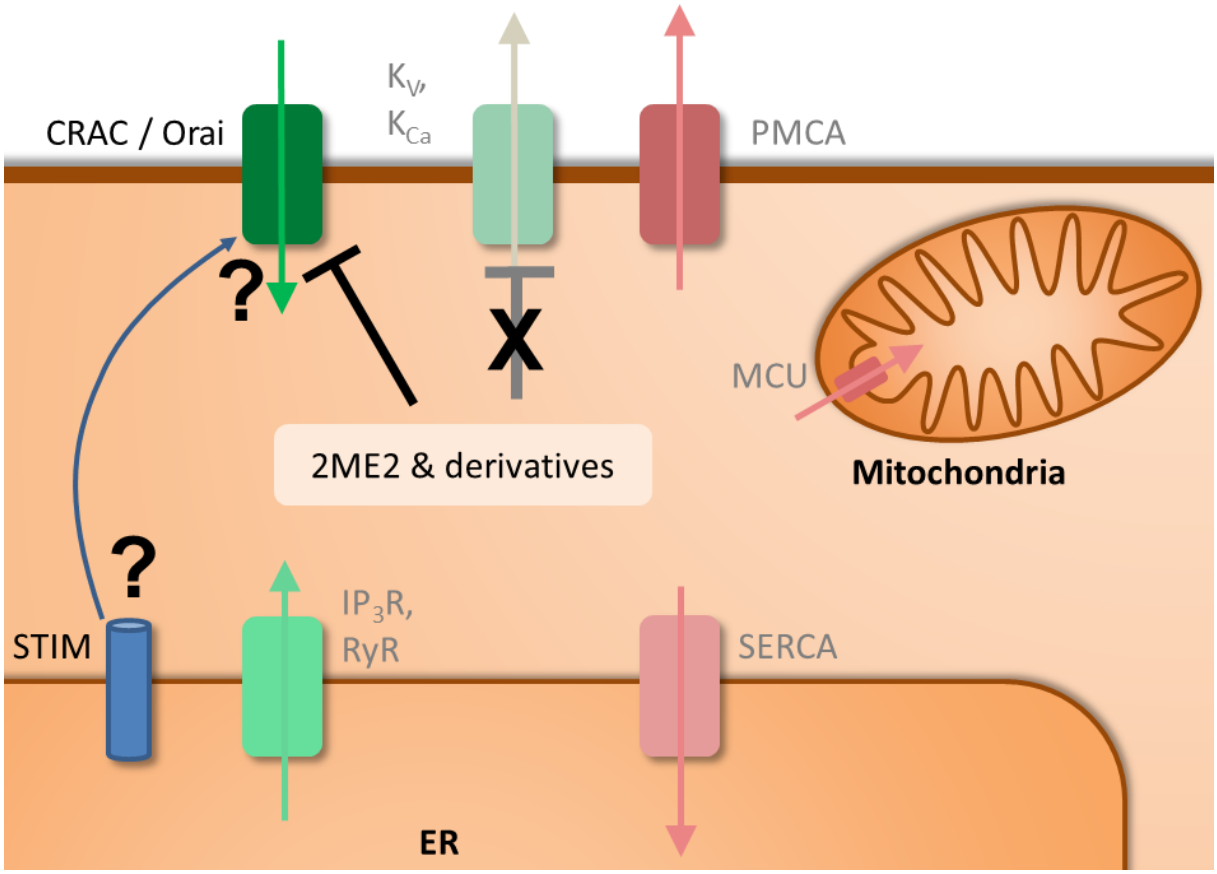

Figure 20: Targets of 2ME2 and its derivatives.

The current study revealed that 2ME2 and its derivatives inhibit Ca^{2+} entry by CRAC channels in T lymphocytes. 2ME2 and its derivatives do not inhibit K^+ channels. Ca^{2+} clearance mediated by PMCAs, MCUs and SERCAs as well as on Ca^{2+} release channels IP_3R and RyR do not account as primary targets for inhibiting SOCE. SERCAs were inhibited by TG before compound addition leading to ER depletion. Thus, SOCE inhibition is independent of Ca^{2+} release. Further, Ca^{2+} clearance require Ca^{2+} entry first which is inhibited by 2ME2 and its derivatives. Ion channels and pumps which are not affected by 2ME2 and its derivatives are shown in desaturated colors.

to pass through the gel and thereby, this technique provides a better separation of phosphorylated proteins compared to conventional acrylamide gels.

Further, interaction between STIM and Orai dependent on STIM phosphorylation, can be investigated by using the Förster resonance energy transfer (FRET; Shrestha et al., 2015). This technique uses the fluorescence of yellow fluorescent protein (YFP) to stimulate cyan fluorescent protein (CFP). One of these fluorophores is covalently bound to STIM while the other is covalently bound to Orai channels (Muik et al., 2008). By exciting only YFP, the CFP can be excited by YFP emission which only takes place if YFP is in close proximity (distance below 10 nm) to CFP so that an energy transfer can take place (reviewed in Shrestha et al., 2015).

As it is discussed in section 5.3.5 “Further putative targets”, there are some studies who claim that 2ME2 interferes with tubulin polymerization in dividing tumor cells. It would be interesting to investigate if 2ME2 also disrupts tubulin polymerization in T lymphocytes. 2ME2’s impact on tubulin polymerization can be analysed by staining tubulin in T lymphocytes and treating cells with 2ME2 or its derivatives. As tubulin polymerization is also Ca^{2+} dependent (Tombes & Borisy, 1989) and 2ME2 inhibits Ca^{2+} entry, it would be necessary to control $[Ca^{2+}]_i$. This would be possible by using a micropipette which is used in electrophysiology in performing whole cell recordings. As the volume within the micropipette is much larger than the volume of the cell, $[Ca^{2+}]_i$ within cells would be the same as within the micropipette solution. One problem might arise from diluting cytosolic structures by the micropipette solution. Thus, another possibility would be to treat the cells with ionomycin. Thus, $[Ca^{2+}]_i$ can be increased although Orai channels are blocked by 2ME2 or its derivatives. Thereby, a Ca^{2+} independent effect of 2ME2 and its derivatives on tubulin can be determined.

5.5 Summary

In summary, my thesis reveals that the endogenous steroid hormones E2 and Prog inhibit Ca^{2+} entry in T lymphocytes with IC_{50} values of 55 and 19 µM, respectively. The endogenous E2 metabolite 2ME2 inhibits Ca^{2+} entry more potently than E2 with an IC_{50} of 20 µM. By derivatisation of 2ME2, even more potent compounds were identified. The most potent of these compounds showed an IC_{50} of about 1 µM in Jurkat T lymphocytes and restimulated primary rat T lymphocytes. As Ca^{2+} signalling depends on many ion channels and pumps, I also investigated the impact of 2ME2 and its derivatives on these putative targets. This study reveals that the main target of Ca^{2+} entry inhibition are Orai channels mediating Ca^{2+} entry. An impact on K^+ channels maintaining Ca^{2+} entry was not found. Ca^{2+} release mediated by IP_3R and RyR and Ca^{2+} clearance mediated by PMCAs, SERCAs and MCUs can be excluded as primary targets for this mechanism.

6. References

Achrem-Achremowicz, J., Kępczyńska, E., Żylewski, M., & Janeczko, Z. (2010). Synthesis of betulin derivatives and the determination of their relative lipophilicities using reversed-phase thin-layer chromatography. *Biomed. Chromatogr.*, *24*(3), 261–267. https://doi.org/10.1002/bmc.1282

Ackerman, L. S. (2006). Sex Hormones and the Genesis of Autoimmunity. *Arch. Dermatol.*, *142*(3), 371–376. https://doi.org/10.1001/archderm.142.3.371

Acuto, O., Bartolo, V. D., & Michel, F. (2008). Tailoring T-cell receptor signals by proximal negative feedback mechanisms. *Nat. Rev. Immunol.*, *8*(9), 699–712. https://doi.org/10.1038/nri2397

Arck, P. C., & Hecher, K. (2013). Fetomaternal immune cross-talk and its consequences for maternal and offspring's health. *Nat. Med.*, *19*(5), 548–556. https://doi.org/10.1038/nm.3160

Artyomov, M. N., Lis, M., Devadas, S., Davis, M. M., & Chakraborty, A. K. (2010). CD4 and CD8 binding to MHC molecules primarily acts to enhance Lck delivery. *Proc. Natl. Acad. Sci.*, *107*(39), 16916–16921. https://doi.org/10.1073/pnas.1010568107

Attaf, M., Legut, M., Cole, D. K., & Sewell, A. K. (2015). The T cell antigen receptor: the Swiss army knife of the immune system. *Clin. Exp. Immunol.*, *181*(1), 1–18. https://doi.org/10.1111/cei.12622

Attalla, H., Mäkelä, T. P., Adlercreutz, H., & Andersson, L. C. (1996). 2-Methoxyestradiol Arrests Cells in Mitosis without Depolymerizing Tubulin. *Biochem. Biophys. Res. Commun.*, *228*(2), 467–473. https://doi.org/10.1006/bbrc.1996.1683

Azenabor, A. A., & Hoffman-Goetz, L. (2001). 17β-Estradiol Increases Ca2+ Influx and Down Regulates Interleukin-2 Receptor in Mouse Thymocytes. *Biochem. Biophys. Res. Commun.*, *281*(2), 277–281. https://doi.org/10.1006/bbrc.2001.4341

Bansil, S., Lee, H. J., Jindal, S., Holtz, C. R., & Cook, S. O. (1999). Correlation between sex hormones and magnetic resonance imaging lesions in multiple sclerosis. *Acta Neurol. Scand.*, *99*(2), 91–94. https://doi.org/10.1111/j.1600-0404.1999.tb00663.x

Bassnett, S., Reinisch, L., & Beebe, D. C. (1990). Intracellular pH measurement using single excitation-dual emission fluorescence ratios. *Am. J. Physiol.-Cell Physiol.*, *258*(1), C171–C178. https://doi.org/10.1152/ajpcell.1990.258.1.C171

Bebo, B. F., Fyfe-Johnson, A., Adlard, K., Beam, A. G., Vandenbark, A. A., & Offner, H. (2001). Low-Dose Estrogen Therapy Ameliorates Experimental Autoimmune

Encephalomyelitis in Two Different Inbred Mouse Strains. *J. Immunol.*, *166*(3), 2080–2089. https://doi.org/10.4049/jimmunol.166.3.2080

Beeton, C., Barbaria, J., Giraud, P., Devaux, J., Benoliel, A.-M., Gola, M., Sabatier, J. M., Bernard, D., Crest, M., & Béraud, E. (2001a). Selective Blocking of Voltage-Gated K+ Channels Improves Experimental Autoimmune Encephalomyelitis and Inhibits T Cell Activation. *J. Immunol.*, *166*(2), 936–944. https://doi.org/10.4049/jimmunol.166.2.936

Beeton, C., Wulff, H., Barbaria, J., Clot-Faybesse, O., Pennington, M., Bernard, D., Cahalan, M. D., Chandy, K. G., & Béraud, E. (2001b). Selective blockade of T lymphocyte K+ channels ameliorates experimental autoimmune encephalomyelitis, a model for multiple sclerosis. *Proc. Natl. Acad. Sci. U. S. A.*, *98*(24), 13942–13947. https://doi.org/10.1073/pnas.241497298

Behl, C., & Holsboer, F. (1999). The female sex hormone oestrogen as a neuroprotectant. *Trends Pharmacol. Sci.*, *20*(11), 441–444. https://doi.org/10.1016/S0165-6147(99)01392-9

Ben-Nun, A., Wekerle, H., & Cohen, I. R. (1981). The rapid isolation of clonable antigen-specific T lymphocyte lines capable of mediating autoimmune encephalomyelitis. *Eur. J. Immunol.*, *11*(3), 195–199. https://doi.org/10.1002/eji.1830110307

Benten, W. P., Lieberherr, M., Giese, G., & Wunderlich, F. (1998). Estradiol binding to cell surface raises cytosolic free calcium in T cells. *FEBS Lett.*, *422*(3), 349–353.

Benten, W. P. M., Lieberherr, M., Giese, G., Wrehlke, C., Stamm, O., Sekeris, C. E., Mossmann, H., & Wunderlich, F. (1999). Functional testosterone receptors in plasma membranes of T cells. *FASEB J.*, *13*(1), 123–133.

Benten, W. P. M., Lieberherr, M., Sekeris, C. E., & Wunderlich, F. (1997). Testosterone induces Ca2+ influx via non-genomic surface receptors in activated T cells. *FEBS Lett.*, *407*(2), 211–214. https://doi.org/10.1016/S0014-5793(97)00346-3

Berger, T., Rubner, P., Schautzer, F., Egg, R., Ulmer, H., Mayringer, I., Dilitz, E., Deisenhammer, F., & Reindl, M. (2003). Antimyelin Antibodies as a Predictor of Clinically Definite Multiple Sclerosis after a First Demyelinating Event. *N. Engl. J. Med.*, *349*(2), 139–145. https://doi.org/10.1056/NEJMoa022328

Bers, D. M., Patton, C. W., & Nuccitelli, R. (2010). Chapter 1 - A Practical Guide to the Preparation of Ca2+ Buffers. In M. Whitaker (Ed.), *Methods in Cell Biology* (Vol. 99, pp. 1–26). Academic Press. Retrieved from http://www.sciencedirect.com/science/article/pii/B9780123748416000013

Birnbaum, M. E., Mendoza, J. L., Sethi, D. K., Dong, S., Glanville, J., Dobbins, J., Özkan, E., Davis, M. M., Wucherpfennig, K. W., & Garcia, K. C. (2014). Deconstructing the Peptide-MHC Specificity of T Cell Recognition. *Cell*, *157*(5), 1073–1087. https://doi.org/10.1016/j.cell.2014.03.047

Bittar, E. E., & Bittar, N. (Eds.). (1996). *Immunobiology*. Greenwich, Conn: JAI Press.

Brownlie, R. J., & Zamoyska, R. (2013). T cell receptor signalling networks: branched, diversified and bounded. *Nat. Rev. Immunol.*, *13*(4), 257–269. https://doi.org/10.1038/nri3403

Bruce, J. Y., Eickhoff, J., Pili, R., Logan, T., Carducci, M., Arnott, J., Treston, A., Wilding, G., & Liu, G. (2012). A phase II study of 2-methoxyestradiol nanocrystal colloidal dispersion alone and in combination with sunitinib malate in patients with metastatic renal cell carcinoma progressing on sunitinib malate. *Invest. New Drugs*, *30*(2), 794–802. https://doi.org/10.1007/s10637-010-9618-9

Bubert, C., Leese, M. P., Mahon, M. F., Ferrandis, E., Regis-Lydi, S., Kasprzyk, P. G., Newman, S. P., Ho, Y. T., Purohit, A., Reed, M. J., & Potter, B. V. L. (2007). 3,17-Disubstituted 2-Alkylestra-1,3,5(10)-trien-3-ol Derivatives: Synthesis, In Vitro and In Vivo Anticancer Activity. *J. Med. Chem.*, *50*(18), 4431–4443. https://doi.org/10.1021/jm070405v

Bunge, R. P. (1968). Glial cells and the central myelin sheath. *Physiol. Rev.*, *48*(1), 197–251. https://doi.org/10.1152/physrev.1968.48.1.197

Cahalan, M. D., Wulff, H., & Chandy, K. G. (2001). Molecular Properties and Physiological Roles of Ion Channels in the Immune System. *J. Clin. Immunol.*, *21*(4), 235–252. https://doi.org/10.1023/A:1010958907271

Cairrão, E., Alvarez, E., Carvas, J. M., Santos-Silva, A. J., & Verde, I. (2012). Non-genomic vasorelaxant effects of 17β-estradiol and progesterone in rat aorta are mediated by L-type Ca2+ current inhibition. *Acta Pharmacol. Sin.*, *33*(5), 615–624. https://doi.org/10.1038/aps.2012.4

Chandy, K. G., Williams, C. B., Spencer, R. H., Aguilar, B. A., Ghanshani, S., Tempel, B. L., & Gutman, G. A. (1990). A family of three mouse potassium channel genes with intronless coding regions. *Science*, *247*(4945), 973–975. https://doi.org/10.1126/science.2305265

Chari, D. M. (2007). Remyelination In Multiple Sclerosis. In B.-I. R. of Neurobiology (Ed.) (Vol. 79, pp. 589–620). Academic Press. Retrieved from http://www.sciencedirect.com/science/article/pii/S0074774207790268

Chen, S., Sun, X., Wu, B., & Lian, X. (2015). Pregnancy in Women with Systemic Lupus Erythematosus: A Retrospective Study of 83 Pregnancies at a Single Centre. *Int. J. Environ. Res. Public. Health*, *12*(8), 9876–9888. https://doi.org/10.3390/ijerph120809876

Chiang, C. S., Powell, H. C., Gold, L. H., Samimi, A., & Campbell, I. L. (1996). Macrophage/microglial-mediated primary demyelination and motor disease induced by the central nervous system production of interleukin-3 in transgenic mice. *J. Clin. Invest.*, *97*(6), 1512–1524.

Chiang, H.-T., & Wu, S.-N. (2001). Inhibition of Large-Conductance Calcium-Activated Potassium Channel by 2-Methoxyestradiol in Cultured Vascular Endothelial (HUV-EC-C) Cells. *J. Membr. Biol.*, *182*(3), 203–212. https://doi.org/10.1007/s00232-001-0044-y

Clark, E. A., & Ledbetter, J. A. (1994). How B and T cells talk to each other. *Nature*, *367*(6462), 425–428. https://doi.org/10.1038/367425a0

Confavreux, C., Hutchinson, M., Hours, M. M., Cortinovis-Tourniaire, P., & Moreau, T. (1998). Rate of Pregnancy-Related Relapse in Multiple Sclerosis. *N. Engl. J. Med.*, *339*(5), 285–291. https://doi.org/10.1056/NEJM199807303390501

Confavreux, C., & Vukusic, S. (2002). Natural history of multiple sclerosis: implications for counselling and therapy. *Curr. Opin. Neurol.*, *15*(3), 257–266.

Correale, J., Arias, M., & Gilmore, W. (1998). Steroid Hormone Regulation of Cytokine Secretion by Proteolipid Protein-Specific CD4+ T Cell Clones Isolated from Multiple Sclerosis Patients and Normal Control Subjects. *J. Immunol.*, *161*(7), 3365–3374.

Correale, J., Gilmore, W., McMillan, M., Li, S., McCarthy, K., Le, T., & Weiner, L. P. (1995). Patterns of cytokine secretion by autoreactive proteolipid protein-specific T cell clones during the course of multiple sclerosis. *J. Immunol.*, *154*(6), 2959–2968.

D'Amato, R. J., Lin, C. M., Flynn, E., Folkman, J., & Hamel, E. (1994). 2-Methoxyestradiol, an endogenous mammalian metabolite, inhibits tubulin polymerization by interacting at the colchicine site. *Proc. Natl. Acad. Sci. U. S. A.*, *91*(9), 3964–3968.

Danel, L., Souweine, G., Monier, J. C., & Saez, S. (1983). Specific estrogen binding sites in human lymphoid cells and thymic cells. *J. Steroid Biochem.*, *18*(5), 559–563. https://doi.org/10.1016/0022-4731(83)90131-0

de Man, Y. A., Dolhain, R. J. E. M., van de Geijn, F. E., Willemsen, S. P., & Hazes, J. M. W. (2008). Disease activity of rheumatoid arthritis during pregnancy: results from a nationwide prospective study. *Arthritis Rheum.*, *59*(9), 1241–1248. https://doi.org/10.1002/art.24003

DeHaven, W. I., Jones, B. F., Petranka, J. G., Smyth, J. T., Tomita, T., Bird, G. S., & Putney, J. W. (2009). TRPC channels function independently of STIM1 and Orai1. *J. Physiol.*, *587*(10), 2275–2298. https://doi.org/10.1113/jphysiol.2009.170431

Deindl, S., Kadlecek, T. A., Brdicka, T., Cao, X., Weiss, A., & Kuriyan, J. (2007). Structural Basis for the Inhibition of Tyrosine Kinase Activity of ZAP-70. *Cell*, *129*(4), 735–746. https://doi.org/10.1016/j.cell.2007.03.039

Del Prete, G., De Carli, M., Almerigogna, F., Daniel, C. K., D'Elios, M. M., Zancuoghi, G., Vinante, F., Pizzolo, G., & Romagnani, S. (1995). Preferential expression of

CD30 by human CD4+ T cells producing Th2-type cytokines. *FASEB J.*, *9*(1), 81–86. https://doi.org/10.1096/fasebj.9.1.7821763

Djillani, A., Nüße, O., & Dellis, O. (2014). Characterization of novel store-operated calcium entry effectors. *Biochim. Biophys. Acta BBA - Mol. Cell Res.*, *1843*(10), 2341–2347. https://doi.org/10.1016/j.bbamcr.2014.03.012

Dohle, W., Leese, M. P., Jourdan, F. L., Chapman, C. J., Hamel, E., Ferrandis, E., & Potter, B. V. L. (2014a). Optimisation of Tetrahydroisoquinoline-Based Chimeric Microtubule Disruptors. *ChemMedChem*, *9*(8), 1783–1793. https://doi.org/10.1002/cmdc.201402025

Dohle, W., Leese, M. P., Jourdan, F. L., Major, M. R., Bai, R., Hamel, E., Ferrandis, E., Kasprzyk, P. G., Fiore, A., Newman, S. P., Purohit, A., & Potter, B. V. L. (2014b). Synthesis, Antitubulin, and Antiproliferative SAR of C3/C1-Substituted Tetrahydroisoquinolines. *ChemMedChem*, *9*(2), 350–370. https://doi.org/10.1002/cmdc.201300412

Domi, T., Di Leva, F., Fedrizzi, L., Rimessi, A., & Brini, M. (2007). Functional Specificity of PMCA Isoforms? *Ann. N. Y. Acad. Sci.*, *1099*(1), 237–246. https://doi.org/10.1196/annals.1387.043

Doria, A., Cutolo, M., Ghirardello, A., Zampieri, S., Vescovi, F., Sulli, A., Giusti, M., Piccoli, A., Grella, P., & Gambari, P. F. (2002). Steroid hormones and disease activity during pregnancy in systemic lupus erythematosus. *Arthritis Care Res.*, *47*(2), 202–209. https://doi.org/10.1002/art.10248

Dubey, R. K. (2017). 2-Methoxyestradiol: A 17β-Estradiol Metabolite With Gender-Independent Therapeutic Potential. *Hypertens. Dallas Tex 1979*. https://doi.org/10.1161/HYPERTENSIONAHA.117.09265

Duncan, G. S., Brenner, D., Tusche, M. W., Brüstle, A., Knobbe, C. B., Elia, A. J., Mock, T., Bray, M. R., Krammer, P. H., & Mak, T. W. (2012). 2-Methoxyestradiol inhibits experimental autoimmune encephalomyelitis through suppression of immune cell activation. *Proc. Natl. Acad. Sci.*, *109*(51), 21034–21039. https://doi.org/10.1073/pnas.1215558110

Dynes, J. L., Amcheslavsky, A., & Cahalan, M. D. (2016). Genetically targeted single-channel optical recording reveals multiple Orai1 gating states and oscillations in calcium influx. *Proc. Natl. Acad. Sci.*, *113*(2), 440–445. https://doi.org/10.1073/pnas.1523410113

Ehring, G. R., Kerschbaum, H. H., Eder, C., Neben, A. L., Fanger, C. M., Khoury, R. M., Negulescu, P. A., & Cahalan, M. D. (1998). A Nongenomic Mechanism for Progesterone-mediated Immunosuppression: Inhibition of K+ Channels, Ca2+ Signaling, and Gene Expression in T Lymphocytes. *J. Exp. Med.*, *188*(9), 1593–1602. https://doi.org/10.1084/jem.188.9.1593

Elenkov, I. J., Wilder, R. L., Bakalov, V. K., Link, A. A., Dimitrov, M. A., Fisher, S., Crane, M., Kanik, K. S., & Chrousos, G. P. (2001). IL-12, TNF-α, and Hormonal

Changes during Late Pregnancy and Early Postpartum: Implications for Autoimmune Disease Activity during These Times. *J. Clin. Endocrinol. Metab.*, *86*(10), 4933–4938. https://doi.org/10.1210/jcem.86.10.7905

Engler, J. B., Kursawe, N., Solano, M. E., Patas, K., Wehrmann, S., Heckmann, N., Lühder, F., Reichardt, H. M., Arck, P. C., Gold, S. M., & Friese, M. A. (2017). Glucocorticoid receptor in T cells mediates protection from autoimmunity in pregnancy. *Proc. Natl. Acad. Sci.*, *114*(2), E181–E190. https://doi.org/10.1073/pnas.1617115114

Falcone, M., & Bloom, B. R. (1997). A T helper cell 2 (Th2) immune response against non-self antigens modifies the cytokine profile of autoimmune T cells and protects against experimental allergic encephalomyelitis. *J. Exp. Med.*, *185*(5), 901–907.

Falkenstein, E., Tillmann, H.-C., Christ, M., Feuring, M., & Wehling, M. (2000). Multiple Actions of Steroid Hormones—A Focus on Rapid, Nongenomic Effects. *Pharmacol. Rev.*, *52*(4), 513–556.

Fanger, C. M., Neben, A. L., & Cahalan, M. D. (2000). Differential Ca^{2+} Influx, K_{Ca} Channel Activity, and Ca^{2+} Clearance Distinguish Th1 and Th2 Lymphocytes. *J. Immunol.*, *164*(3), 1153–1160. https://doi.org/10.4049/jimmunol.164.3.1153

Fanger, C. M., Rauer, H., Neben, A. L., Miller, M. J., Rauer, H., Wulff, H., Rosa, J. C., Ganellin, C. R., Chandy, K. G., & Cahalan, M. D. (2001). Calcium-activated Potassium Channels Sustain Calcium Signaling in T Lymphocytes SELECTIVE BLOCKERS AND MANIPULATED CHANNEL EXPRESSION LEVELS. *J. Biol. Chem.*, *276*(15), 12249–12256. https://doi.org/10.1074/jbc.M011342200

Feske, S. (2007). Calcium signalling in lymphocyte activation and disease. *Nat. Rev. Immunol.*, *7*(9), 690–702. https://doi.org/10.1038/nri2152

Finkelsztejn, A., Brooks, J., Paschoal, F., & Fragoso, Y. (2011). What can we really tell women with multiple sclerosis regarding pregnancy? A systematic review and meta-analysis of the literature. *BJOG Int. J. Obstet. Gynaecol.*, *118*(7), 790–797. https://doi.org/10.1111/j.1471-0528.2011.02931.x

Fiorelli, G., Gori, F., Frediani, U., Franceschelli, F., Tanini, A., Tosti-Guerra, C., Benvenuti, S., Gennari, L., Becherini, L., & Brandi, M. L. (1996). Membrane binding sites and non-genomic effects of estrogen in cultured human preosteoclastic cells. *J. Steroid Biochem. Mol. Biol.*, *59*(2), 233–240. https://doi.org/10.1016/S0960-0760(96)00092-1

Fontenot, J. D., Gavin, M. A., & Rudensky, A. Y. (2017). Pillars Article: Foxp3 Programs the Development and Function of CD4+CD25+ Regulatory T Cells. Nat. Immunol. 2003. 4: 330–336. *J. Immunol.*, *198*(3), 986–992.

Foster, P. A., Ho, Y. T., Newman, S. P., Kasprzyk, P. G., Leese, M. P., Potter, B. V. L., Reed, M. J., & Purohit, A. (2007). 2-MeOE2bisMATE and 2-EtE2bisMATE induce cell cycle arrest and apoptosis in breast cancer xenografts as shown by

a novel ex vivo technique. *Breast Cancer Res. Treat.*, *111*(2), 251–260. https://doi.org/10.1007/s10549-007-9791-5

Fotsis, T., Zhang, Y., Pepper, M. S., Adlercreutz, H., Montesano, R., Nawroth, P. P., & Schweigerer, L. (1994). The endogenous oestrogen metabolite 2-methoxyoestradiol inhibits angiogenesis and suppresses tumour growth. *Nature*, *368*(6468), 237–239. https://doi.org/10.1038/368237a0

Frischer, J. M., Bramow, S., Dal-Bianco, A., Lucchinetti, C. F., Rauschka, H., Schmidbauer, M., Laursen, H., Sorensen, P. S., & Lassmann, H. (2009). The relation between inflammation and neurodegeneration in multiple sclerosis brains. *Brain*, *132*(5), 1175–1189. https://doi.org/10.1093/brain/awp070

Frisullo, G., Nociti, V., Iorio, R., Patanella, A. K., Caggiula, M., Marti, A., Sancricca, C., Angelucci, F., Mirabella, M., Tonali, P. A., & Batocchi, A. P. (2009). Regulatory T cells fail to suppress CD4T+-bet+ T cells in relapsing multiple sclerosis patients. *Immunology*, *127*(3), 418–428. https://doi.org/10.1111/j.1365-2567.2008.02963.x

Garidou, L., Laffont, S., Douin-Echinard, V., Coureau, C., Krust, A., Chambon, P., & Guéry, J.-C. (2004). Estrogen Receptor α Signaling in Inflammatory Leukocytes Is Dispensable for 17β-Estradiol-Mediated Inhibition of Experimental Autoimmune Encephalomyelitis. *J. Immunol.*, *173*(4), 2435–2442. https://doi.org/10.4049/jimmunol.173.4.2435

Gasser, A., Bruhn, S., & Guse, A. H. (2006). Second messenger function of nicotinic acid adenine dinucleotide phosphate revealed by an improved enzymatic cycling assay. *J. Biol. Chem.*, *281*(25), 16906–16913. https://doi.org/10.1074/jbc.M601347200

Ghanshani, S., Wulff, H., Miller, M. J., Rohm, H., Neben, A., Gutman, G. A., Cahalan, M. D., & Chandy, K. G. (2000). Up-regulation of the IKCa1 Potassium Channel during T-cell Activation MOLECULAR MECHANISM AND FUNCTIONAL CONSEQUENCES. *J. Biol. Chem.*, *275*(47), 37137–37149. https://doi.org/10.1074/jbc.M003941200

Gilmore, W., Weiner, L. P., & Correale, J. (1997). Effect of estradiol on cytokine secretion by proteolipid protein-specific T cell clones isolated from multiple sclerosis patients and normal control subjects. *J. Immunol.*, *158*(1), 446–451.

Goodnow, C. C., Sprent, J., Groth, B. F. de S., & Vinuesa, C. G. (2005, June 1). Cellular and genetic mechanisms of self tolerance and autoimmunity [Special Features]. https://doi.org/10.1038/nature03724

Gorska-Ponikowska, M., Kuban-Jankowska, A., Eisler, S. A., Perricone, U., Bosco, G. L., Barone, G., & Nussberger, S. (2018). 2-Methoxyestradiol Affects Mitochondrial Biogenesis Pathway and Succinate Dehydrogenase Complex Flavoprotein Subunit A in Osteosarcoma Cancer Cells. *Cancer Genomics - Proteomics*, *15*(1), 73–89.

Grissmer, S., Lewis, R. S., & Cahalan, M. D. (1992). Ca(2+)-activated K+ channels in human leukemic T cells. *J. Gen. Physiol.*, *99*(1), 63–84. https://doi.org/10.1085/jgp.99.1.63

Grissmer, S., Nguyen, A. N., & Cahalan, M. D. (1993). Calcium-activated potassium channels in resting and activated human T lymphocytes. Expression levels, calcium dependence, ion selectivity, and pharmacology. *J. Gen. Physiol.*, *102*(4), 601–630. https://doi.org/10.1085/jgp.102.4.601

Grossman, C. J. (1985). Interactions between the gonadal steroids and the immune system. *Science*, *227*(4684), 257–261. https://doi.org/10.1126/science.3871252

Grynkiewicz, G., Poenie, M., & Tsien, R. Y. (1985). A new generation of Ca2+ indicators with greatly improved fluorescence properties. *J. Biol. Chem.*, *260*(6), 3440–3450.

Gunter, T. E., Restrepo, D., & Gunter, K. K. (1988). Conversion of esterified fura-2 and indo-1 to Ca2+-sensitive forms by mitochondria. *Am. J. Physiol.-Cell Physiol.*, *255*(3), C304–C310. https://doi.org/10.1152/ajpcell.1988.255.3.C304

Guse, A. H., da Silva, C. P., Berg, I., Skapenko, A. L., Weber, K., Heyer, P., Hohenegger, M., Ashamu, G. A., Schulze-Koops, H., Potter, B. V. L., & Mayr, G. W. (1999). Regulation of calcium signalling in T lymphocytes by the second messenger cyclic ADP-ribose. *Nature*, *398*(6722), 70–73. https://doi.org/10.1038/18024

Guse, A. H., Roth, E., & Emmrich, F. (1993). Intracellular Ca2+ pools in Jurkat T-lymphocytes. *Biochem. J.*, *291*(Pt 2), 447–451.

Hato, T., & Dagher, P. C. (2015). How the Innate Immune System Senses Trouble and Causes Trouble. *Clin. J. Am. Soc. Nephrol.*, *10*(8), 1459–1469. https://doi.org/10.2215/CJN.04680514

Hill, B. J. F., Gebre, S., Schlicker, B., Jordan, R., & Necessary, S. (2010). Nongenomic inhibition of coronary constriction by 17β-estradiol, 2- hydroxyestradiol, and 2-methoxyestradiol. *Can. J. Physiol. Pharmacol.*, *88*(2), 147–152. https://doi.org/10.1139/y09-120

Hoffman, G. E., Le, W. W., Murphy, A. Z., & Koski, C. L. (2001). Divergent Effects of Ovarian Steroids on Neuronal Survival during Experimental Allergic Encephalitis in Lewis Rats. *Exp. Neurol.*, *171*(2), 272–284. https://doi.org/10.1006/exnr.2001.7783

Hogan, P. G., Lewis, R. S., & Rao, A. (2010). Molecular basis of calcium signaling in lymphocytes: STIM and ORAI. *Annu. Rev. Immunol.*, *28*, 491–533. https://doi.org/10.1146/annurev.immunol.021908.132550

Hohlfeld, R. (1997). Biotechnological agents for the immunotherapy of multiple sclerosis. Principles, problems and perspectives. *Brain*, *120*(5), 865–916. https://doi.org/10.1093/brain/120.5.865

Hori, S., Nomura, T., & Sakaguchi, S. (2003). Control of Regulatory T Cell Development by the Transcription Factor Foxp3. *Science*, *299*(5609), 1057–1061. https://doi.org/10.1126/science.1079490

Hoth, M., Button, D. C., & Lewis, R. S. (2000). Mitochondrial control of calcium-channel gating: A mechanism for sustained signaling and transcriptional activation in T lymphocytes. *Proc. Natl. Acad. Sci. U. S. A.*, *97*(19), 10607–10612.

Hou, X., Pedi, L., Diver, M. M., & Long, S. B. (2012). Crystal Structure of the Calcium Release–Activated Calcium Channel Orai. *Science*, *338*(6112), 1308–1313. https://doi.org/10.1126/science.1228757

Huang, G. N., Zeng, W., Kim, J. Y., Yuan, J. P., Han, L., Muallem, S., & Worley, P. F. (2006). STIM1 carboxyl-terminus activates native SOC, Icrac and TRPC1 channels. *Nat. Cell Biol.*, *8*(9), 1003–1010. https://doi.org/10.1038/ncb1454

Hutchison, S. J., Sudhir, K., Chou, T. M., & Chatterjee, K. (1997). Sex hormones and vascular reactivity. *Herz*, *22*(3), 141–150. https://doi.org/10.1007/BF03044351

Ireson, C. R., Chander, S. K., Purohit, A., Perera, S., Newman, S. P., Parish, D., Leese, M. P., Smith, A. C., Potter, B. V. L., & Reed, M. J. (2004). Pharmacokinetics and efficacy of 2-methoxyoestradiol and 2-methoxyoestradiol-bis-sulphamate in vivo in rodents. *Br. J. Cancer*, *90*(4), 932–937. https://doi.org/10.1038/sj.bjc.6601591

Ito, A., Bebo, B. F., Matejuk, A., Zamora, A., Silverman, M., Fyfe-Johnson, A., & Offner, H. (2001). Estrogen Treatment Down-Regulates TNF-α Production and Reduces the Severity of Experimental Autoimmune Encephalomyelitis in Cytokine Knockout Mice. *J. Immunol.*, *167*(1), 542–552. https://doi.org/10.4049/jimmunol.167.1.542

Jäger, H., Adelman, J. P., & Grissmer, S. (2000). SK2 encodes the apamin-sensitive Ca2+-activated K+ channels in the human leukemic T cell line, Jurkat. *FEBS Lett.*, *469*(2–3), 196–202. https://doi.org/10.1016/S0014-5793(00)01236-9

Jenkins, J. K., Suwannaroj, S., Elbourne, K. B., Ndebele, K., & McMurray, R. W. (2001). 17-β-Estradiol alters Jurkat lymphocyte cell cycling and induces apoptosis through suppression of Bcl-2 and cyclin A. *Int. Immunopharmacol.*, *1*(11), 1897–1911. https://doi.org/10.1016/S1567-5769(01)00114-X

Jin, S., Chin, J., Kitson, C., Woods, J., Majmudar, R., Carvajal, V., Allard, J., DeMartino, J., Narula, S., & Thomas-Karyat, D. A. (2013). Natural regulatory T cells are resistant to calcium release-activated calcium (CRAC/ORAI) channel inhibition. *Int. Immunol.*, *25*(9), 497–506. https://doi.org/10.1093/intimm/dxt013

Josefsson, E., & Tarkowski, A. (1997). Suppression of type II collagen-induced arthritis by the endogenous estrogen metabolite 2-methoxyestradiol. *Arthritis Rheum.*, *40*(1), 154–163. https://doi.org/10.1002/art.1780400120

Jourdan, F., Leese, M. P., Dohle, W., Ferrandis, E., Newman, S. P., Chander, S., Purohit, A., & Potter, B. V. L. (2011). Structure–Activity Relationships of C-17-Substituted Estratriene-3-O-sulfamates as Anticancer Agents. *J. Med. Chem.*, *54*(13), 4863–4879. https://doi.org/10.1021/jm200483x

Jourdan, F., Leese, M. P., Dohle, W., Hamel, E., Ferrandis, E., Newman, S. P., Purohit, A., Reed, M. J., & Potter, B. V. L. (2010). Synthesis, Antitubulin, and Antiproliferative SAR of Analogues of 2-Methoxyestradiol-3,17-O,O-bis-sulfamate. *J. Med. Chem.*, *53*(7), 2942–2951. https://doi.org/10.1021/jm9018806

Kar, P., Mirams, G. R., Christian, H. C., & Parekh, A. B. (2016). Control of NFAT Isoform Activation and NFAT-Dependent Gene Expression through Two Coincident and Spatially Segregated Intracellular Ca2+ Signals. *Mol. Cell*, *64*(4), 746–759. https://doi.org/10.1016/j.molcel.2016.11.011

Kärre, K., Ljunggren, H. G., Piontek, G., & Kiessling, R. (1986). Selective rejection of H–2-deficient lymphoma variants suggests alternative immune defence strategy. *Nature*, *319*(6055), 675–678. https://doi.org/10.1038/319675a0

Kawasaki, T., Lange, I., & Feske, S. (2009). A minimal regulatory domain in the C terminus of STIM1 binds to and activates ORAI1 CRAC channels. *Biochem. Biophys. Res. Commun.*, *385*(1), 49–54. https://doi.org/10.1016/j.bbrc.2009.05.020

Khan, D., & Ahmed, S. A. (2016). The Immune System Is a Natural Target for Estrogen Action: Opposing Effects of Estrogen in Two Prototypical Autoimmune Diseases. *Front. Immunol.*, *6*. https://doi.org/10.3389/fimmu.2015.00635

Kinoshita, E., Takahashi, M., Takeda, H., Shiro, M., & Koike, T. (2004). Recognition of phosphate monoester dianion by an alkoxide-bridged dinuclear zinc(ii) complex. *Dalton Trans.*, *0*(8), 1189–1193. https://doi.org/10.1039/B400269E

Kitazawa, T., Hamada, E., Kitazawa, K., & Gaznabi, A. K. (1997). Non-genomic mechanism of 17 beta-oestradiol-induced inhibition of contraction in mammalian vascular smooth muscle. *J. Physiol.*, *499*(2), 497–511. https://doi.org/10.1113/jphysiol.1997.sp021944

Kovats, S. (2015). Estrogen receptors regulate innate immune cells and signaling pathways. *Cell. Immunol.*, *294*(2), 63–69. https://doi.org/10.1016/j.cellimm.2015.01.018

Krell, T., Lacal, J., García-Fontana, C., Silva-Jiménez, H., Rico-Jiménez, M., Lugo, A. C., Darias, J. A. R., & Ramos, J.-L. (2014). Characterization of Molecular Interactions Using Isothermal Titration Calorimetry. In *Pseudomonas Methods*

and Protocols (pp. 193–203). Humana Press, New York, NY. https://doi.org/10.1007/978-1-4939-0473-0_16

Kulke, M. H., Chan, J. A., Meyerhardt, J. A., Zhu, A. X., Abrams, T. A., Blaszkowsky, L. S., Regan, E., Sidor, C., & Fuchs, C. S. (2011). A prospective phase II study of 2-methoxyestradiol administered in combination with bevacizumab in patients with metastatic carcinoid tumors. *Cancer Chemother. Pharmacol.*, *68*(2), 293–300. https://doi.org/10.1007/s00280-010-1478-7

Kunerth, S., Langhorst, M. F., Schwarzmann, N., Gu, X., Huang, L., Yang, Z., Zhang, L., Mills, S. J., Zhang, L.-H., Potter, B. V. L., & Guse, A. H. (2004). Amplification and propagation of pacemaker Ca2+ signals by cyclic ADP-ribose and the type 3 ryanodine receptor in T cells. *J. Cell Sci.*, *117*(Pt 10), 2141–2149. https://doi.org/10.1242/jcs.01063

Langhorst, M. F., Schwarzmann, N., & Guse, A. H. (2004). Ca2+ release via ryanodine receptors and Ca2+ entry: major mechanisms in NAADP-mediated Ca2+ signaling in T-lymphocytes. *Cell. Signal.*, *16*(11), 1283–1289. https://doi.org/10.1016/j.cellsig.2004.03.013

Laufer, T. M., DeKoning, J., Markowitz, J. S., Lo, D., & Glimcher, L. H. (1996). Unopposed positive selection and autoreactivity in mice expressing class II MHC only on thymic cortex. *Nature*, *383*(6595), 81–85. https://doi.org/10.1038/383081a0

LaVallee, T. M., Zhan, X. H., Herbstritt, C. J., Kough, E. C., Green, S. J., & Pribluda, V. S. (2002). 2-Methoxyestradiol Inhibits Proliferation and Induces Apoptosis Independently of Estrogen Receptors α and β. *Cancer Res.*, *62*(13), 3691–3697.

Lee, J.-S., Kim, Y.-K., Yang, H., Kang, H. Y., Ahn, C., & Jeung, E.-B. (2015). Two faces of the estrogen metabolite 2-methoxyestradiol in vitro and in vivo. *Mol. Med. Rep.*, *12*(4), 5375–5382.

Leese, M. P., Hejaz, H. A. M., Mahon, M. F., Newman, S. P., Purohit, A., Reed, M. J., & Potter, B. V. L. (2005). A-Ring-Substituted Estrogen-3-O-sulfamates: Potent Multitargeted Anticancer Agents. *J. Med. Chem.*, *48*(16), 5243–5256. https://doi.org/10.1021/jm050066a

Leese, M. P., Jourdan, F. L., Gaukroger, K., Mahon, M. F., Newman, S. P., Foster, P. A., Stengel, C., Regis-Lydi, S., Ferrandis, E., Fiore, A. D., De Simone, G., Supuran, C. T., Purohit, A., Reed, M. J., & Potter, B. V. L. (2008). Structure–Activity Relationships of C-17 Cyano-Substituted Estratrienes as Anticancer Agents†. *J. Med. Chem.*, *51*(5), 1295–1308. https://doi.org/10.1021/jm701319c

Leese, M. P., Jourdan, F., R. Kimberley, M., E. Cozier, G., Thiyagarajan, N., Stengel, C., Regis-Lydi, S., A. Foster, P., P. Newman, S., Ravi Acharya, K., Ferrandis, E., Purohit, A., J. Reed, M., & L. Potter, B. V. L. (2010). Chimeric microtubule disruptors. *Chem. Commun.*, *46*(17), 2907–2909. https://doi.org/10.1039/C002558E

Leese, M. P., Leblond, B., Smith, A., Newman, S. P., Di Fiore, A., De Simone, G., Supuran, C. T., Purohit, A., Reed, M. J., & Potter, B. V. L. (2006). 2-Substituted Estradiol Bis-sulfamates, Multitargeted Antitumor Agents: Synthesis, In Vitro SAR, Protein Crystallography, and In Vivo Activity†. *J. Med. Chem.*, *49*(26), 7683–7696. https://doi.org/10.1021/jm060705x

Lélu, K., Laffont, S., Delpy, L., Paulet, P.-E., Périnat, T., Tschanz, S. A., Pelletier, L., Engelhardt, B., & Guéry, J.-C. (2011). Estrogen receptor α signaling in T lymphocytes is required for estradiol-mediated inhibition of Th1 and Th17 cell differentiation and protection against experimental autoimmune encephalomyelitis. *J. Immunol. Baltim. Md 1950*, *187*(5), 2386–2393. https://doi.org/10.4049/jimmunol.1101578

Lewis, R. S., & Cahalan, M. D. (1995). Potassium and Calcium Channels in Lymphocytes. *Annu. Rev. Immunol.*, *13*(1), 623–653. https://doi.org/10.1146/annurev.iy.13.040195.003203

Lieberherr, M., & Grosse, B. (1994). Androgens increase intracellular calcium concentration and inositol 1,4,5-trisphosphate and diacylglycerol formation via a pertussis toxin-sensitive G-protein. *J. Biol. Chem.*, *269*(10), 7217–7223.

Lin, A., & Loré, K. (2017). Granulocytes: New Members of the Antigen-Presenting Cell Family. *Front. Immunol.*, *8*. https://doi.org/10.3389/fimmu.2017.01781

Linington, C., Bradl, M., Lassmann, H., Brunner, C., & Vass, K. (1988). Augmentation of demyelination in rat acute allergic encephalomyelitis by circulating mouse monoclonal antibodies directed against a myelin/oligodendrocyte glycoprotein. *Am. J. Pathol.*, *130*(3), 443–454.

Liou, J., Kim, M. L., Heo, W. D., Jones, J. T., Myers, J. W., Ferrell, J. E., & Meyer, T. (2005). STIM is a Ca2+ sensor essential for Ca2+-store-depletion-triggered Ca2+ influx. *Curr. Biol. CB*, *15*(13), 1235–1241. https://doi.org/10.1016/j.cub.2005.05.055

Lippert, C., Seeger, H., Mueck, A. O., & Lippert, T. H. (2000). The effects of A-ring and D-ring metabolites of estradiol on the proliferation of vascular endothelial cells. *Life Sci.*, *67*(13), 1653–1658. https://doi.org/10.1016/S0024-3205(00)00747-5

Liu, X., Berry, C. T., Ruthel, G., Madara, J. J., MacGillivray, K., Gray, C. M., Madge, L. A., McCorkell, K. A., Beiting, D. P., Hershberg, U., May, M. J., & Freedman, B. D. (2016). T cell receptor-induced NF-κB signaling and transcriptional activation are regulated by STIM1- and Orai1-mediated calcium entry. *J. Biol. Chem.*, jbc.M115.713008. https://doi.org/10.1074/jbc.M115.713008

Logsdon, N. J., Kang, J., Togo, J. A., Christian, E. P., & Aiyar, J. (1997). A Novel Gene, hKCa4, Encodes the Calcium-activated Potassium Channel in Human T Lymphocytes. *J. Biol. Chem.*, *272*(52), 32723–32726. https://doi.org/10.1074/jbc.272.52.32723

Lovatt, M., Filby, A., Parravicini, V., Werlen, G., Palmer, E., & Zamoyska, R. (2006). Lck Regulates the Threshold of Activation in Primary T Cells, While both Lck and Fyn Contribute to the Magnitude of the Extracellular Signal-Related Kinase Response. *Mol. Cell. Biol.*, *26*(22), 8655–8665. https://doi.org/10.1128/MCB.00168-06

Luik, R. M., Wang, B., Prakriya, M., Wu, M. M., & Lewis, R. S. (2008). Oligomerization of STIM1 couples ER calcium depletion to CRAC channel activation. *Nature*, *454*(7203), 538–542. https://doi.org/10.1038/nature07065

Lytton, J., Westlin, M., & Hanley, M. R. (1991). Thapsigargin inhibits the sarcoplasmic or endoplasmic reticulum Ca-ATPase family of calcium pumps. *J. Biol. Chem.*, *266*(26), 17067–17071.

Marino, M., Pallottini, V., & Trentalance, A. (1998). Estrogens Cause Rapid Activation of IP3-PKC-α Signal Transduction Pathway in HEPG2 Cells. *Biochem. Biophys. Res. Commun.*, *245*(1), 254–258. https://doi.org/10.1006/bbrc.1998.8413

Martin, R., McFarland, H. F., & Boggs, J. M. (1995). Immunological Aspects of Experimental Allergic Encephalomyelitis and Multiple Sclerosis. *Crit. Rev. Clin. Lab. Sci.*, *32*(2), 121–182. https://doi.org/10.3109/10408369509084683

Martucci, C. P., & Fishman, J. (1979). Impact of Continuously Administered Catechol Estrogens on Uterine Growth and Luteinizing Hormone Secretion. *Endocrinology*, *105*(6), 1288–1292. https://doi.org/10.1210/endo-105-6-1288

Marzi, M., Vigano, A., Trabattoni, D., Villa, M. L., Salvaggio, A., Clerici, E., & Clerici, M. (1996). Characterization of type 1 and type 2 cytokine production profile in physiologic and pathologic human pregnancy. *Clin. Exp. Immunol.*, *106*(1), 127–133.

Maselli, A., Conti, F., Alessandri, C., Colasanti, T., Barbati, C., Vomero, M., Ciarlo, L., Patrizio, M., Spinelli, F. R., Ortona, E., Valesini, G., & Pierdominici, M. (2016). Low expression of estrogen receptor β in T lymphocytes and high serum levels of anti-estrogen receptor α antibodies impact disease activity in female patients with systemic lupus erythematosus. *Biol. Sex Differ.*, *7*. https://doi.org/10.1186/s13293-016-0057-y

Matei, D., Schilder, J., Sutton, G., Perkins, S., Breen, T., Quon, C., & Sidor, C. (2009). Activity of 2 methoxyestradiol (Panzem® NCD) in advanced, platinum-resistant ovarian cancer and primary peritoneal carcinomatosis: A Hoosier Oncology Group trial. *Gynecol. Oncol.*, *115*(1), 90–96. https://doi.org/10.1016/j.ygyno.2009.05.042

Matejuk, A., Adlard, K., Zamora, A., Silverman, M., Vandenbark, A. A., & Offner, H. (2001). 17β-estradiol inhibits cytokine, chemokine, and chemokine receptor mRNA expression in the central nervous system of female mice with experimental autoimmune encephalomyelitis. *J. Neurosci. Res.*, *65*(6), 529–542. https://doi.org/10.1002/jnr.1183

McMurray, R. W., Ndebele, K., Hardy, K. J., & Jenkins, J. K. (2001). 17-β-ESTRADIOL SUPPRESSES IL-2 AND IL-2 RECEPTOR. *Cytokine*, *14*(6), 324–333. https://doi.org/10.1006/cyto.2001.0900

Melcangi, R. C., Giatti, S., & Garcia-Segura, L. M. (2016). Levels and actions of neuroactive steroids in the nervous system under physiological and pathological conditions: Sex-specific features. *Neurosci. Biobehav. Rev.*, *67*, 25–40. https://doi.org/10.1016/j.neubiorev.2015.09.023

Merwe, P. A. van der, & Dushek, O. (2011). Mechanisms for T cell receptor triggering. *Nat. Rev. Immunol.*, *11*(1), 47–55. https://doi.org/10.1038/nri2887

Miller, V. (2010). Sex-based differences in vascular function. *Womens Health*, *6*(5), 737–752. https://doi.org/10.2217/whe.10.53

Morley, P., Whitfield, J. F., Vanderhyden, B. C., Tsang, B. K., & Schwartz, J. L. (1992). A new, nongenomic estrogen action: the rapid release of intracellular calcium. *Endocrinology*, *131*(3), 1305–1312. https://doi.org/10.1210/endo.131.3.1505465

Muik, M., Frischauf, I., Derler, I., Fahrner, M., Bergsmann, J., Eder, P., Schindl, R., Hesch, C., Polzinger, B., Fritsch, R., Kahr, H., Madl, J., Gruber, H., Groschner, K., & Romanin, C. (2008). Dynamic Coupling of the Putative Coiled-coil Domain of ORAI1 with STIM1 Mediates ORAI1 Channel Activation. *J. Biol. Chem.*, *283*(12), 8014–8022. https://doi.org/10.1074/jbc.M708898200

Negulescu, P. A., Shastri, N., & Cahalan, M. D. (1994). Intracellular calcium dependence of gene expression in single T lymphocytes. *Proc. Natl. Acad. Sci.*, *91*(7), 2873–2877. https://doi.org/10.1073/pnas.91.7.2873

Ng, S. W., Capite, J. di, Singaravelu, K., & Parekh, A. B. (2008). Sustained Activation of the Tyrosine Kinase Syk by Antigen in Mast Cells Requires Local Ca2+ Influx through Ca2+ Release-activated Ca2+ Channels. *J. Biol. Chem.*, *283*(46), 31348–31355. https://doi.org/10.1074/jbc.M804942200

Nishigaki, I., Sasaguri, Y., & Yagi, K. (1995). Anti-proliferative effect of 2-methoxyestradiol on cultured smooth muscle cells from rabbit aorta. *Atherosclerosis*, *113*(2), 167–170. https://doi.org/10.1016/0021-9150(94)05442-L

Paavonen, T., Andersson, L. C., & Adlercreutz, H. (1981). Sex hormone regulation of in vitro immune response. Estradiol enhances human B cell maturation via inhibition of suppressor T cells in pokeweed mitogen-stimulated cultures. *J. Exp. Med.*, *154*(6), 1935–1945. https://doi.org/10.1084/jem.154.6.1935

Pani, B., & Singh, B. B. (2009). Lipid rafts/caveolae as microdomains of calcium signaling. *Cell Calcium*, *45*(6), 625–633. https://doi.org/10.1016/j.ceca.2009.02.009

Pankratz, S., Ruck, T., Meuth, S. G., & Wiendl, H. (2016). CD4+HLA-G+ regulatory T cells: Molecular signature and pathophysiological relevance. *Hum. Immunol.*, *77*(9), 727–733. https://doi.org/10.1016/j.humimm.2016.01.016

Pennell, L. M., Galligan, C. L., & Fish, E. N. (2012). Sex affects immunity. *J. Autoimmun.*, *38*(2–3), J282–J291. https://doi.org/10.1016/j.jaut.2011.11.013

Piccinni, M. P., Giudizi, M. G., Biagiotti, R., Beloni, L., Giannarini, L., Sampognaro, S., Parronchi, P., Manetti, R., Annunziato, F., & Livi, C. (1995). Progesterone favors the development of human T helper cells producing Th2-type cytokines and promotes both IL-4 production and membrane CD30 expression in established Th1 cell clones. *J. Immunol.*, *155*(1), 128–133.

Piccioni, M., Chen, Z., Tsun, A., & Li, B. (2014). Regulatory T-Cell Differentiation and Their Function in Immune Regulation. In *T Helper Cell Differentiation and Their Function* (pp. 67–97). Springer, Dordrecht. https://doi.org/10.1007/978-94-017-9487-9_4

Pinheiro, M. A. L., Kooij, G., Mizee, M. R., Kamermans, A., Enzmann, G., Lyck, R., Schwaninger, M., Engelhardt, B., & de Vries, H. E. (2016). Immune cell trafficking across the barriers of the central nervous system in multiple sclerosis and stroke. *Biochim. Biophys. Acta BBA - Mol. Basis Dis.*, *1862*(3), 461–471. https://doi.org/10.1016/j.bbadis.2015.10.018

Polanczyk, M. J., Carson, B. D., Subramanian, S., Afentoulis, M., Vandenbark, A. A., Ziegler, S. F., & Offner, H. (2004). Cutting Edge: Estrogen Drives Expansion of the CD4+CD25+ Regulatory T Cell Compartment. *J. Immunol.*, *173*(4), 2227–2230. https://doi.org/10.4049/jimmunol.173.4.2227

Potter, B. V. L. (2018). Steroid Sulfatase Inhibition by Aryl Sulfamates: Clinical Progress, Mechanism and Future Prospects. *J. Mol. Endocrinol.*, JME-18-0045. https://doi.org/10.1530/JME-18-0045

Pozzilli, C., Falaschi, P., Mainero, C., Martocchia, A., D'Urso, R., Proietti, A., Frontoni, M., Bastianello, S., & Filippi, M. (1999). MRI in multiple sclerosis during the menstrual cycle: Relationship with sex hormone patterns. *Neurology*, *53*(3), 622–622. https://doi.org/10.1212/WNL.53.3.622

Prossnitz, E. R., & Barton, M. (2014). Estrogen biology: New insights into GPER function and clinical opportunities. *Mol. Cell. Endocrinol.*, *389*(1), 71–83. https://doi.org/10.1016/j.mce.2014.02.002

Quintana, A., & Hoth, M. (2004). Apparent cytosolic calcium gradients in T-lymphocytes due to fura-2 accumulation in mitochondria. *Cell Calcium*, *36*(2), 99–109. https://doi.org/10.1016/j.ceca.2004.01.003

Quintana, A., Schwindling, C., Wenning, A. S., Becherer, U., Rettig, J., Schwarz, E. C., & Hoth, M. (2007). T cell activation requires mitochondrial translocation to the immunological synapse. *Proc. Natl. Acad. Sci.*, *104*(36), 14418–14423. https://doi.org/10.1073/pnas.0703126104

Redondo, P. C., Salido, G. M., Pariente, J. A., Sage, S. O., & Rosado, J. A. (2008). SERCA2b and 3 play a regulatory role in store-operated calcium entry in human platelets. *Cell. Signal.*, *20*(2), 337–346. https://doi.org/10.1016/j.cellsig.2007.10.019

Reed, M. J., Purohit, A., Woo, L. W. L., Newman, S. P., & Potter, B. V. L. (2005). Steroid Sulfatase: Molecular Biology, Regulation, and Inhibition. *Endocr. Rev.*, *26*(2), 171–202. https://doi.org/10.1210/er.2004-0003

Robinson, A. P., Harp, C. T., Noronha, A., & Miller, S. D. (2014). Chapter 8 - The experimental autoimmune encephalomyelitis (EAE) model of MS: utility for understanding disease pathophysiology and treatment. In D. S. Goodin (Ed.), *Handbook of Clinical Neurology* (Vol. 122, pp. 173–189). Elsevier. Retrieved from http://www.sciencedirect.com/science/article/pii/B978044452001200008X

Roe, M. W., Lemasters, J. J., & Herman, B. (1990). Assessment of Fura-2 for measurements of cytosolic free calcium. *Cell Calcium*, *11*(2–3), 63–73. https://doi.org/10.1016/0143-4160(90)90060-8

Ropero, A. B., Fuentes, E., Rovira, J. M., Ripoll, C., Soria, B., & Nadal, A. (1999). Non-genomic actions of 17β-oestradiol in mouse pancreatic β-cells are mediated by a cGMP-dependent protein kinase. *J. Physiol.*, *521*(2), 397–407. https://doi.org/10.1111/j.1469-7793.1999.00397.x

Rubtsova, K., Marrack, P., & Rubtsov, A. V. (2015). Sexual dimorphism in autoimmunity. *J. Clin. Invest.*, *125*(125(6)), 2187–2193. https://doi.org/10.1172/JCI78082

Ruehlmann, D. O., Steinert, J. R., Valverde, M. A., Jacob, R., & Mann, G. E. (1998). Environmental estrogenic pollutants induce acute vascular relaxation by inhibiting L-type Ca2+ channels in smooth muscle cells. *FASEB J.*, *12*(7), 613–619.

Sage, S. O., Merritt, J. E., Hallam, T. J., & Rink, T. J. (1989). Receptor-mediated calcium entry in fura-2-loaded human platelets stimulated with ADP and thrombin. Dual-wavelengths studies with Mn2+. *Biochem. J.*, *258*(3), 923–926. https://doi.org/10.1042/bj2580923

Scanlon, M., Williams, D. A., & Fay, F. S. (1987). A Ca2+-insensitive form of fura-2 associated with polymorphonuclear leukocytes. Assessment and accurate Ca2+ measurement. *J. Biol. Chem.*, *262*(13), 6308–6312.

Schaufelberger, S. A., Rosselli, M., Barchiesi, F., Gillespie, D. G., Jackson, E. K., & Dubey, R. K. (2016). 2-Methoxyestradiol, an endogenous 17β-estradiol metabolite, inhibits microglial proliferation and activation via an estrogen receptor-independent mechanism. *Am. J. Physiol. - Endocrinol. Metab.*, *310*(5), E313–E322. https://doi.org/10.1152/ajpendo.00418.2015

Seegers, J. C., Aveling, M.-L., van Aswegen, C. H., Cross, M., Koch, F., & Joubert, W. S. (1989). The cytotoxic effects of estradiol-17β, catecholestradiols and

methoxyestradiols on dividing MCF-7 and Hela cells. *J. Steroid Biochem.*, *32*(6), 797–809. https://doi.org/10.1016/0022-4731(89)90455-X

Sewell, A. K. (2012). Why must T cells be cross-reactive? *Nat. Rev. Immunol.*, *12*(9), 669–677. https://doi.org/10.1038/nri3279

Shen, Z., Wu, Y., Chen, X., Chang, X., Zhou, Q., Zhou, J., Ying, H., Zheng, J., Duan, T., & Wang, K. (2014). Decreased Maternal Serum 2-Methoxyestradiol Levels are Associated with the Development of Preeclampsia. *Cell. Physiol. Biochem.*, *34*(6), 2189–2199. https://doi.org/10.1159/000369662

Sheridan, J. T., Gilmore, R. C., Watson, M. J., Archer, C. B., & Tarran, R. (2013). 17β-Estradiol Inhibits Phosphorylation of Stromal Interaction Molecule 1 (STIM1) Protein IMPLICATION FOR STORE-OPERATED CALCIUM ENTRY AND CHRONIC LUNG DISEASES. *J. Biol. Chem.*, *288*(47), 33509–33518. https://doi.org/10.1074/jbc.M113.486662

Shivaji, S., & Jagannadham, M. V. (1992). Steroid-induced perturbations of membranes and its relevance to sperm acrosome reaction. *Biochim. Biophys. Acta BBA - Biomembr.*, *1108*(1), 99–109. https://doi.org/10.1016/0005-2736(92)90119-7

Shrestha, D., Jenei, A., Nagy, P., Vereb, G., & Szöllősi, J. (2015). Understanding FRET as a Research Tool for Cellular Studies. *Int. J. Mol. Sci.*, *16*(4), 6718–6756. https://doi.org/10.3390/ijms16046718

Sica, A., Dorman, L., Viggiano, V., Cippitelli, M., Ghosh, P., Rice, N., & Young, H. A. (1997). Interaction of NF-κB and NFAT with the Interferon-γ Promoter. *J. Biol. Chem.*, *272*(48), 30412–30420. https://doi.org/10.1074/jbc.272.48.30412

Stefano, G. B., Cadet, P., Breton, C., Goumon, Y., Prevot, V., Dessaint, J. P., Beauvillain, J.-C., Roumier, A. S., Welters, I., & Salzet, M. (2000). Estradiol-stimulated nitric oxide release in human granulocytes is dependent on intracellular calcium transients: evidence of a cell surface estrogen receptor. *Blood*, *95*(12), 3951–3958.

Stubelius, A., Andréasson, E., Karlsson, A., Ohlsson, C., Tivesten, Å., Islander, U., & Carlsten, H. (2011). Role of 2-methoxyestradiol as inhibitor of arthritis and osteoporosis in a model of postmenopausal rheumatoid arthritis. *Clin. Immunol.*, *140*(1), 37–46. https://doi.org/10.1016/j.clim.2011.03.006

Stubelius, A., Erlandsson, M. C., Islander, U., & Carlsten, H. (2014). Immunomodulation by the estrogen metabolite 2-methoxyestradiol. *Clin. Immunol.*, *153*(1), 40–48. https://doi.org/10.1016/j.clim.2014.03.011

Stuke, K., Flachenecker, P., Zettl, U. K., Elias, W. G., Freidel, M., Haas, J., Pitschnau-Michel, D., Schimrigk, S., & Rieckmann, P. (2009). Symptomatology of MS: results from the German MS Registry. *J. Neurol.*, *256*(11), 1932–1935. https://doi.org/10.1007/s00415-009-5257-5

Stys, P. K., Zamponi, G. W., Minnen, J. van, & Geurts, J. J. G. (2012). Will the real multiple sclerosis please stand up? *Nat. Rev. Neurosci.*, *13*(7), 507. https://doi.org/10.1038/nrn3275

Tevaarwerk, A. J., Holen, K. D., Alberti, D. B., Sidor, C., Arnott, J., Quon, C., Wilding, G., & Liu, G. (2009). Phase I Trial of 2-Methoxyestradiol (2ME2, Panzem®) NanoCrystal® Dispersion (NCD®) in Advanced Solid Malignancies. *Clin. Cancer Res. Off. J. Am. Assoc. Cancer Res.*, *15*(4), 1460–1465. https://doi.org/10.1158/1078-0432.CCR-08-1599

Thakur, P., & Fomina, A. F. (2010). Whole-Cell Recording of Calcium Release-Activated Calcium (CRAC) Currents in Human T Lymphocytes. *J. Vis. Exp. JoVE*, (46). https://doi.org/10.3791/2346

Tian, C., Du, L., Zhou, Y., & Li, M. (2016). Store-operated CRAC channel inhibitors: opportunities and challenges. *Future Med. Chem.*, *8*(7), 817–832. https://doi.org/10.4155/fmc-2016-0024

Tiller, G. E., Mueller, T. J., Dockter, M. E., & Struve, W. G. (1984). Hydrogenation of Triton X-100 eliminates its fluorescence and ultraviolet light absorption while preserving its detergent properties. *Anal. Biochem.*, *141*(1), 262–266. https://doi.org/10.1016/0003-2697(84)90455-X

Tombes, R. M., & Borisy, G. G. (1989). Intracellular free calcium and mitosis in mammalian cells: anaphase onset is calcium modulated, but is not triggered by a brief transient. *J. Cell Biol.*, *109*(2), 627–636.

Tsien, R., & Pozzan, T. (1989). [14] Measurement of cytosolic free Ca2+ with quin2. In *Methods in Enzymology* (Vol. 172, pp. 230–262). Academic Press. https://doi.org/10.1016/S0076-6879(89)72017-6

Tsien, R. Y., Rink, T. J., & Poenie, M. (1985). Measurement of cytosolic free Ca2+ in individual small cells using fluorescence microscopy with dual excitation wavelengths. *Cell Calcium*, *6*(1–2), 145–157. https://doi.org/10.1016/0143-4160(85)90041-7

Veillette, A., Bookman, M. A., Horak, E. M., & Bolen, J. B. (1988). The CD4 and CD8 T cell surface antigens are associated with the internal membrane tyrosine-protein kinase p56lck. *Cell*, *55*(2), 301–308. https://doi.org/10.1016/0092-8674(88)90053-0

Viglietta, V., Baecher-Allan, C., Weiner, H. L., & Hafler, D. A. (2004). Loss of Functional Suppression by CD4+CD25+ Regulatory T Cells in Patients with Multiple Sclerosis. *J. Exp. Med.*, *199*(7), 971–979. https://doi.org/10.1084/jem.20031579

Vono, M., Lin, A., Norrby-Teglund, A., Koup, R. A., Liang, F., & Loré, K. (2017). Neutrophils acquire the capacity for antigen presentation to memory CD4+ T cells in vitro and ex vivo. *Blood*, *129*(14), 1991–2001. https://doi.org/10.1182/blood-2016-10-744441

Voskuhl, R. R., Martin, R., Bergman, C., Dalal, M., Ruddle, N. H., & McFarland, H. F. (1993). T helper 1 (Th1) functional phenotype of human myelin basic protein-specific T lymphocytes. *Autoimmunity*, *15*(2), 137–143.

Voskuhl, R. R., & Palaszynski, K. (2001). Sex Hormones in Experimental Autoimmune Encephalomyelitis: Implications for Multiple Sclerosis. *The Neuroscientist*, *7*(3), 258–270. https://doi.org/10.1177/107385840100700310

Wegmann, T. G., Lin, H., Guilbert, L., & Mosmann, T. R. (1993). Bidirectional cytokine interactions in the maternal-fetal relationship: is successful pregnancy a TH2 phenomenon? *Immunol. Today*, *14*(7), 353–356. https://doi.org/10.1016/0167-5699(93)90235-D

Wehling, M. (1997). Specific, Nongenomic Actions of Steroid Hormones. *Annu. Rev. Physiol.*, *59*(1), 365–393. https://doi.org/10.1146/annurev.physiol.59.1.365

Whitacre, C. C. (1999). BIOMEDICINE:A Gender Gap in Autoimmunity. *Science*, *283*(5406), 1277–1278. https://doi.org/10.1126/science.283.5406.1277

Wucherpfennig, K. W., & Strominger, J. L. (1995). Molecular mimicry in T cell-mediated autoimmunity: Viral peptides activate human T cell clones specific for myelin basic protein. *Cell*, *80*(5), 695–705. https://doi.org/10.1016/0092-8674(95)90348-8

Xu, L., Yang, T., Su, S., & Wang, F. (2016). 2-Methoxyestradiol Alleviates Experimental Autoimmune Uveitis by Inhibiting Lymphocytes Proliferation and T Cell Differentiation. *BioMed Res. Int.*, *2016*, e7948345. https://doi.org/10.1155/2016/7948345

Yang, J., & Reth, M. (2015). Receptor Dissociation and B-Cell Activation. *Curr. Top. Microbiol. Immunol.* https://doi.org/10.1007/82_2015_482

Yates, M. A., Li, Y., Chlebeck, P. J., & Offner, H. (2010). GPR30, but not estrogen receptor-alpha, is crucial in the treatment of experimental autoimmune encephalomyelitis by oral ethinyl estradiol. *BMC Immunol.*, *11*, 20. https://doi.org/10.1186/1471-2172-11-20

Zhang, Y., Song, L., Gu, S., Lu, S., & Zhou, Z. (1999). Inhibitory effects of estradiol on inward rectifier and delayed rectifier K+ currents in guinea pig ventricular myocytes. *Zhongguo Yao Li Xue Bao*, *20*(7), 631–634.

Zhu, B. T., & Conney, A. H. (1998). Functional role of estrogen metabolism in target cells: review and perspectives. *Carcinogenesis*, *19*(1), 1–27.

Zhu, J., & Paul, W. E. (2008). CD4 T cells: fates, functions, and faults. *Blood*, *112*(5), 1557–1569. https://doi.org/10.1182/blood-2008-05-078154

7. Eidesstattliche Versicherung

Name: Johnsen Vorname: Anke

Hiermit erkläre ich an Eides statt, dass ich die vorliegende Dissertationsschrift selbst verfasst und keine anderen als die angegebenen Quellen und Hilfsmittel benutzt habe.

_____ _____

Ort, Datum Unterschrift

8. Acknowledgements

I thank Prof. Andreas Guse for the project, for supervision and many discussions which were always interesting and inspiring.

I thank Prof. Christian Lohr for evaluating my thesis.

Further, I thank our collaborator Prof. Barry Potter from the University of Oxford for many inspiring ideas and for proofreading my thesis. I thank Dr. Wolfgang Dohle from the University of Oxford for providing the 2ME2 derivatives. I am grateful to Prof. Alexander Flügel, Dr. Dmitri Lodygin and Leon Hosang from the University Medical Center Göttingen for the supply of T_{MBP} lymphocytes.

Special thanks go to Dr. Ralf Fliegert. Thank you for every single discussion, support and proofreading my thesis.

I thank the Ca^{2+} signalling group, esp. Andreas Bauche, Dr. Björn-Phillip Diercks and Ellen Gattkowski for all the support, discussions, fun, cocktails and cakes. Further, I thank the medical student Sissy-Alina Waschkowski for performing Ca^{2+} measurements during her practical training.

Mein besonderer Dank geht an meine Familie, insbesondere an Reiner und Inka Johnsen sowie Uwe und Lore Nothdurft. Vielen Dank für eure finanzielle und mentale Unterstützung in all den Jahren. Ohne euch wäre ich nicht da, wo ich jetzt bin.

Außerdem möchte ich Helmut, Monika und Anne Löhndorf für all den Spaß und die Entspannung danken.

Meinen größten Dank möchte ich Tim Löhndorf aussprechen. Seitdem unsere Lebenswege sich trafen, ist jeder Tag wie ein Geschenk: Du überrascht mich jeden Tag aufs Neue, ich weiß nie ganz genau, was mich erwartet, aber am Ende ist es wunderschön. Vielen Dank für jeden einzelnen Tag, den ich mit dir verbringen darf.